Prediction of the Off-Road Rigid-Ring Model Parameters for Truck Tire and Soft Soil Interactions

By

Kristian Lee Lardner

A Thesis Presented in Partial Fulfillment
of the Requirements for the Degree of

Master of Applied Science
in
Automotive Engineering

Faculty of Engineering and Applied Science
University of Ontario Institute of Technology
Oshawa, Ontario, Canada

July 2017

ABSTRACT

Significant time and cost savings can be realized through the use of virtual simulation of testing procedures across diverse areas of research and development. Fully detailed virtual truck models using the simplified off-road rigid-ring model parameters may further increase these economical savings within the automotive industry. The determination of the off-road rigid-ring parameters is meant to facilitate the simulation of full vehicle models developed by Volvo Group Trucks Technology. This works features new FEA (Finite Element Analysis) tire and SPH (Smoothed Particle Hydrodynamics) soil interaction modeling techniques. The in-plane and out-of-plane off-road rigid-ring parameters are predicted for an RHD (Regional Haul Drive) truck tire at varying operating conditions. The tire model is validated through static and dynamic virtual tests that are compared to previously published literature.

Both the in-plane and out-of-plane off-road rigid-ring RHD parameters were successfully predicted. The majority of the in-plane parameters are strongly influenced by the inflation pressure of the tire because the in-plane parameters are derived with respect to the mode of vibration of the tire. The total equivalent vertical stiffness on a dry sand is not as heavily influenced by the inflation pressure compared to predictions on a hard surface. For perspective, at 110 psi, the dry sand total vertical stiffness is nearly nine times smaller than that determined on the hard surface, while the lateral stiffness on soft soil (Dry Sand) is at a minimal of three times higher than that of the corresponding values tested on a hard surface. The cornering stiffness is primarily load dependant because the inflation pressure is only noticeably influential at high vertical loads. More importantly, the soil builds in front of the tire, creating what is called a bulldozing effect, during high slip angles. The additional lateral force of the soil exerted onto the tire during cornering maneuvers may contribute to higher than expected results and may be confirmed through future investigation of the cohesion of the soil model.

Key Words: FEA (Finite Element Analysis), SPH (Smoothed Particle Hydrodynamics), RHD (Regional Haul Drive truck tire), Off-Road Rigid-Ring Tire Model

TABLE OF CONTENTS

CHAPTER 6 DETERMINATION OF THE OUT-OF-PLANE OFF-ROAD RIGID-RING MODEL PARAMETERS 78

LIST OF FIGURES

LIST OF TABLES

NOMENCLATURE

In-Plane Rigid-Ring Parameters

$2_{a,soil}$	Effective Contact Patch, Soil	m
c_{bz}	Vertical Damping Constant	kN-s/m
c_{tot}	Tire Damping Constant	kN-s/m
c_{vr}	Residual Damping Constant	kN-s/m
$c_{b\theta}$	Rotational Damping Constant	kN-m-s/rad
k_{bz}	Sidewall Stiffness	kN/m
$k_{b\theta}$	Rotational Stiffness	kN-m/rad
$k_{cx,soil}$	Longitudinal Tread Stiffness, Soil	kN/ m
$k_{k,soil}$	Longitudinal Tire Stiffness, Soil	kN/unit slip
$k_{k,soil/v_{tr}}$	Longitudinal Tread Damping, Soil	kNs/m
k_{soil}	Soil Stiffness, Soil	kN/m
k_{tot}	Total Vertical Stiffness	kN/m
$k_{tot,soil}$	Total Vertical Stiffness, Soil	kN/m
k_{vr}	Residual Vertical Stiffness	kN/m
$R_{r,soil}$	Effective rolling radius, soil	m

Out-of-Plane Rigid-Ring Parameters

c_{by}	Translational Damping Constant	kN-s/m
c_{l}	Lateral Damping Constant	kN-s/m
$c_{l,soil}$	Lateral Damping Constant, Dry Sand	kN-s/m
$c_{b\gamma}$	Rotational Damping Constant	kN-s/rad
k_{by}	Translational Stiffness	kN/m
$k_{b\gamma}$	Translational Stiffness	kN-m/rad
$k_{f,soil}$	Cornering Stiffness, Soil	kN/rad
k_{l}	Lateral Tire Stiffness	kN/m
$k_{l,tot,Soil}$	Total Lateral Slip Stiffness, Soil	kN/m
$k_{l,Soil}$	Lateral Slip Stiffness, Soil	kN/m
$k_{M,soil}$	Self-Aligning Torque Stiffness, Soil	kN-m/rad
$RRC_{,soil}$	Rolling Resistance Coefficient, soil	-
$\sigma_{,\mathrm{soil}}$	Relaxation Length, soil	m

Additional Parameters

b	Loading plate radius	m
C_1	Bulk modulus (of soil)	-
$c_{2,3}$	Tire coefficient	-
$C_{4,5,6}$	Dimensionless material constants	-
c	Cohesion (of soil)	kPa
c_c	Critical damping constant	kN-m-s/rad
E_i	Internal energy	-
f	First nodal frequency	Hz
F_x	Longitudinal force	kN
F_y	Lateral force	kN
F_z	Normal force	kN
I_{bx}	Tire belt moment of inertia	kg-m^2
I_{by}	Tire belt moment of inertia	kg-m^2
k_c	Cohesive modulus of terrain deformation	kN/m
k_φ	Frictional modulus of terrain deformation	kN/m
m_a	Mass of rim	kg
m_b	Mass of tire belt	kg
m_{tot}	Total mass of tire model	kg
m_{wheel}	Mass of tire and rim	kg
M_x	Overturning moment	Nm
M_y	Rolling resistance moment	Nm
M_z	Self-Aligning moment	Nm
n	Exponent of terrain deformation	-
p	Pressure	MPa
p	Applied loading on plate	kPa
t_1	Time of first peak of logarithmic decay	s
t_2	Time of second peak logarithmic decay	s
v_{tr}	Tire velocity	m/s
V_x or v	Velocity	km/hr
y_1	First peak of translational displacement	mm
y_2	Second peak of translational displacement	mm
$\mathrm{y}_{l,1}$	First peak of translational displacement	mm
$\mathrm{y}_{l,2}$	Second peak of translational displacement	mm
$\mathrm{y}_{l,ss}$	Steady state translational displacement	mm
y_{ss}	Steady state translational displacement	mm
z	Sinkage (of soil)	m
α	Proportional sidewall nodal damping factor	rad/s
δ	Logarithmic decrement	-
θ_{ss}	Steady state angular displacement	rad
θ_1	First peak angular displacement	rad
θ_2	Second peak angular displacement	rad

Additional Parameters

μ	$\mu = \left(\frac{\rho}{\rho_o}\right) - 1$	-
ξ	Critical damping ratio	-
ξ_{tot}	Total damping ratio	-
τ_{d}	Damped period of vibration	s
ρ_o	Internal material density	kg/m^3
ρ	Material density	kg/m^3
τ_{max}	Maximum shear strength of soil	MPa
γ	Camber angle	deg
Φ	Angle of internal shearing resistance	deg
ω	Natural frequency of vibration	rad/s
ω_n	Undammed natural frequency	rad/s
ω_d	Dammed natural frequency	rad/s

Acronyms

ARSM	Adaptive Response Surface Method	-
FDERP	Force Dependant Effective Road Profile	-
FEA	Finite Element Analysis	-
FIERP	Force Independent Effective Road Profile	-
RHD	Regional Haul Drive (truck tire)	-
RRQVM	Rigid-Ring Quarter Vehicle Model	-
SAE	Society of Automotive Engineers	-
SPH	Smoothed Particle Hydrodynamics	-

ACKNOWLEDGEMENTS

The author expresses gratitude to Volvo Group Trucks Technology, in particular to Inge Johansson and Fredrik Öijer, for their continuous technical and financial support during the development of this research. Further appreciation is expressed towards AUTO 21, Canada Foundation for Innovation (CFI) and Infrastructure Operating Fund (IOF) for further funding supporting this work.

More importantly, sincere gratitude is owed towards Dr. Moustafa El-Gindy for his steady support and guidance as mentor and supervising professor of the Vehicle Dynamics and Crash Simulation Laboratory at the University of Ontario Institute of Technology (U.O.I.T). It is an honor to be a contributor to such a long-standing research project that has over a decade in industry partnership.

On a personal note, the author would like to thank all colleagues, friends, and family whose support indorsed the completion of this work. Finally, I would like to dedicate this to my father.

CHAPTER 1

INTRODUCTION

This chapter introduces the work to this thesis; the motivation, problem statement, and objectives of the work is discussed in detail. Also presented within this chapter is the working fundamentals of the basic tire concepts.

1.1 Motivation

The computational efficiency of computers and advancements in programming algorithms have allowed for the shift towards virtual simulation research and development within the automotive industry. The purpose is to reduce the amount of time, cost and man power required to design, develop, and test vehicles through the use of virtual simulations.

Tires are arguably the most important component of a wheeled vehicle because they are the direct link between the vehicle and the road surface. The prediction of a tire's behaviour is important to understand the stability, control, handling, and performance of the vehicle [1]. Often, these vehicular characteristics are determined through virtual testing methodologies in the vested interest of economic savings. However, these virtual full vehicle models often lack detailed and accurate tire models. This may be explained by the boundary presented upon automotive engineers by the confidentiality of tire manufacturers.

1.2 Problem Statement

With the understanding of the dynamics, a fully complex, 3D FEA pneumatic tire model may be used as a means to predict the characteristics of a tire at particular operating conditions. The simplified prediction of these parameters requires isolated virtual testing procedures through the determination of the rigid-ring model parameters.

Significant amounts of time is saved with the use of the simplified rigid-ring tire parameters implemented within complex full vehicle model simulations. The determination of the off-road rigid-ring parameters will facilitate the simulation of full vehicle models developed by Volvo Group Truck Technology with detailed and accurate tire models. More importantly, the discovery of a tires behaviour on soft soil is to be determined. This will be accomplished using a validated FEA (Finite Element Analysis) truck tire model and SPH (Smoothed Particle Hydrodynamics) soft soil (Dry Sand) to determine the in-plane and out-of-plane off-road rigid-ring model parameters with the use of the ESI program PAM-CRASH.

1.3 Objectives and Scope

The objective of this thesis is to predict the off-road rigid-ring parameters of an FEA (Finite Element Analysis) RHD (Regional Haul Drive) truck tire running over SPH (Smoothed Particle Hydrodynamics) soft soil (Dry Sand) for the implementation within the customer's full vehicle model. The contribution of this work features new FEA tire and SPH soil interaction modeling techniques. Further contributions include the determination of the behaviour of the tire on soft soil and the influence of varying the tire's operating conditions on that behaviour. The scope is to predict the in-plane and out-of-plane rigid-ring parameters and tire characteristics of the RHD truck tire on the SPH soft soil (Dry Sand) at varying operating conditions; three applied loadings, and three tire inflation pressures. The applied loadings considered are 13.34 kN (3,000 lbs.), 26.69 kN (6,000 lbs.), and 40.03 kN (9,000 lbs.). The studied operating inflation pressure will include 55 psi, 85 psi, and 110 psi. These parameters are recommended by Volvo and supporting literature to capture the tire's parameters above, below, and upon the manufactured recommended operating conditions. It is determined that these three step inputs of varying operating conditions satisfy the interest of this study due to the linearity of the rigid-ring parameters with respect to the operating load and inflation pressure of the tire.

1.4 Working Fundamentals

This section outlines the basic principles of pneumatic tires, to establish and define a fundamental understanding for the concepts presented within this work.

In 1839, Charles Goodyear developed the process of generating a pliable material from rubber, and thus begun manufacturing solid rubber bicycle tires. The pneumatic air filled tire was initially patented by Thomson, a Scottish engineer, ahead of his time. The first to successfully manufacture the pneumatic bicycle tire was John Dunlop in 1888 [2]. However, the Michelin brothers are credited with generating popularity in favour of the pneumatic tire among the automotive manufactures by creating a version of the pneumatic tire that was detachable from its solid rim in 1891 [3].

A vehicle tire is a toroid shape entity, often referred to as a pneumatic tire, that is a layered rubber composite flexible membrane shell filled with atmospheric air [4]. Tires are arguably the most important component of a wheeled vehicle; with the tire being responsible for supporting the vehicle sprung mass and cushioning the vehicle, therefore providing a quality ride. Tires are also responsible for the handling and performance, steering control, and directional stability of the vehicle while maintaining traction forces suitable to support the vehicle's movement. These characteristics are mainly influenced by the construction, materials of the tire and the forces and moments acting on the tire. [1]

1.4.1 Construction of Pneumatic Tires

The main structural components of a pneumatic tire are illustrated within Figure 1-1 and includes the tread, sidewall, under-tread, belt plies, carcass, and beads [5]. It is the construction and design of the plies, specifically the crown angle that determines the characteristics of the tire. With any crown angle less than twenty-five degrees, the tire sacrifices a poor ride quality for good cornering characteristics. The angle between the cord and the centerline of the tire is defined as the crown angle, and is depicted within Figure 1-2. [1]

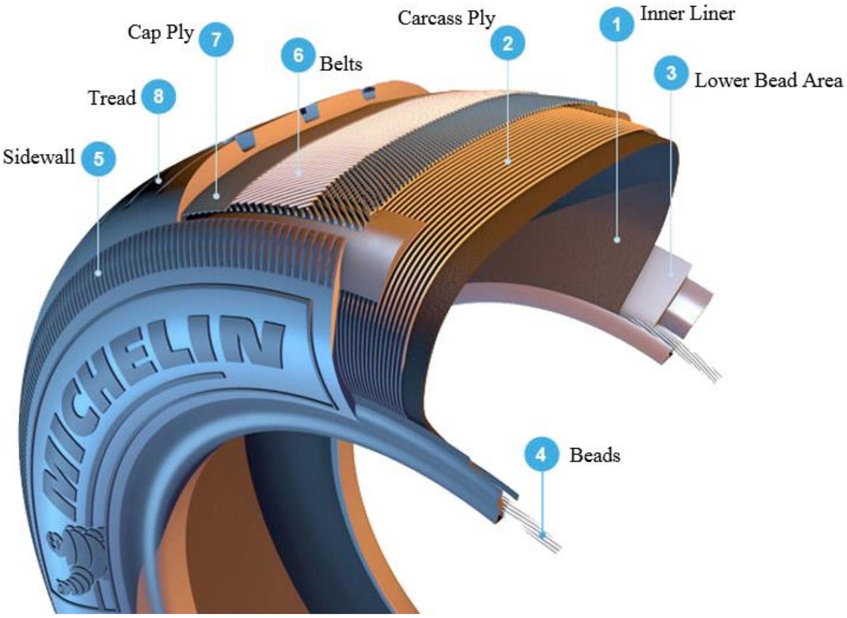

Figure 1-1: Pneumatic (Radial-Ply) Tire Construction [5]

Bias-ply tires and radial ply tires are the two types of tires important to the automotive industry. Bias-ply tires have diagonally run reinforcing cords, whereas a radial tire has cords running in radial directions, this phenomenon is highlighted in Figure 1-2 [1].The typical automotive passenger car tire is classified as a radial tire due to its good cornering, small flexing action of the tread, low wear, and lower rolling resistance. [1]

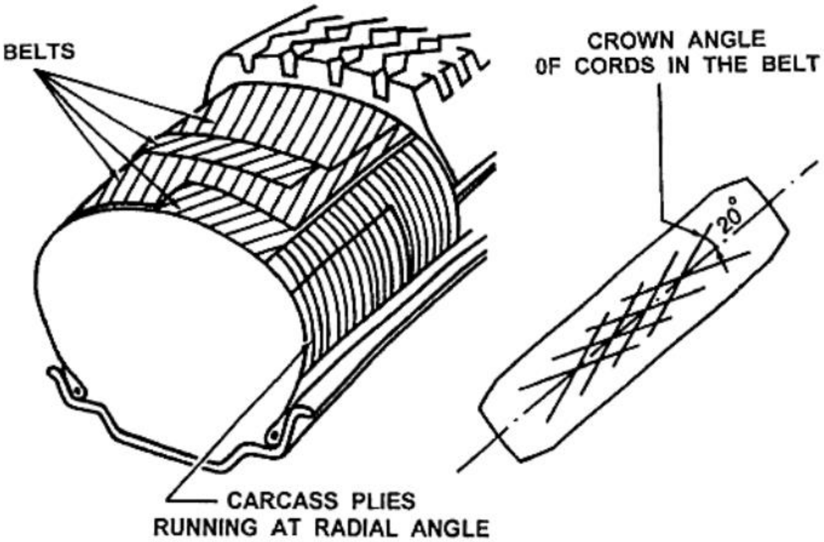

Figure 1-2: Radial-Ply Pneumatic Tire [1]

Truck tires are designed using the same principles as described for the passenger car tire. However, they are engineered to withstand higher inflation pressures and higher applied loadings. Therefore, truck tires are made of a heavier construction with a more rigid sidewall and steel cords reinforcing the carcass.

1.4.2 Dynamics of Pneumatic Tires

To be able to predict a tire's performance and characteristics it is important to understand fundamentals of the forces acting upon the tire. Before the forces and moments may be described, it is important to have the ability to visualize the forces and moments acting on the tire within an axis system. The SAE (Society of Automotive Engineers) coordinate system is the referenced coordinate system for this thesis, as shown in Figure 1-3 [1].

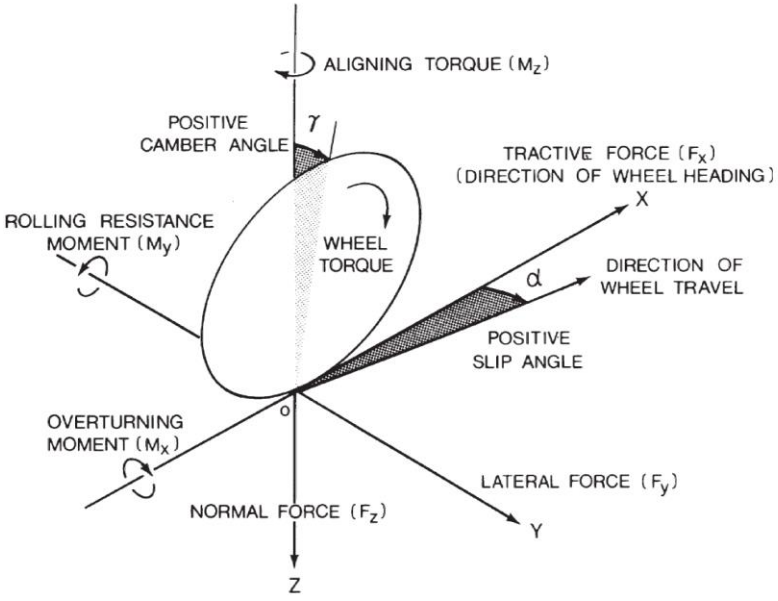

Figure 1-3: Forces and Moments Acting on a Tire in the SAE Coordinate System [1]

It is illustrated in Figure 1-3 that the positive x-axis is the direction of the wheel heading; the x-axis is the plane of interaction between the road and wheel contact. The tractive force, F_x acts in the direction of the wheel and is often termed tractive or longitudinal forces because they are the forces developed during braking and acceleration of the vehicle. The vehicle's control is governed by the lateral forces produced by the cornering force of the tire and other external lateral forces acting on the vehicle such as cross winds. The normal force, F_Z is the resultant of the vertical loading in the z-axis causing deflection within the tire. The moment about the x-axis is called the overturning moment, M_x, and is caused by the applied camber. The rolling resistance moment, M_y is the moment about the y-axis that resists the rolling motion of the tire in both positive and negative directions. The moment about the z-axis is called the self-aligning moment or aligning-torque moment, M_z, and is caused by the reaction forces from steering the tire. The slip angle, α is the angle between the direction of the wheel heading and the direction of the wheel travel. The camber angle, γ is created between the wheel and x-z plane. [1]

1.5 Thesis Outline

This work is delivered in seven chapters, listed below in synapsis;

Chapter 1: The motivation, problem definition, scope and objective of this thesis along within the description of the most basic tire fundamentals are initially presented in the first chapter.

Chapter 2: The necessary background is presented within chapter two for the conceptual understanding of the work(s) presented within this thesis. The analytical and virtual methods for expressing the tire-soil interaction characteristics are discussed in detail within this chapter.

Chapter 3: The details of the development and validation of both the FEA truck tire and SPH soft soil (Dry Sand) models are presented within chapter three.

Chapter 4: The sensitivity analysis of the influence of three key tire operating conditions on the first mode of vibrations of the tire are discussed within chapter four; the linear speed, the inflation pressure, and the applied loading are the varying parameters. The analysis is conducted using the drum-cleat testing procedure on a 2.5 m diameter drum model with a 10mm cleat. The mode frequency is important because it influences numerous tire characteristic parameters. Further purpose of this sensitivity analysis is to provide further validation of the FEA tire model.

Chapter 5: The in-plane off-road rigid-ring parameters are predicted for the RHD truck tire on SPH soft soil (Dry Sand) at varying loads and inflation pressure conditions.

Chapter 6: The out-of-plane off-road rigid-ring model parameters are discussed in detail within chapter six at varying operating conditions. The steering characteristics on dry sand are also discussed in detail.

Chapter 7: The conclusions, main contributions, and recommendations for future work(s) surrounding the thesis content is presented in the seventh chapter.

CHAPTER 2

LITERATURE REVIEW

2.1 Chapter Introduction

This chapter presents fundamental background on the modeling of tires and road surfaces such as soil using virtual simulations to predict tire characteristics at varying operating conditions. The literature review is further broken down into two sections; tire and soil modeling techniques, both analytical and virtual.

2.2 Tire Modeling

2.2.1 Analytical Tire Modeling

Analytical tire models are mechanical systems that simplify the complexity of a pneumatic tire to a set of equations of motion defined by a system of masses, springs, and dampers. The analytical tire models were used for characteristic prediction before computational efficiency supported FEA analysis, which is capable of sustaining such complex models. Although, some simulation models still use analytical models within real-time controllers.

The single one point mechanism, developed by Captain et al. in 1979 is one of the most simplified analytical tire models. The model only considers the vertical behaviour of the tire, meaning only the vertical stiffness and damping values are considered. Due to its simplicity, most early tire models adopted the point contact mechanism. An example of the single point contact mechanism is illustrated within Figure 2-1. The point contact mechanism has one key assumption for which it is valid; the contact point lies directly under the wheel and never losses contact with the ground. The model was initially used to investigate the ride comfort and vertical responses from road irregularities. The model is effective for its desired purpose with reasonable responses in the low input frequency range (0.1-1 Hz) but, the model overestimated the tire forces within the high to intermediate frequencies (1-10 Hz, and 10-100 Hz) and is therefore unable to predict complex dynamic tire parameters. [6]

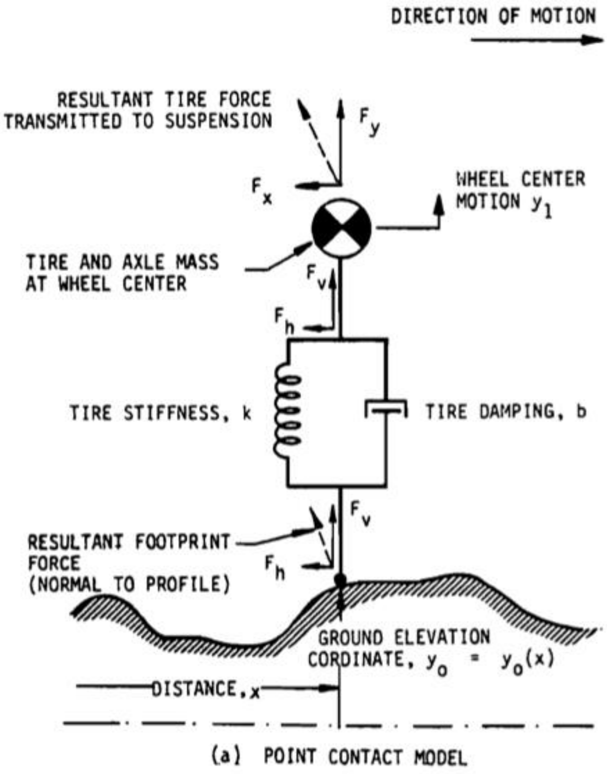

Figure 2-1: Point Contact Mechanism by Captain et al. [6]

To overcome the point contact model's deficiencies the equivalent ground model was developed by Davis in 1997; this model assumes the tire to be a simplified series of 2D radial springs connected to the road centre. The model represents the road profile by determining position and orientation according to the original road profile and the deformed area. The model worked exceptionally well on concave surfaces. [7]

In 1984 Takayama and Yamagishi developed a lumped mass-spring tire model to analyze the in-plane and tangential radial axle forces during the drum-cleat test. The tread and belt were modeled as a rigid-ring with five degrees of freedom with linear springs attached to the rigid-ring enabling tire deflection. The axle was fixed after loading of the tire to measure the vertical reaction forces. It is important to understand that the effects of suspension are ignored along with the displacements and forces outside of the in-plane parameters. Through comprehensive testing, the rigid-ring parameters were determined and agreed with measured data. Also, the longitudinal and vertical vibrational modes were determined to be 67 Hz and 74 Hz respectively. [8]

In 1985, Loo developed an analytical tire model represented by a flexible rigid-ring under tension surrounded by radial springs and dampers. The flexible outer tread band is considered to be massless and represents the contact between the model and the road profile. The model is complete with radial springs and dampers connecting the tread band to the rigid inner rim. The described flexible rigid-ring model is illustrated in Figure 2-2. [9]. The model requires equations of motion to generate the parameters of the model that are approximated using the theory of tensional strings supported by an elastic foundation. It is in theory, that an infinite number of springs and dampers may be placed as close together to accurately represent a tires' characteristic. This model is more capable than the single point mechanism at predicting tire properties; however, it is not an effective tool when regarding rotational dynamic behavior. The model was quantitatively validated by means of comparison to experimental data and was further used to predict the vertical load deflection and rolling resistance of a tire. [9]

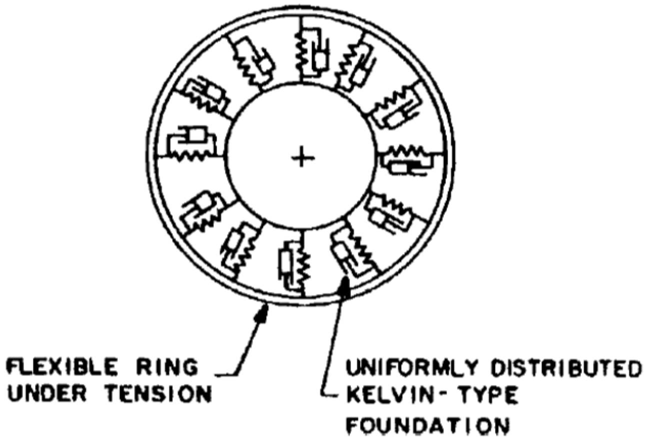

Figure 2-2: Loo's Flexible Rigid-Ring Model [9]

The original rigid-ring tire model presented by Zegelar and Pacejka in 1997, depicted within Figure 2-3, includes rotational stiffness and damping parameters. The in-plane semi-analytical model has freedom within the longitudinal, lateral and rotational directions allowing for the model to describe tire-road interactions more effectively. The tread and steel belts are modeled as a single rigid-ring mounted on an elastic foundation representing the tire sidewall. The residual vertical stiffness spring and damper is located between the rigid-ring and ground to account for the elastic tread while the longitudinal slip stiffness, between the tire and ground, accounts for the change in velocity. The rigid-ring tire model was validated using the 2.5m diameter drum-cleat test model and proved to be very effective in determining the in-plane dynamic behaviours. The purpose of the model was to provide more accurate predictions, specifically regarding the longitudinal force and vertical velocity in response to brake torque variations. [10]

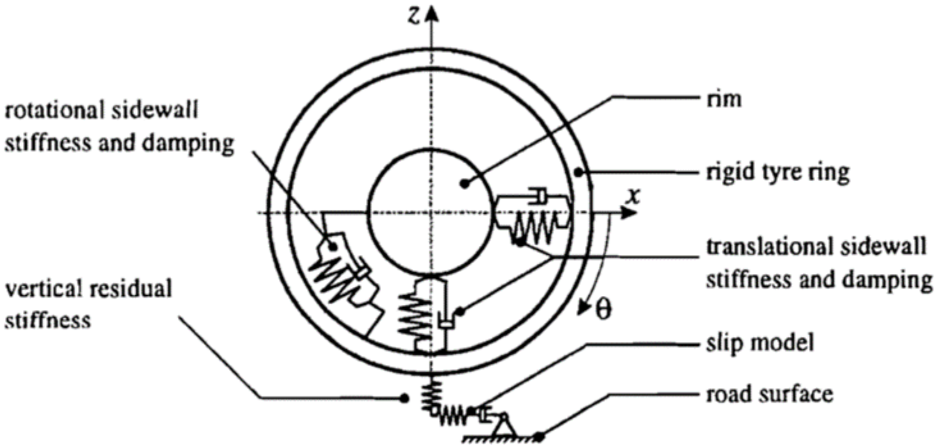

Figure 2-3: Basic Rigid-Ring Tire Model [10]

Kim and Savakor analyzed the issue of defining the in-plane contact of a free rolling pneumatic tire on a flat road. The rigid-ring model they used was an elastic ring on a viscoelastic foundation. Elastic ring components are introduced on the outer surface of the tire to represent the radial and tangential flexibility of the tread. The rigid-ring parameters were determined through measurements of a physical tire. The model predicted the traction force distributions and rolling resistance coefficients. However, these predictions were not validated with any proven experimental measurements. [11]

Two other researchers used the rigid-ring and rigid tread model; Bruni et al. [12], and Allison and Sharp [13]. Each of their work focused on the handling and ride comfort of a vehicle through the vibration frequency range analysis up to 100 Hz. Allision and Sharp used the simplified rigid-ring model approach to consider the problems of in-plane longitudinal vibrations in the low frequency range in 1997 [13]. Bruni et al., in 1997, proposed a method of determining in-plane tire parameters for a rigid-ring model through experimental tests. Bruni's rigid-ring model, depicted in Figure 2-4, was developed with the intent on performing braking, driving, and comfort analysis. Torsional pendulum and free rolling tests were used to directly measure certain parameters to complete the rigid-ring tire model, the remaining parameters were approximated by optimizing the difference between experimental and measured natural frequencies. [12]

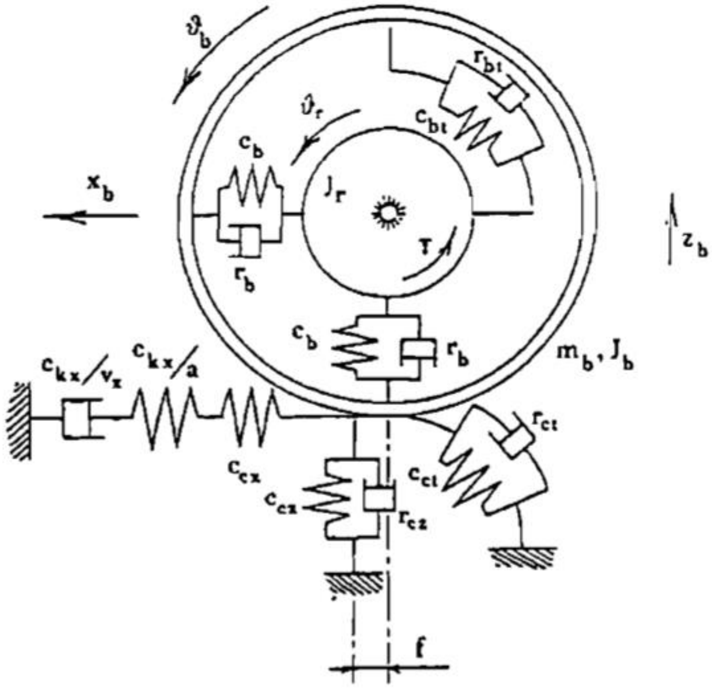

Figure 2-4: Bruni's Rigid-ring Tire Model [12]

Schmeitz expanded this work in 2004 with the development of a quarter vehicle model integrated with a rigid-ring model, and a suspension system comprised of spring and dampers, and a sprung mass. The road profile was produced form elliptical cams. The mode predicted longitudinal forces for different step road height inputs. The model was compared to measurements predicting accurate longitudinal and vertical tire forces. [14]

Allen continued the investigation of the ride comfort and durability predictions in 2007 using a combined Rigid-Ring Quarter Vehicle Model (RRQVM). Two models were compared; the Force Dependent Effective Road Profile (FDERP) and the Force Independent Effective Road Profile (FIERP). It is concluded that the FIERP model yields a smoother effective road profile slope under dynamic loading and therefore predicted the measured data more accurately. [15]

Chae et al. improved Zegelaar and Pacejka’s rigid-ring tire model in 2006 to include the out-of-plane tire parameters. The model incorporates the sidewall behavior, tread band, and slip characteristics and is depicted within Figure 2-5. One such introduction is the radial spring and damper to include the out-of-plane sidewall stiffness and damping. The in-plane and out-of-plane rigid-ring parameters, were predicted for the development of his three-groove truck tire model. [16]

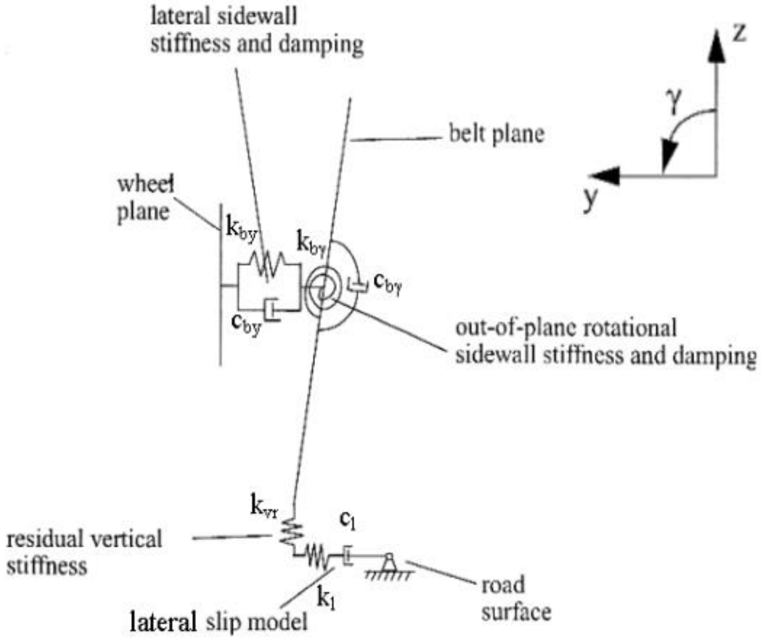

Figure 2-5: Chae's Out-of-Plane Rigid-ring Model [16]

Using ESI PAM-CRASH, Slade modeled and validated a non-linear 3D FEA truck tire model. The Goodyear RHD 315/80R22.5 drive tire was validated by matching simulation static and dynamic test to the tires manufactured published data. The tire in-plane and out of-plane rigid-ring parameters were determined on both an FEA hard surface and soft soil (sandy loam). The sandy loam FEA soil model was represented by elastic plastic materials and validated through the use of previously published techniques. Slade modified Pacejka and Zegelars’s rigid-ring model to include parameters to account for the soils flexibility. The newly developed semi-empirical in-plane and out-of-plane off-road rigid-ring model, illustrated within Figure 2-6 and Figure 2-7, were specifically developed to capture the behaviour of a truck tire driving on soft soil. [15]

It was concluded by Slade that the rolling resistance on a sandy loam are three times higher than that on a rigid surface, that the longitudinal slip stiffness is about a factor of four times lower on a sandy loam than on a rigid surface, and that the tractive forces are a fourth of that of a rigid surface on a sandy loam. It was also observed that the lateral forces on a sandy loam increase linearly with an increase in slip angle. However, this is called into question when a bulldozing effect is observed at high slip angles creating additional lateral forces. This is explained by the lack of a proper representation of the soils cohesion within the elastic plastic model. [17]

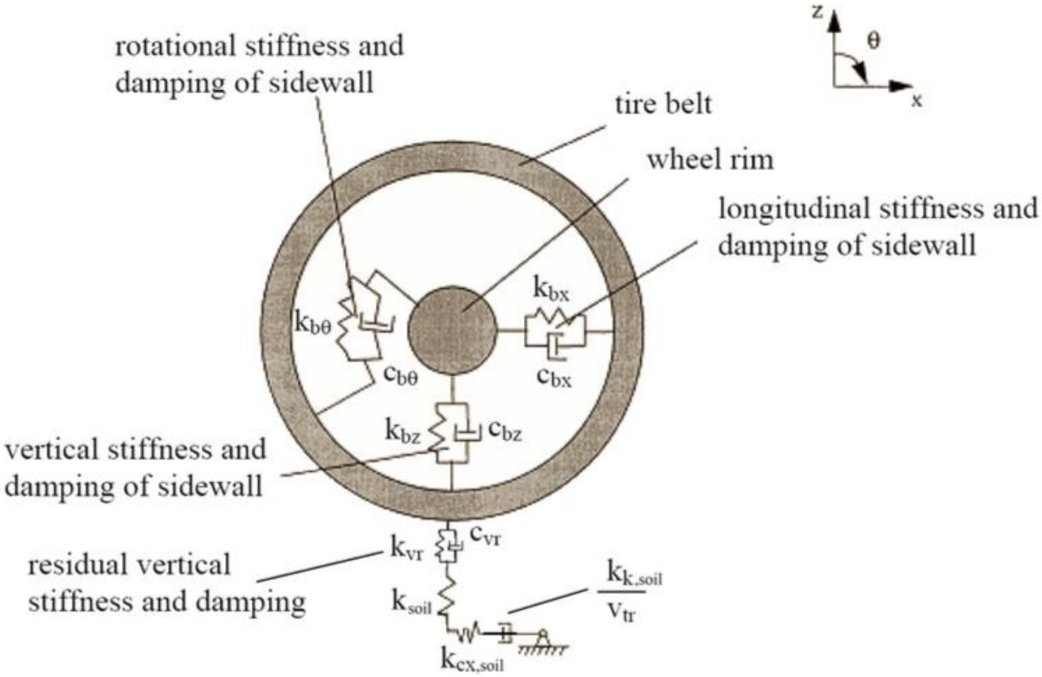

Figure 2-6: Slade's In-Plane Off-Road Rigid-Ring Model [17]

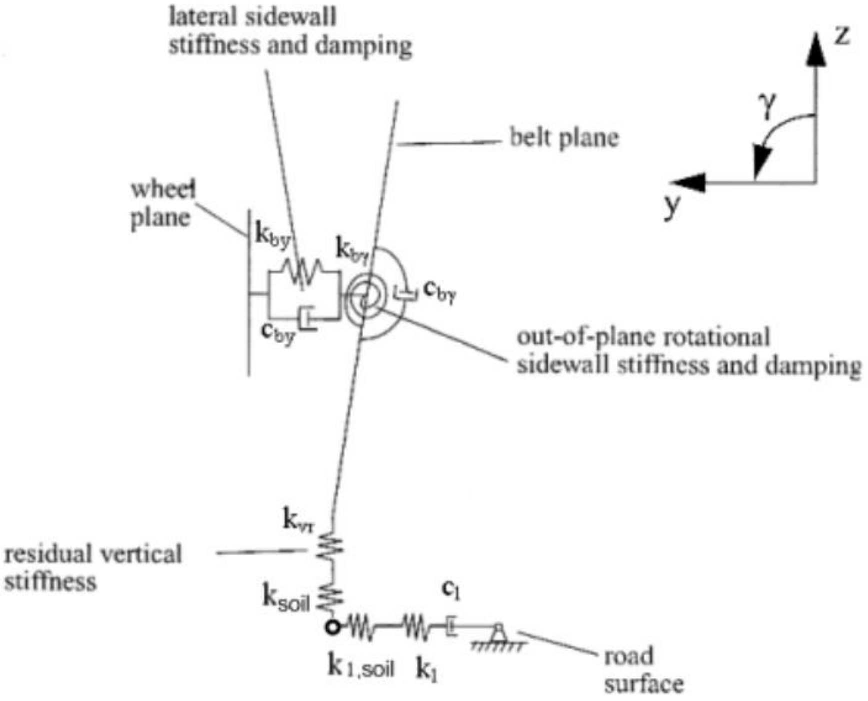

Figure 2-7: Slade's Out-of-Plane Off-Road Rigid-Ring Model [17]

2.2.2 FEA Tire Modeling

FEA tire modeling has grown in popularity since the 1970’s with the advancement in computer technology. Specifically, FEA has been widely adopted to solve problems of stress, strain, and elastic-plastic deformations allowing for extensive mathematical conclusions involving multi layered factors. Therefore, tire modeling requires extensive preparation to produce detailed and accurate results.

Young et al. studied the relationships of a tire and its contact between terra-mechanics in 1978. The tire soil interactions, specifically the stiffness of the tire carcass and tractive forces, were described while the tire was loaded with various inflation pressures using a series of FEA tests. The accuracy and reliability of FEA tire models were supported as the simulations results were comparable to the measured lab test data. [18]

Nakajima and Padovan developed a 2D FEA tire model in ADINA software to run on an arbitrary shaped surface. The tire tread and sidewall consisted of a linear viscoelastic ring on an elastic foundation. Simulated horizontal and vertical forces on the spindle of the tire were measured and found to be in agreement with experimental results. [19]

Rhyne et al. modeled a passenger car tire using 3D membranes in 1994 to study the influence of rim imperfections on the force vibration and ride comfort. The tire was rigid in the transverse shear direction due to computational limitations. An example of the tire model is showcased within Figure 2-8. It was concluded that most forces could be influenced by the radial rim imperfections; this suggests that the non-uniform signal produced by the lateral and radial rim imperfections require further discussion. [20]

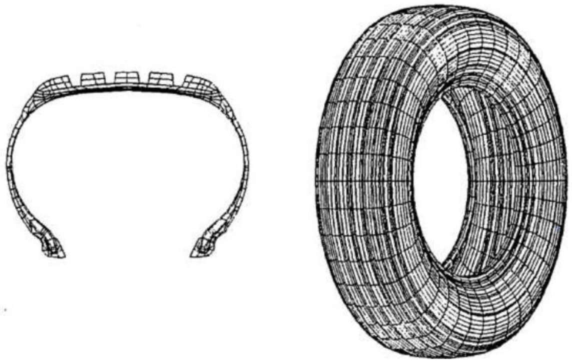

Figure 2-8: Rhyne's 3D Membrane FEA Tire Model [20]

Hiroma et al., in1997, determined that FEA models were capable of predicting tire traction at low slip angles. The developed FEA model could accurately predict pressure distributions and tractive forces under a rolling wheel when compared to measurements. [21]

Yan, in 2003, determined the maximum sectional width and resultant reaction forces with respect to tire speed for an FEA truck tire model. It was concluded that due to the centrifugal inertia forces pushing the tread outwards radially, an increase in speed yields a narrower section width and higher reaction forces. Figure 2-9 observes a section cut of the FEA tire with respect to the completed 3D tire model [22]. In 2005, Yan continued his previous research to study the relative belt edge endurance of a radial truck tire. Throughout the analysis, the relative belt edge endurance predicted reasonable numbers. [23]

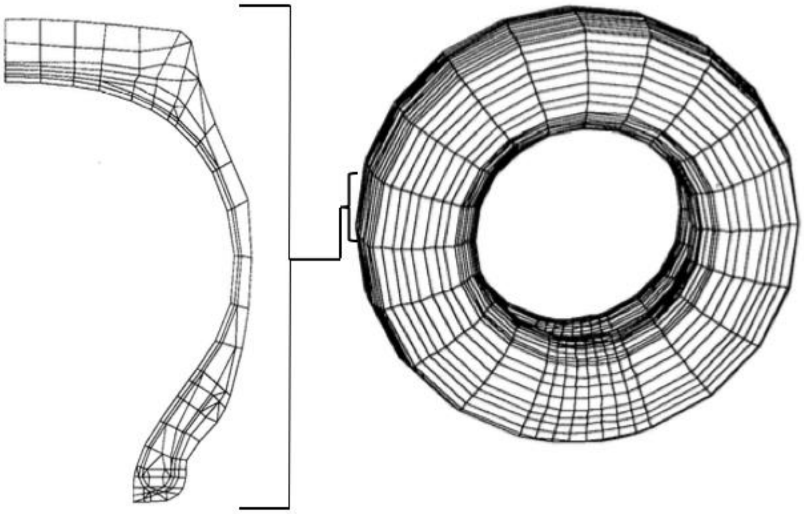

Figure 2-9: A Section Cut (Left) of Yan's Complete FEA Tire Model (Right) [22]

Chang and El Gindy developed an FEA non-linear radial, P185/70R14, passenger car tire. The tires construction is as such; 3D Mooney-Rivlin hyperplastic solid FE elements representing rubber materials, reinforced with fiber layered membrane elements representing rubber composites, and beam elements representing the beads of the tire. The tire was tested on a virtual drum-cleat test revealing the tires in-plane free vibrational modes to be within the range of 84 Hz for the vertical mode and 45Hz for a longitudinal first mode of vibration. [24]

Chang's virtual drum-cleat experimentation methodology was reiterated by Chae Seokyong in 2006 with a three-groove single truck tire (297/75R22.5). The diameter of the drum was 2.5m with a 10mm radius cleat and the truck tire was inflated to 110psi, loaded at 26.7kN (6,000lbs.), and was tested at a linear speed of 50km/h. The drum was able to successfully reach high speeds achievable beyond the standing wave phenomena which is a very challenging concept in physical experimentations. The first vertical mode of vibration was determined to occur at 73Hz. The vertical mode of vibration was then used to determine the vertical stiffness and damping constants of the tire. [16]

Ali et al. created a three-groove FEA radial truck tire, 295/75R22.5 using the software PAM-CRASH. The tire was validated using static vertical stiffness tests, footprint area, and free vibrational tests with results corresponding to published data. Also considered were the enveloping characteristics and combined camber and cornering characteristics. [25]

An FEA tire model was created based on the foundation of a 3D flexible ring on an elastic foundation by Kindt et el. in 2008. The tire model and dynamic behaviour was determined in ABAQUS with reasonable accuracy as compared to analytical calculations. The longitudinal and vertical first mode of vibration was determined via simulation to be 47.5Hz and 64.0Hz, respectively. These results compared to experimental findings with the longitudinal and vertical first modes of vibration being 47.4Hz and 74.3Hz, respectively. [26]

Similar success was shown by Adam Reid in 2015 [27]. Reid details the analysis of the selection, construction, and validation and application for an FEA tire model. An FEA 3D XONE XDA 445/50R22.5 Michelin wide base tire was created using the program PAM-CRASH. The tire was tuned using an Adaptive Response Surface Method (ARSM) optimization algorithm. The optimized tire was validated through a series of simulated experiments compared to measured field data conducted with Volvo at North Carolina. The dynamic test Reid used to validate the tire consisted of the drum-cleat test with a 2.5m diameter drum and a 20mm cleat in PAM-CRASH. The in-plane natural frequency was determined with a variation of load between 22.7kN-68kN (2312.5kg-6937.5kg) and a variance in inflation pressure of 70-150 psi. Reid concluded a vertical natural frequency in the range of 47-55Hz. Furthermore, it is observed that there is a slight increase in the natural frequency as the inflation pressure was increased. However, the load has no obvious effect on the in-plane vibration of the wide base tire. The tire was able to match the behaviour of the physical tire such that the rolling resistance measured during steady state had a minimal percent error of 1.78% between the simulated and physical measurements. When compared to the physical tire the simulated static load deflection yielded only a 0.42% error. After optimization and validation, the tire was used to populate the analytical rigid-ring model on a rigid road through the use of isolated virtual experiments. The in-plane and out-of-plane rigid-ring parameters for the tire at various loads and inflation pressures were predicted. The rigid-ring model trends are as follows; an increase in inflation pressure increases various stiffness, while most translational damping constant decrease with an increasing inflation pressure. However, the rotational damping constant increases with respect to an increasing inflation pressure. [27]

Figure 2-10: Comparison of Reid's Virtual FEA Wide Base Tire (Right) and the Michelin Tire (Left) [27]

2.3 Soil Modeling

It is of great importance that we are able to understand the tire-soil interactions, because accurately predicting vehicles characteristics requires a relationship between the off-road vehicle tires and the terrain characteristics. The second half of this literature review details the terra-mechanics, FEA soil modeling, SPH soil modeling, and hybrid FEA/SPH soil modeling techniques.

2.3.1 Terra-mechanics

The leading investigators of soil deformation predictions through mathematical analysis are Bekker, and the team of Janosi and Hanamoto.

Between the 1950's to the 1960's Bekker investigated the normal forces reacting with the soil [28] [29] [30]. In 1956, Bekker determined equations to describe the relationship of the sinkage of the soil using Mohr-Coulomb failure criterion. The pressure-sinkage relationship equations were developed to predict the interactions of forces normal to the soil. Parameters were tabulated for a range of soils to predict their pressure distribution under a passenger car tire, with Bekker's work spanning two decades focused on the modeling of soil deformation. [28]

In 1961 Janosi and Hanamoto mathematically predicted shear, or traction control characteristics, of the soil using stress strain relationships and a uniform pressure distribution. The equations were used to predict tractive force of a tracked vehicle. [31]

Osman, in 1964, successfully determined the angle of shearing resistance and soil cohesion for three particular soil models; dry sand, wet sand and clay. The purpose was to determine the accuracy of the current testing methodologies such as; the translational shear box, the NIAE shear box, the shear vane, the bevameter, triaxle test, and friction trolley method. Each method proved to be reliable and accurate for predicting soil characteristics. [32]

Both Wismer et al. [33] and Brixius [34] developed equations capable of predicting the tire's tractive performance using soil parameters as known values within the equations. Wismer and Luth used the cone index to predict the tractive performance of a car [33]. Young et al. concluded that shearing slip may not be determined using a cone penetrometer when comparing measured results to terra-mechnic properties [35] .

Wes developed the cone penetrometer, illustrated within Figure 2-11, in WWII; the device is a 30 degree right circular cone with a base area of 0.5in^2. The cone index is defined as the resistance of a soil to penetration by unit cone base area and is one of two methods of measuring soil characteristics by civil engineering standards.

Wittig and Alcock created a single wheel tester in 1990 to determine the traction of soil through measurement of the maximum transferable torque at known wheel loadings. The bulk density or soil water content was concluded to be predicted more accurately using the single wheel tester than Wismer and Luth's equations based on the cone index. [36]

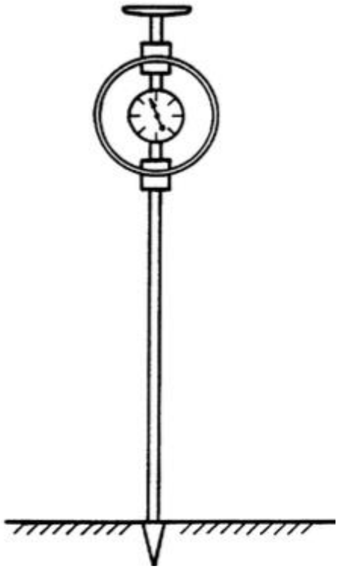

Figure 2-11: Cone Penetrometer (WES) [37]

In 1991 Okello concluded that the bevameter technique is better at determining soil parameters when directly compared to the cone-penetrometer. The Bevameter technique involves two simple tests; the pressure-sinkage test and the shear test. The original bevameter was developed by the University of New Castle and was later modified by Carlton University [37]. The plate penetration test, also known as the pressure-sinkage test determines the pressure-sinkage relationship by loading a plate with a contact area similar to that of the tire's contact patch onto the soil. The shear test measures the soil shear strength using measured friction forces. Okello's results agreed with Wittig and Alcock. However, with the added conclusion was that the bulk modulus and moisture content have a large influence on a tire's performance. [38]

Grahm, in 1991, studied the effects of penetration velocity; penetration velocity is the speed at which a tire requirs in order to avoid sinking into the soil. The dynamic pressure-sinkage properties of soil were studied using a simple model involving pushing a plate at different velocities into the soil and calculating the pressure under the plate. It was determined that when at constant inflation pressure, the soil sinkage decreases and the rolling resistance decreases as the penetration velocity increases. This is due to the point of the highest pressure being located at the front of the tire. [39]

Grahm explains that for a wheel, the penetration velocity is highest towards the front of the wheel this is because the translational and rotational velocities of the tire moves the pentation velocity forward and down the tire where it reduces to zero directly under the wheel. A study on the relationship between penetration velocity and pressure-sinkage was completed based on this observation. It is determined that tire will glide across the soil at high speeds as high penetration velocities induce less soil sinkage. There is an inverse relation between soil sinkage and rolling resistance as the rolling resistance will decrease with an increase in driving speed. [39]

Mosade et al. created a new critical state model including soil structure information in 1998 accounting for the anisotropic nature of soil. The results discovered that certain soils are unstable. Previous work (Cambridge University) describes the direction of voids within the structure of clay influences the soil's stress-strain behaviour as some soils experience a strain softening effect when these particular void structures experience a collapse. Once these structures are broken down the soil is predictable by original cam-clay methodologies. However, Masad's new model proved to be far superior when describing the stress strain of soil. [40]

Al-Shayea et al. developed a model to simulate soils such as dense sands and stiff clays, or soils that have a post peak strain-softening behavior in 2003. The simulation combined this stress-strain behavior with the Drucker-Prager model. It was observed that the simulation results were in good approximations with data from triaxle tests. [41]

2.3.2 FEA Soil Modeling

Tire-soil interactions are difficult and time consuming to model due to the complexity of the relationship between the required accuracy of both the tire and soil models. Advancements in computer computational efficiency and soil modeling techniques have allowed for simpler models to be used that do not compromise accuracy of the soil characteristics, allowing for FEA/FEM soil modeling techniques to become widely accepted

Heroma et al. studied the tire-soil stress distribution at the contact patch of the tire using FEM modeling. The tire was considered rigid and a viscoelastic soil model represented soft soil with a moisture content; the tire is allowed to sink into the soil before rolling at a constant vertical speed. The tractive forces were investigated at various slip angles. [21]

Shoop created a 3D model of a tire on deformable terrain to analyze the tire-ground interactions. Snow and compressed sand were modeled using steady state plasticity. The model was validated with pressure sinkage lab and field testing. [42]

In 2004 Fevers used the Drucker-Prager material with ABAQUS software to model different types of soil; wet loam with a high cohesion and a dry sand with low cohesion. The 2D FEA tire model’s operating conditions consisted of a constant speed with two inflation pressures. It was concluded that at low inflation pressures, the sandy loam compacted less and the sand soil illustrated more soil compaction due to the low cohesion and internal shear. Figure 2-12 illustrates the soil pressure distribution at both low and high inflation pressures. [43]

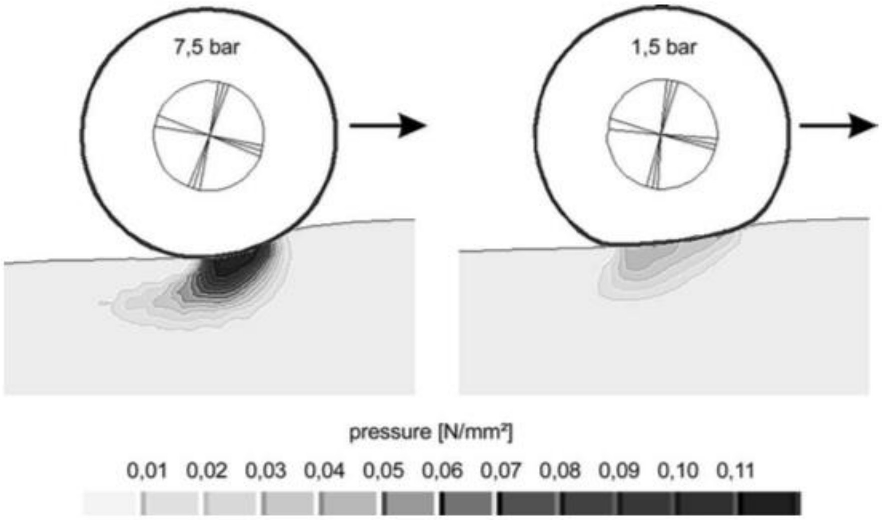

Figure 2-12: Soil Pressure Analysis at High and Low Inflation Pressures [43]

Hambleton and Drescher, investigated wheeled induced rutting in soils using FEM elastic plastic soil models in ABAQUS in the years 2008 and 2009. It was found that the 3D effects of indentation are insignificant for clays and significant for sands. An example is presented within Figure 2-13. It was further concluded that the rutting process of a rolling wheel is steady, meaning the analytical model is able to predict sinkage under steady state conditions. [44] [45]

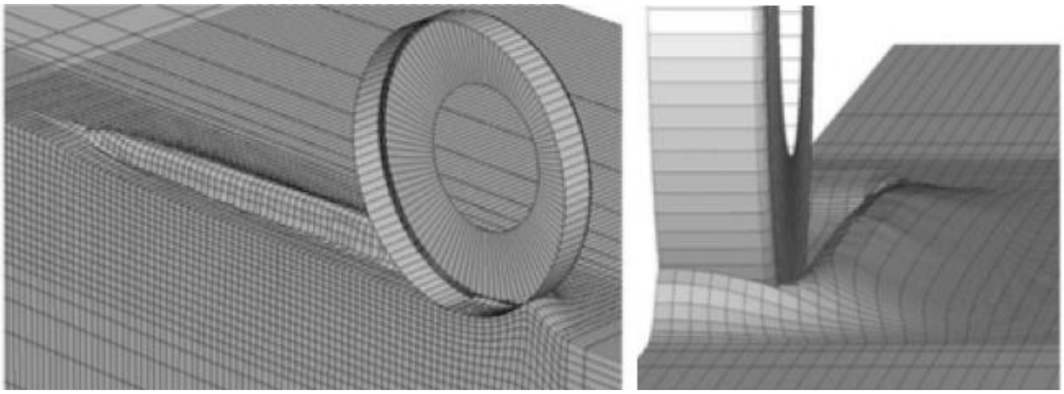

Figure 2-13: Side (Left) and Front (Right) Illustration of Tire Deforming FEA Soil Mesh [45]

In 2005 Chiroux developed a 3D soil model using ABAQUS with a rigid rotating wheel. The objective was to analyze the stress and deflection of the soil under the wheel. The soil type model was a Norfolk Sandy Loam and is modeled with five different mesh densities, with the smallest mesh size located at the contact area between the soil and tire to save on computational time without losing accuracy of the simulation. The experimental results and analytical data were in agreement with each other. This proves that a larger mesh sizing is an appropriate time saving strategy when the larger mesh size is away from the measured area of interest. [46]

Slade successfully predicted the off-road rigid-ring model parameters on an FEA sandy loam soil model in 2009. It was noted that hysteresis and damping effects were not part of the defined elastic-plastic model. The elastic-model itself has the limitation of behaving like springs at stresses below yield and deforming for stresses above yield. Nor was the Druker-Prager or Mohr-Coulomb failure criterion able to be implemented due to the software limitations using FEA techniques. He recommended the investigation of SPH techniques to improve the soil model's accuracy. [17]

2.3.3 SPH Soil Modeling

FEA modeling has been the predominant way to represent soil characteristics during recent years, but, FEA modeling has some limitations. One of which is its inability to characterize shear properties due to observed sponge behaviour during pressure-sinkage tests. Smoothed Particle Hydrodynamics (SPH) was originally cited by Schlatter in 1999 as a meshless form of modeling to represent a compact group of particles representing galaxy formations [47]. Currently, SPH modeling has been adopted to be used for multiple types of models including fluid dynamics, body impacts and soil flow analysis models. The SPH particles are defined by a smoothing length, or a radius of interaction that allows for multiple particle interactions compared to FEA elements, which are limited to interact with only their direct neighbors in contact. Figure 2-14 illustrates the allowance of interaction relationship of neighboring SPH particles. The smoothing length may be varied or constant depending on the real-time particle density. [47]

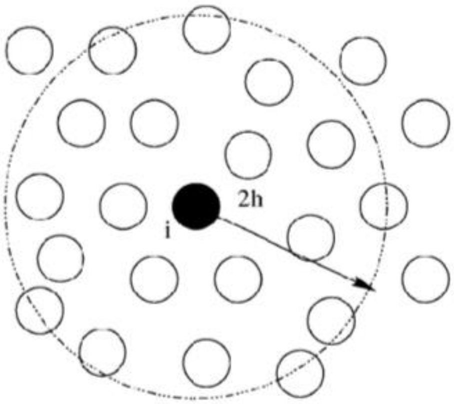

Figure 2-14: Allowance of Interaction (2h) of Particle (i) [47]

In 1997 Groenboom modeled 2D and 3D hypervelocity impacts with SPH particles using PAM-SHOCK. The shapes of craters, ejected trajectories and debris clouds computed were in agreement with experimental data. It was determined that using a varied smoothing length yields more accurate results. Combined FEA/SPH models determined a 0.1% standard deviation between the full SPH and the combined FEA/SPH results. [48]

Clegg et al., in 1997, choose to use SPH over FEA soil modeling because SPH is able to represent fracture and fragmentation of soils more naturally. Three models were used to compare penetrator impacts on multilayered soils; SPH/Lagrange, Euler/Lagrange, and Lagrange/Lagrange. It is noted that the SPH/Lagrange soil model has a level of accuracy equivalent to the Euler/Lagrange method. But the SPH model under predicts the tire deceleration up to 30%. [49]

In 1999 Faraud et al. simulated debris impacts using the 3D PAM-SHOCK and 2D AUTIDYN programs. It was realized that the FEA models require less simulation time than the equivalent SPH models. PAM-SHOCK was concluded to be the promising software. [50]

In 2004 McCarthy et al. modeled the impacts of fluid like behaviour of a bird strike on an airplane wing. The relevant conclusion was that SPH has the ability to represent variable connectivity allowing for the modeling of severe distortion. [51]

Johnsosn and Holzapel published a paper in 2006 on the modeling of soft body impacts on aircraft structures. They concluded that the SPH impactor model methodology was promising for simulating soft body impacts. [52]

Maeda et al. published a paper in 2006 on seepage failure; it was determined that SPH was capable of modeling soil, water, and air, or a solid, liquid and a gas. [53]

Bui et al. investigates soil water interactions using SPH. The water was modeled as viscous and the soil was modeled to be elastic plastic. The model proved to be stable with large deformation problems. [54, 55] Bui et al. describe the methods of using SPH to model the behaviour of soil using the Mohr-Coloumb failure criterion in 2006. The model simulates dry sand collapse and soil erosion via a water jet. The treatment of frictional boundary conditions is discussed in detail within their work. The SPH model was validated through numerical analysis of dry soil collapse tests and erosion processes providing stable results. It was determined that SPH is an advanced soil modeling method with advantages including a simplified concept, the ease of incorporating physical characteristics, the ability to simulate large deformations during soil collapse, and most importantly the robustness of the model [54]. Bui et al. continues to extend his work to include the pore water seepage in 2007. The model, represented within Figure 2-15, provided evidence that SPH is capable of representing gross discontinuities of soil failure. [55]

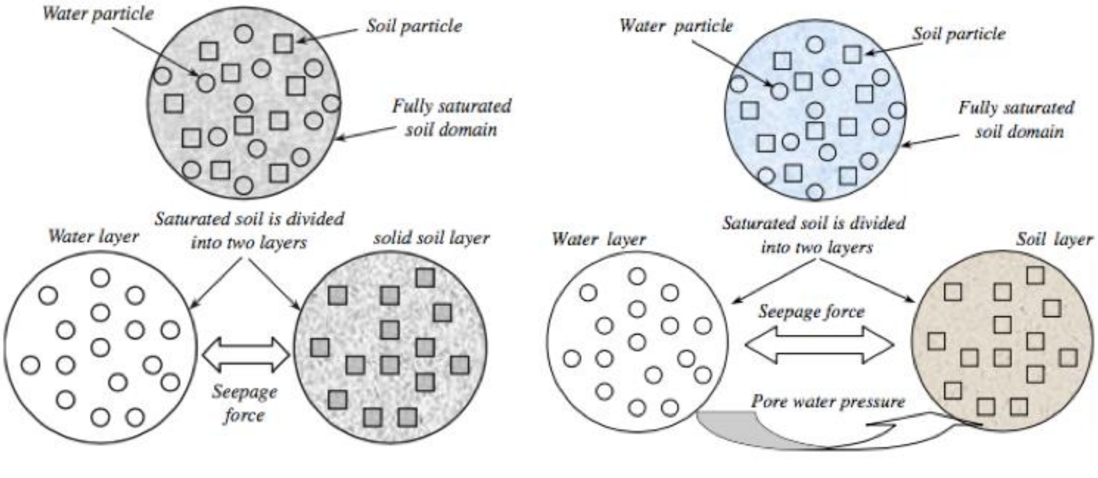

Figure 2-15: Saturated SPH Soil Schematics with Seepage Force (Left, [54]) and Pore Water Pressure (Right, [55])

In 2008 Bui et al. adapted his previous work in SPH soil modeling for geotechnical engineering to investigate the interaction between solid structures and soil. It was determined that the failure discontinuities of geometrical is well represented using SPH modeling techniques. [56]

In 2008 Bui et al. also influenced an artificial stress method to deteriorate the unsteadiness of the SPH soil cohesion. It was determined that the SPH particles repel another when under compression and attract to another during stretching. When under tension, SPH particles may illustrate some clumping. Using the Druker-Prager model for elastic plastic and cohesive soils, SPH may be used and that the soil instability may be overcome through different means such as the artificial stress method. The results were comparable to FEM results and proved that SPH may be used to solve geothermal problems. [57]

Bui et al., in 2011, evaluated the use of SPH to determine the stability of a slope and simulate the soil's post-failure behaviour as a means of overcoming the limitations of FEM modeling. The results were comparable to previously used techniques but proved advantageous for reasons previously stated. This works proposed new SPH formulations in regard to soil to account for the pore water pressure [58]. This new SPH formulation was then re-instated into the modeling of dry and saturated soils by Bui et al. in 2012; the new method recommended is more accurate and saves on computational time [59].

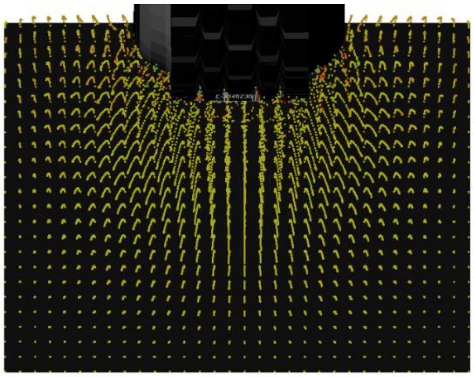

Figure 2-16: SPH Soil Deformation under a Tire [60]

In 2013 Dhillion used two tire models; a three-groove highway truck tire and an off-road RHD truck tire to investigate clayey soil created using the traditional FEA techniques and the newer mesh-less SPH method. The SPH soil model is illustrated in Figure 2-16. These FEA and SPH models were validated through previously determined methods; the pressure-sinkage and shear strength simulation tests. The rolling resistance trends for both soil models followed published trends with the SPH qualitatively yielding results closest to the experimental data. It was also noticed that the SPH soil model produced higher deflection and high rolling resistance coefficient compared to its FEA counterpart. [60]

2.3.4 Hybrid Soil Modeling

Hybrid soil modeling are compositions of FEA elements and SPH particles, tied by links and contacts to create a full soil model. The composition of the FEA/SPH models varies with the intended application. The use of hybrid models to represent a soil model is a fairly new concept.

Groenenboom, in 1997, used PAM-SHOCK and tied links to connect FEA and SPH particles to model 2D and 3D hypervelocity impacts [48]. In 2010, he used another combination of FEA and SPH modeling to represent hydrodynamics and fluid structure interactions [61].

In 2010 Lescoe first captured the computational time difference between FEA and SPH soil models. The SPH soil model was created through conversion of the FEA elements to SPH particles. The rolling resistance was tested on both FEA and SPH soil models using a rigid and pneumatic tire model. It was discovered that the SPH soil model produced an increased rolling resistance coefficient compared to the FEA soil model. The viability of SPH used to simulate soil in place or integrated with FEA soil models to capture the deformation of soil was discussed. It was even determined that the SPH part and particle density parameters had no large influence on the rolling resistance coefficient. It was determined that the SPH particle depth had the largest influence and that the SPH soil model behaved more like clay during initial shearing and more like a dry sand in relation to an increase in loading having a direct relation to shear. Figure 2-17 illustrates the soil deformation under a tire with hybrid and full FEA soil models. [62]

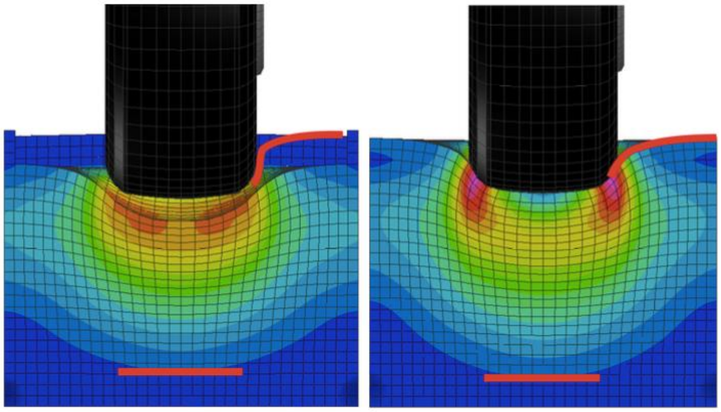

Figure 2-17: Soil Deformation of FEA/SPH (Left) and Full FEA (Right) Soil Models [62]

Marjani investigated different soil modeling techniques in 2016, specifically FEA, SPH and the combination of ½ and ¼ SPH/FEA hybrid soil models. The approach included the FEA analysis of creating a 3D Michelin XONE Line Energy T wide base FEA truck tire model and studying the rolling resistance of the tire on a hard surface. Examples of the FEA wide base tire model rolling on the varying soil models is observed within Figure 2-18. The Micheline tire was modeled in PAM-CRASH and validated through a series of virtual tests; the vertical stiffness test and static footprint, and the dynamic drum-cleat test, measuring the tires mode of vibration. Marjani's results were then compared to published data provided by Michelin supporting the validity of the tire with the vertical stiffness yielding a 5% error and the static footprint length measuring less than a 4mm difference. Further validation was approached through the analysis between virtual rolling resistance test on a hard surface to field test measurements taken with Volvo Trucks Inc. at North Carolina. Dry Sand was then modeled, as mentioned through various mediums and validated with pressure-sinkage and shear box simulations. The same soil models were then tested with accuracy to measured rolling resistance tests and computational time. It was determined that the ¼ SPH/FEA model decreasing CPU time by up to 50% and qualitatively measured the best accuracy with a 5.3% error. More detail will be discussed on these SPH Dry Sand soil models within CHAPTER 3, as this is the soil models used within the study of this thesis to predict the RHD parameters. [63]

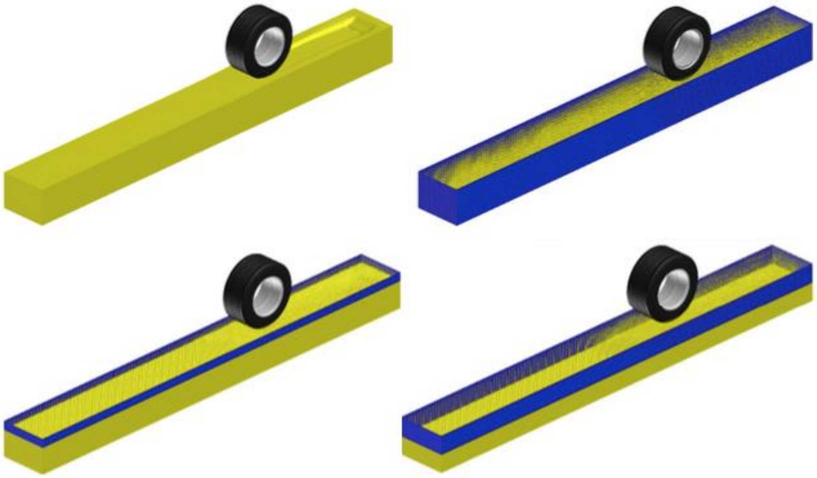

Figure 2-18: Full FEA, Full SPH, 1/4 SPH/FEA, and 1/2 SPH/FEA Soil Models [63]

2.4 Chapter Summary

In this chapter, the background required to understand the concepts presented within the following chapters of this work has been provided.

The drum-cleat test is a commonly accepted dynamic test used to authenticate the FEA tire modeling; the average mode frequency is determined to occur within a range of 80-90 Hz and the longitudinal first mode of vibration occurs within the range of 30-60 Hz according to previously published findings, the majority of which were surveying passenger car tires.

With the advancement of computers enabling the progression of advanced 3D FEA tire modeling, the analytical rigid-ring model parameters are often populated with a series of virtual simulation tests to save on time while providing authentic tire characteristic predictions. The present state of the art considering off-road rigid-ring modeling techniques may be summarized as follows;

- Chae (2006) developed the out-of-plane rigid-ring model using to predict the new parameters of a three-groove truck tire on a rigid road. The tire's operating conditions include a single inflation pressure of 0.759 MPa and three applied tire loadings; 13.3 kN (3000 lbs.), 26.7 kN (6000 lbs.), and 40.0 kN (9000 lbs.).

Selected predicted in-plane and out-of-plane parameters were compared to physical data measurements.

- Slade (2009) developed the off-road rigid-ring tire model (in-plane and out-of-plane parameters) to account for soil parameters. These parameters were then predicted for an RHD (PSU 09) truck tire on FEA soil model representing a sandy loam. The tire’s operating conditions were static at 85 psi and 18.9 kN (4250 lbs.). Determined trends illustrate that the tire’s rolling resistance is greater on soil than on a hard surface. The longitudinal slip stiffness and tractive forces were four times lower on soil than that measured on a hard surface. More importantly, a bulldozing phenomenon is observed.
- Reid (2015) predicted the in-plane and out-of-plane rigid-ring parameters of a wide base truck tire on a hard surface. The operating tire conditions were dynamic, changing the applied loading and inflation pressure each three times; at, above, and below manufactured recommended operating conditions. It was concluded that the majority of the rigid-ring parameters, excluding some outlying damping constants, have direct and linear relations with respect to the applied loading and inflation pressure of the tire.

Several analytical tire models have been developed to predict the in-plane and out-of-plane characteristics of tires on different road surfaces such as a hard surface and soft soils. However, there are distinct research gaps within the state of the art. There has not been an analysis on the prediction of the off-road rigid-ring parameters with the inclusion of varying the tire’s operating conditions, specifically the applied tire loading and inflation pressure. Furthermore, there has been no attempt to make such predictions on neither a specific dry sand soil model nor the SPH soil modeling technique; thus far all studied off-road parameters on soil have used the FEA soil modeling technique. As discussed, the modeling of soils has substantially progressed from FEA elements to SPH particle modeling techniques to improve the soil characteristics in the interest of providing more accurate results.

Therefore, the contributions of this work(s) includes the following;

- Investigation of SPH soil (Dry Sand) modeling techniques and the corresponding interaction with an FEA truck tire.
- Prediction of the off-road rigid-ring model parameters specifically for an RHD (UOIT 2017) truck tire on a SPH soft soil (Dry Sand) model.
- Determine influence of varying both the applied tire loading and inflation pressure on the off-road or soil interactions.

CHAPTER 3

DEVELOPMENT AND VALIDATION OF THE FEA RHD TRUCK TIRE AND SPH DRY SAND MODELS

3.1 Chapter Introduction

In this chapter, the development of the RHD truck tire and SPH soft soil (Dry Sand) models used for the study of this work are reviewed in detail. The RHD 315/80R22.5 was originally composed by Jeff Slade in 2009 [17] and the SPH soft soil (Dry Sand) parameters were developed and validated by Mehrssa Marjani [63] in 2016. The objective of this thesis is to predict the off-road rigid-ring parameters for the U.O.I.T Regional Haul Drive (RHD) truck tire on the SPH soft soil (Dry Sand) model developed by Marjani. .

3.2 RHD Tire Modeling

Originally a three-groove FEA truck tire was developed in 2005 by Chae within his materials thesis [16] . It is this specific tire that was further modified by Slade in 2009 to become an off-road Regional Haul Drive (RHD) 315/80R22.5 Goodyear truck tire [17]. The FEA tire model is rather detailed, including multiple layered membranes, materials, and Mooney-Rivlin elements. [17].

Slade took a single section cut piece of Chae's three-groove tire and modified the tread to make the transformation into the RHD tire. The RHD tread is asymmetric in nature with the objective of preventing stones and debris from sticking into the tread. Although highly effective in practical use, in the interests of containing a reasonable simulation time while maintaining design fundamentals. The complex geometry is simplified such that any possible curves were made straight. This means that the lugs were simplified to rectangular shapes and that the grooves between the lugs became basic "V" or triangular shapes; the important thing is that the tread groove depth is maintained at 27mm as per Goodyear's technical data specifications. The tread is comprised of solid tetrahedron (TET4) elements and Mooney-Rivlin material properties. The tread is pictured within Figure 3-1 and is followed by illustrations of a section cut of the RHD tire, Figure 3-2. [17]

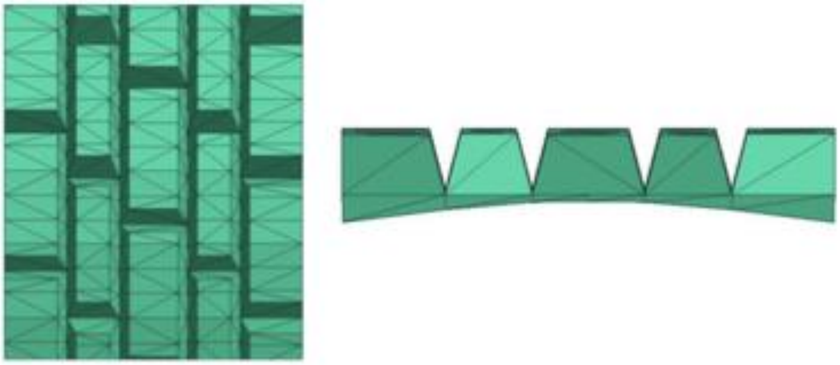

Figure 3-1: RHD Tread [17]

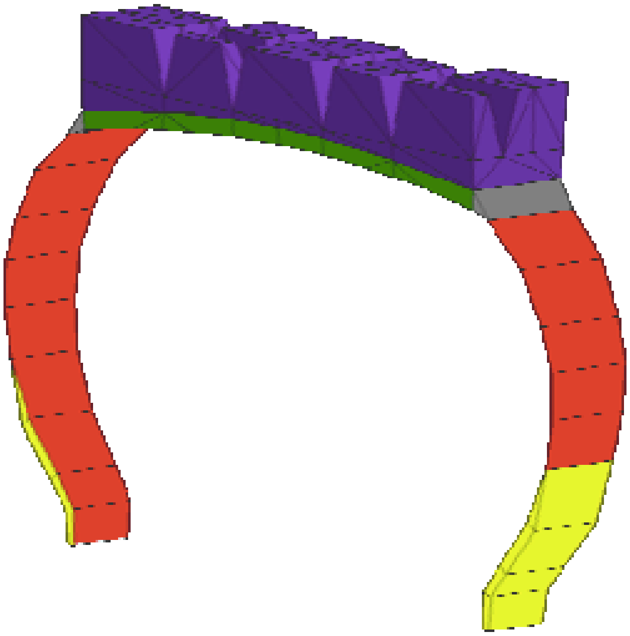

Figure 3-2: RHD Section Cut [17]

The tire was created in PANTRAN by building exactly half of a 3D cross section in detail, node by node. This cross section is then rotated about the axis of the tire in increments separated by six degrees to create a completely round tire with a total of 60 cross sectional pieces fused together. The tire carcass is comprised of layered membrane elements. The bead fillers, shoulders, tread, and under-tread are represented by Mooney-Rivilin elements. The advantages of using a three layered membrane is the ability to have different material properties and multiple orientations within a single part; Figure 3-3 highlights the layered membrane structural composite. For instance, the tire carcass includes the rubber carcass, the steel belts, and radially oriented steel cords. The tire bead is represented by circular beam elements that have steel properties and a defined cross-sectional area; the bead elements are located at the bottom of the bead fillers. [17]

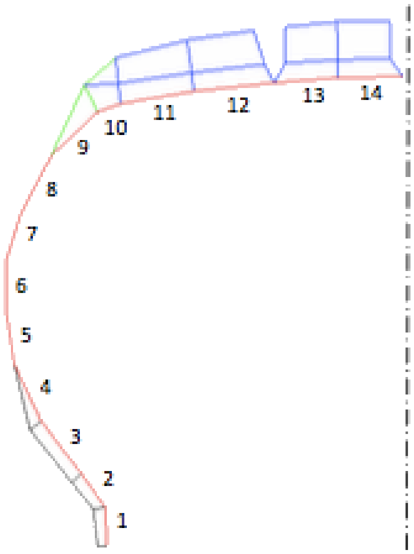

Figure 3-3: Layered Membrane Elements [16]

3.2.1 Final FEA Tire Model

The tire model investigated within this report is the Goodyear RHD 315/80R22.5 drive tire for tractor semi-trailers. The tire model is that as described by Slade, but with some minor modifications completed by the author with the interest of improvement, specifically within the beading of the tire. The tire model is designed to match manufacturer's specifications as shown in Figure 3-4 and Table 3-1: RHD Tire Specifications

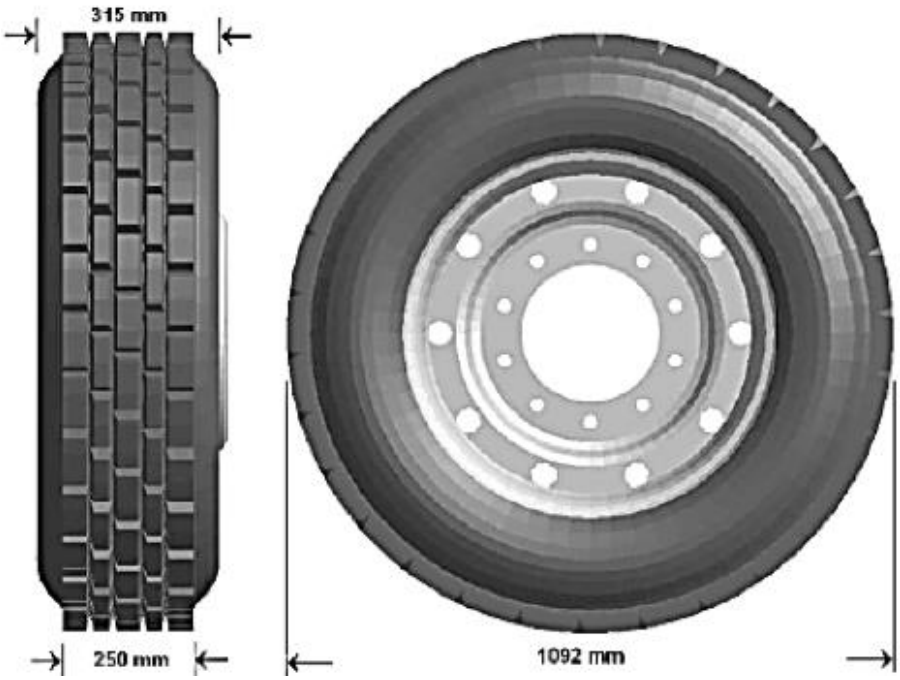

Figure 3-4: RHD FEA Tire Model [17]

Table 3-1: RHD Tire Specifications [17]

Tread Depth	27 mm
Rim Width	229 mm
Rim Weight (m_a)	34.8 kg
Tire Weight	72 kg
Total Tire Weight	106.8 kg
Mass of Belt (m_b)	43.4406 kg
Overall Width	315 mm
Overall Diameter	1092 mm
Static Loaded Radius	505 mm
FSpeed Rating	120 km/h
Single Inflation	8.5 bar
Dual Max Load	3350 kg
Max Dual Inflation Pressure	8.5 bar

3.2.2 Tire Validation

The purpose of calibrating the tire is to achieve an appropriate tire response from the FEA virtual tire model that closely matches its simulation results to that of measurements and/or published data. The calibration of the tire involves two simple tests; a static and dynamic tests. The static test includes the vertical stiffness test, and the dynamic test consists of the drum-cleat test.

The vertical stiffness test is applied to tune the tire to match the given load-deflection curves. The simulation test involves constraining the tire in all directions, with the only exception being the vertical direction, or z-axis. After the tire is settled onto a rigid road, a ramp load is applied to the tire, causing the tire deformation. Through this deformation the load-deflection curves are observed, Figure 3-5 and Figure 3-6.

Slade's RHD tire was developed to tune the following parameters; the sidewall thickness (h), the modulus of elasticity (E) of the sidewall and under-tread, the Mooney-Rivlin coefficients of the rubber compounds of the tread and under-tread [17]. Figure 3-5 illustrates the accuracy of Slade's RHD tire in comparison to provided curves for a generic Goodyear 315/80R22.5 truck tire under different inflation pressures.

The RHD tire used within this thesis has slight modifications, specifically towards the beading of the tire. The static vertical test is repeated with the U.O.I.T 2017 version of the RHD tire. Results for the new RHD tire model are presented within Figure 3-6 and compared within Table 3-2 to the approximations of the slope of other tire models presented within Figure 3-5. The new RHD tire model is comparable to the data provided by Slade and Goodyear, with a 3% difference to the vertical stiffness at 85 psi and a 4.3 % difference at 110 psi.

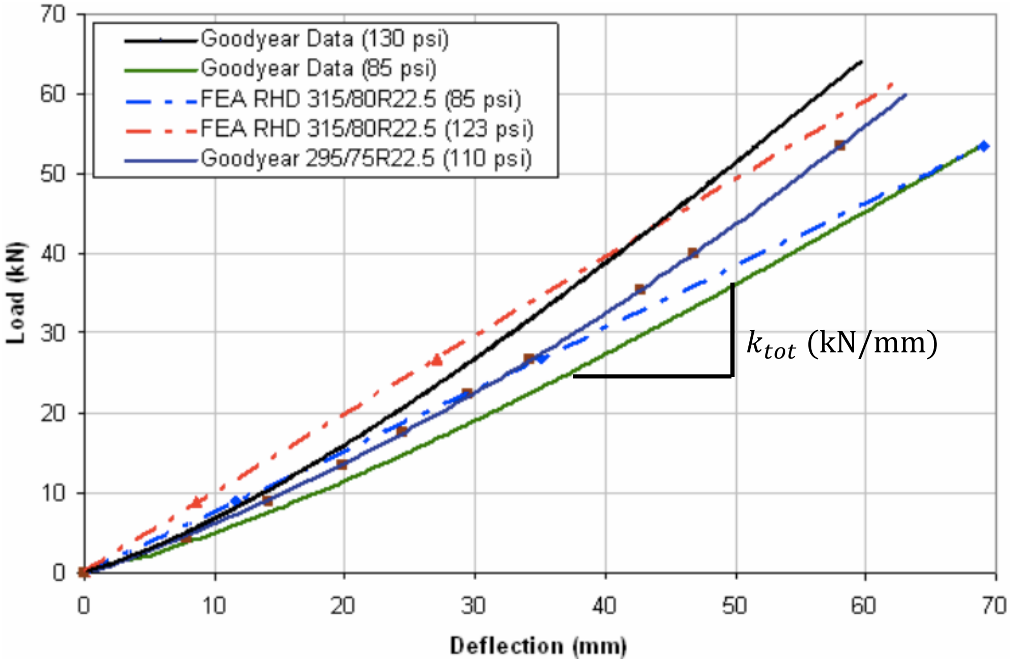

Figure 3-5: Load Deflection Curves for the Pen-State 2009 RHD Tire Compared to Other Models [17]

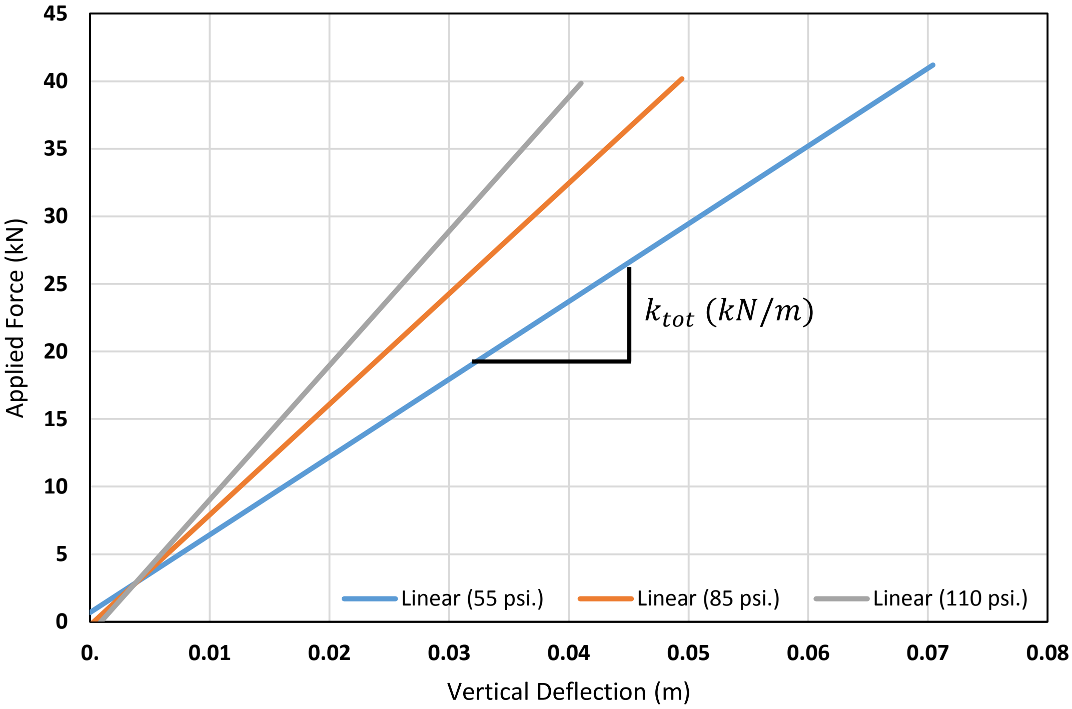

Figure 3-6: Load Deflection Curves for the U.O.I.T 2017 RHD Tire

Table 3-2: Comparison of Static Vertical Deflection of the U.O.I.T 2017 RHD Tire to Other Models

Parameter	55 PSI	85 PSI	110 PSI	123 PSI	130 PSI	Units
U.O.I.T 2017 RHD	575.45	817.91	993.65			kN/m
PSU 2009 RHD		794		1000		
Goodyear RHD		794	952		1085	

The final test to validate the tire is the dynamic drum-cleat test, which includes the investigation of important dynamic properties, being the tire's vertical and horizontal first modes of vibration. Once a tire is mounted onto a rim it become classified as a mass-spring damper system. The stiffness of this system is dependent on the on the sidewall stiffness, which is influenced by the applied loading, inflation pressure, and the material properties of the tire. This means that the tread is able to resonate vertically and horizontally, creating modes of vibration. The frequency at which these modes of vibration occur vary depending on the tire's internal damping.

The drum-cleat test is comprised of a fixed circular drum with a cleat designed to excite or vibrate the tire. The drum-cleat testing procedure will be described in further detail within CHAPTER 4. Figure 3-7 illustrates the mode analysis of Pen-State's (PSU) 2004 RHD tire model. It is observed that the first mode of vibration occurs at 45Hz, as represented by the second peak. The third peak illustrates the first vertical mode of vibration at 53Hz. The second horizontal mode occurs at 67Hz.

The U.O.I.T 2017 RHD tire model undergoes an extensive mode analysis, as to be discussed within CHAPTER 4. It is observed that the changes to the tire model shifts the location of the nodal frequency, to a higher frequency range, within Figure 3-8. The vertical first mode of vibration of the RHD tire now occurs within the frequency range of 46-57 Hz.

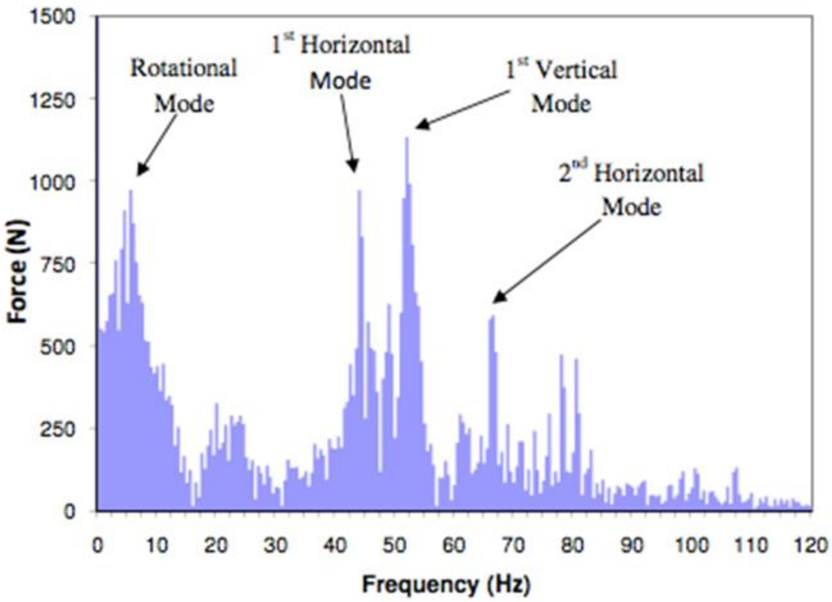

Figure 3-7: RHD Tire's Free Mode of Vibration at 18.9 kN (4,4250 lbs) and 85 psi. [17]

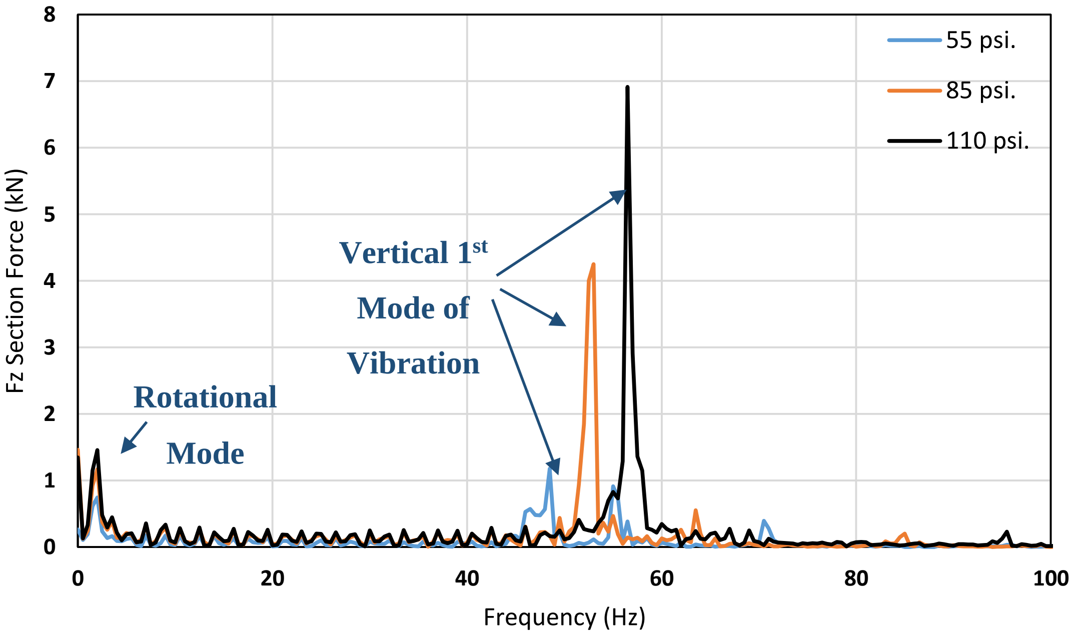

Figure 3-8: RHD (U.O.I.T 2017) Vertical First Mode of Vibration at 26.69 kN (6,000 lbs.) and Varying Inflation Pressures

3.3 Dry Sand SPH Soft Soil Modeling

The purpose of this section is to review the modeling and validation of the Dry Sand SPH soft soil that is to be the focus of this thesis. The soil model(s) were created and validated by Mehrsa Marjani in her 2016 M.A.S.c thesis and ASME (American Society of Mechanical Engineers) paper [63] [64]. An FEA analysis was used to create and validate a virtual 3D Michelin XONE Line Energy T wide base truck tire within PAM-CRASH. The tire was validated through a series of virtual tests compared to published data (i.e. the tire's manufactured specifications made public). The virtual stiffness test came within a 5% error, and the static footprint test produced less than a 4mm difference to the measured data. The tire's validation was further strengthened by the virtual rolling resistance tests on a hard surface proved to be comparable to field measurements taken with Volvo in North Carolina using wheel transducers. These virtual and physical tests were also repeated and completed on the Dry Sand soft soil with a small percentage of error between the measurements and simulation results. [63]

The Dry Sand SPH soil model was modeled and validated as one of various soil model mediums; FEA, SPH, ½, and ¼ SPH/FEA hybrid soil models. However, this section will begin on discussing in depth the creation of the SPH soil model, as it is within the direct interest of this thesis of study. The soil model properties used were provided by Wong's Theory of Ground Vehicles and are presented within Table 3-3 [1]. The soil was calibrated and validated though the use of two simulation tests; the pressure-sinkage and shear strength procedures. [63]

Table 3-3: Empirical Properties of Dry Sand as Provided by Wong [1]

Soil	Moisture	n	k_c	k_Φ	c	Φ
Dry Sand	%	Constant	kN/m^{n+1}	kN/m^{n+2}	kPa	deg.
	0	1.1	0.99	1528.43	1.04	28

3.3.1 Pressure-Sinkage Relationship

Bekker's pressure sinkage relationship was used by Marjani to determine the pressure distribution at the contact patch of the tire [63]. Bekker's equation, Equation 3-1, illustrates the soil's reaction to the nominal load of the tire, represented by an applied

300mm diameter plate. The calculated values are compared to simulated results within Figure 3-10 and are deemed acceptable to announce the virtual FEA soil model as acceptable. The soil is constrained by a fixed 800x600 mm box with six different loading pressures between 0-200kPa applied to the loading of the plate; the procedure is illustrated within Figure 3-9.

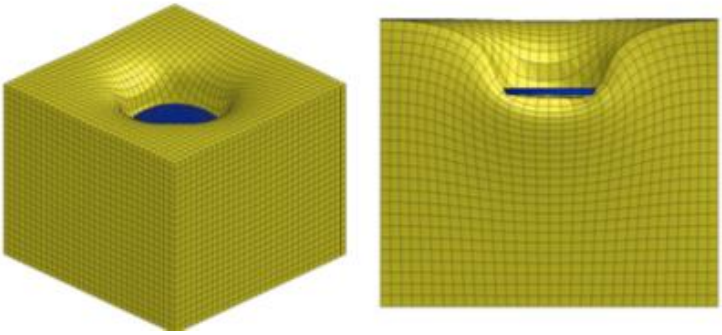

Figure 3-9: FEA Dry Sand Pressure-Sinkage Model [63]

Bekker's equations, Equation 3-1 [28];

$$p = \left(\frac{k_\varphi}{b} + k_\phi\right) z^n \tag{3-1}$$

Where, k_φ and k_ϕ and n are pressure sinkage parameters,

p is the applied loading on the plate,

b is the radius if the loading plate and,

z is the sinkage of the soil (mm).

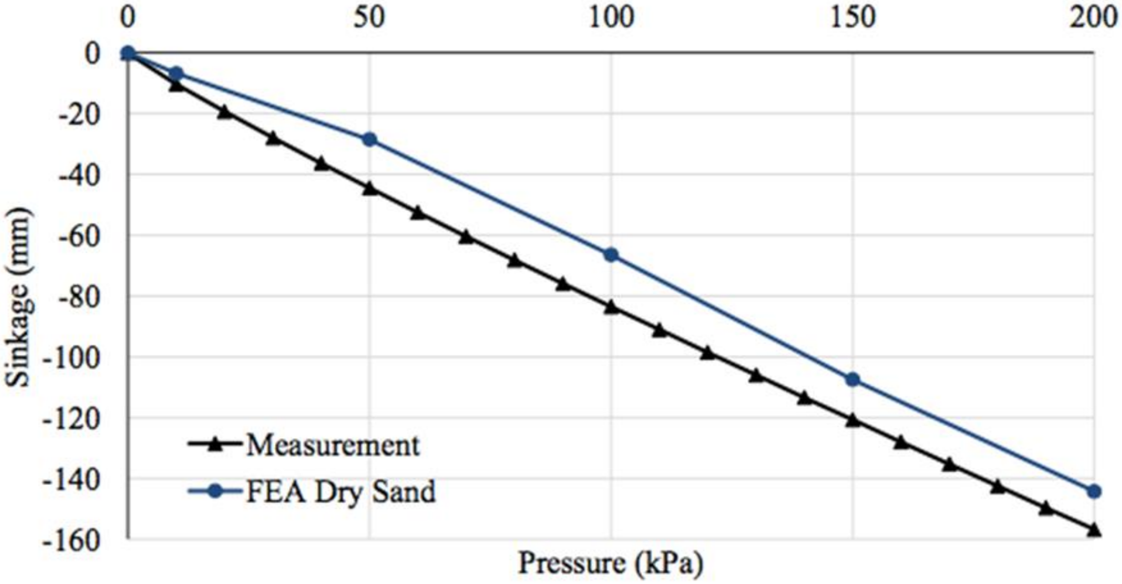

Figure 3-10: FEA Dry Sand Pressure-Sinkage Relationship [63]

The FEA soil originally created was comprised of a 25mm mesh size. The trend for both the simulated and calculated pressure-relationships of the FEA Dry Sand were comparable, as observed within Figure 3-10. However, a sponge effect is observed. This is explained by the connection or sharing nodes between neighboring elements. Therefore, from the FEA elements a collection of SPH (Smoothed Particle Hydrodynamics) is created with the use of PAM-MESH, complete with a particle separation distance of 25mm (centre-to-centre); Figure 3-11 illustrates the creation of SPH particles from FEA elements. [63]

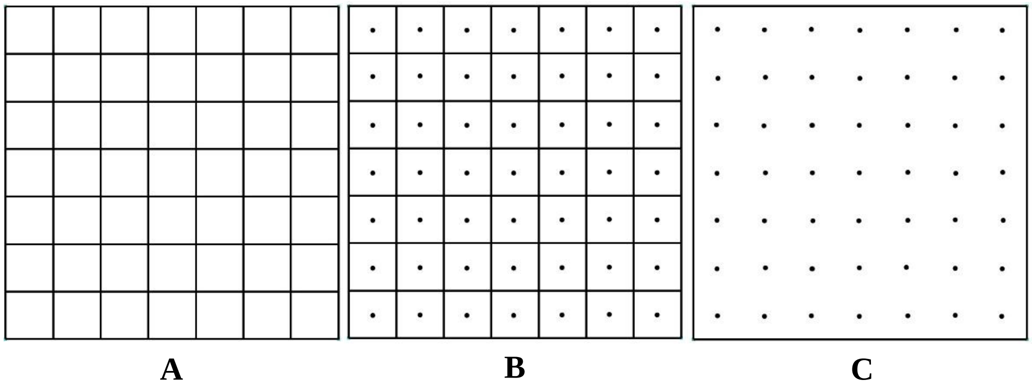

Figure 3-11: Mapping (b) from FEA (a) to SPH Soil Particles (c)

The material properties as described by Wong are the same as defined for the FEA model, though further specifications are required to complete the SPH model. The material is classified as hydrodynamic elastic plastic, complete with an equation of state, as defined within Equation 3-2. [63]

$$p = C_o + C_1 u + C_2 u^2 + C_3 u^3 + [C_4 + C_5 u + C_6 u^2] E_i \tag{3-2}$$

Where $u = \left(\frac{p}{p_o}\right) - 1$,

p is the material density,

p_o is the initial material density,

C_i is the material constant,

E_i is the internal energy and,

C_1 is the bulk modulus.

Other defining parameters, as specified by the program PAM-SHOCK include the minimum and maximum smoothing length, to be 1 and 100 respectively, and the particle density ratio is defined to be 1.21-2.1. [63]

The SPH soil pressure-sinkage relationship is observed to be in good relation with respect to the calculated data using Bekker's equation as illustrated within Figure 3-13. The key difference between the SPH and FEA results is that the SPH proves to have a more accurate and honest representation of soil characteristics when regarding penetration of the soil. Figure 3-12 highlights the pressure-sinkage procedure of the SPH soft soil (Dry Sand).

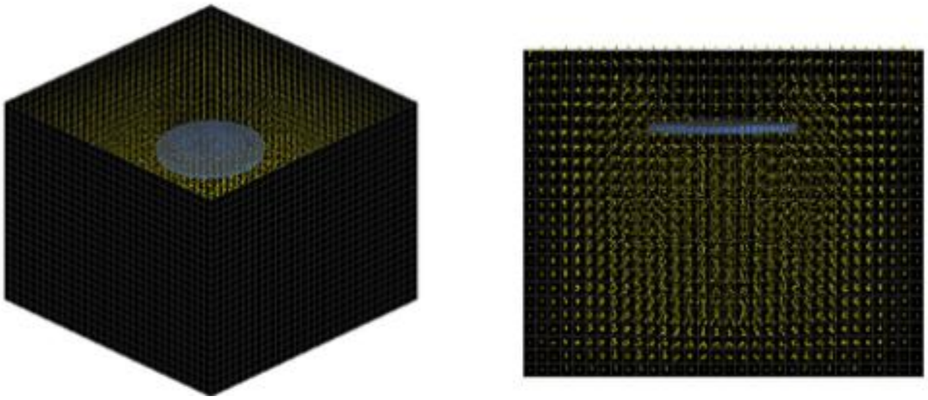

Figure 3-12: SPH Dry Sand Pressure-Sinkage Soil Model [63]

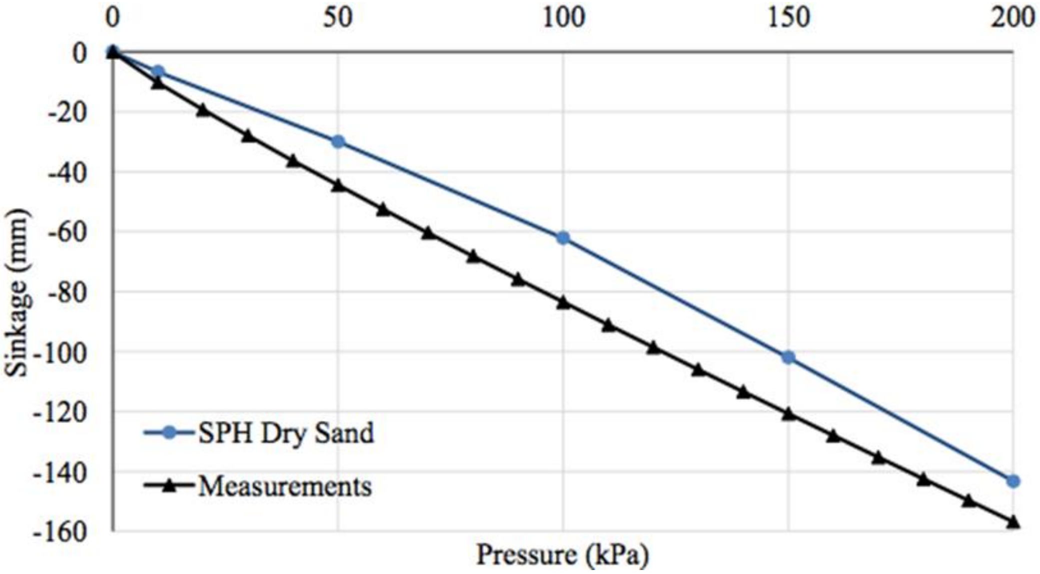

Figure 3-13: SPH Dry Sand Pressure-Sinkage Relationship [63]

3.3.2 Shear Strength

The second virtual test to complete the validation process is called the shear strength, or shear box test. The purpose of this test, as per the name suggests, is to analyze the shear stress and displacement of the soil. These are important characteristics to determine because the soil shear layer is responsible for the tire to incur longitudinal slip, ultimately reducing traction. The maximum shear strength may be determined using the Equation 3-3 for the Mohr-Coulomb failure criterion;

$$\tau_{max} = c + p.\tan\varphi \qquad 3\text{-}3$$

Where, φ is the soil internal friction angle and,

c is the soil cohesion.

The virtual shear box environment consists of two boxes; the bottom box has a solid bottom; the top box is open to the bottom box with a loading plate as a lid. The boxes are filled with the SPH soil and each box section is pulled horizontally at a fixed displacement of 70 mm in 80 sec. The shear box sectional area is 0.15m^2 with an applied loading varying between 10-200 kPa. The shear box soft soil simulation is depicted within Figure 3-14. In conclusion, the dry sand was calibrated through qualitative analysis between the simulated and known dry sand properties. The simulated and calculated results are acceptably comparable and presented within Table 3-4 and Figure 3-15.

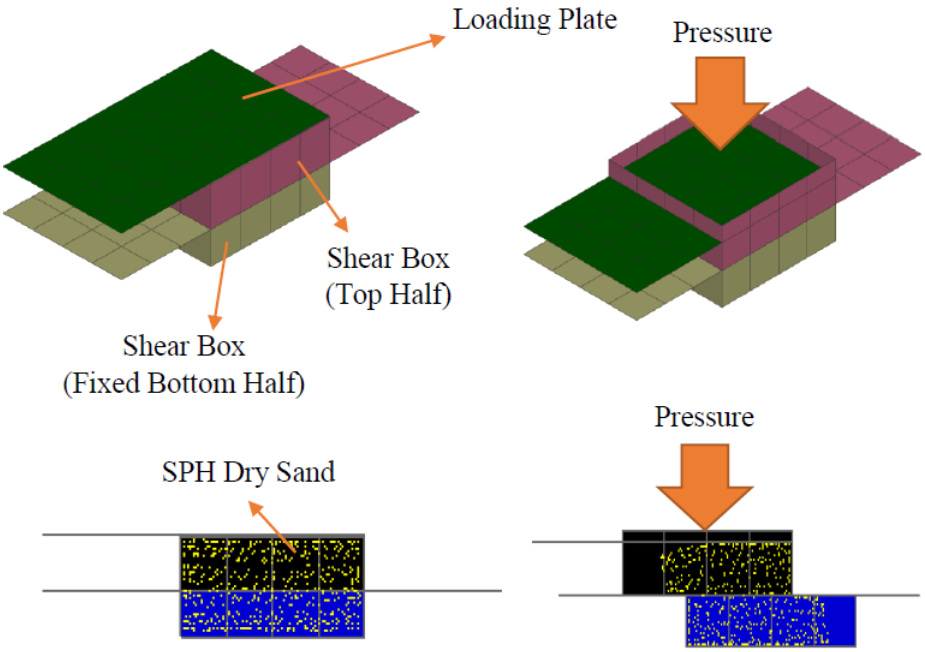

Figure 3-14: Dry Sand Shear Box Simulation [63]

Table 3-4: Shear Strength Parameters [63]

Soil Shear Strength	*c*	*n*
Dry Sand Simulation	5.516	24.8
Dry Sand Measurement	1.04	28

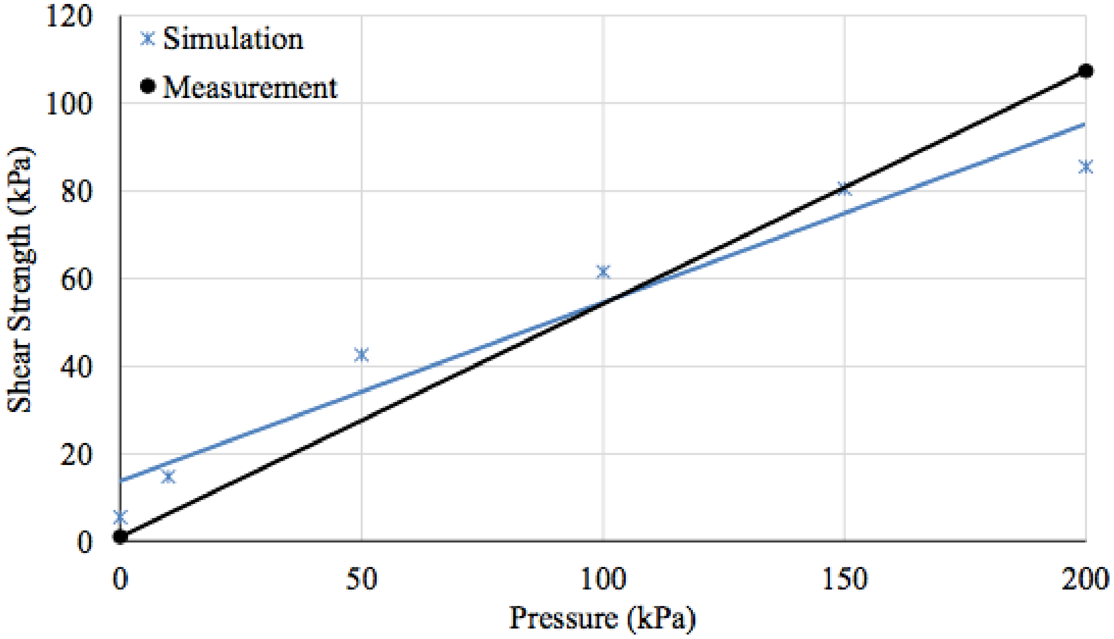

Figure 3-15: SPH Shear Strength Simulation and Measurement Results [63]

3.4 Chapter Summary

This chapter presented the details of the modeling and validation of the two main components at the centre of this thesis; the U.O.I.T RHD 315/80R22.5 truck tire and the SPH soft soil (Dry Sand) model. CHAPTER 5 and CHAPTER 6 employ the analysis of the U.O.I.T RHD tire on the full SPH (Dry Sand) soil model to predict the in-plane and out-of-plane parameters.

CHAPTER 4

DRUM-CLEAT SENSITIVITY ANALYSIS

4.1 Chapter Introduction

This chapter is a direct adaptation of the authors SAE paper, please see PUBLICATIONS. The purpose of this chapter is to determine the effect of tire operating conditions, such as the tire inflation pressure, speed, and loading on the change of the first mode of vibration. The two rationales for this is to;

1) Further validate the FEA tire model by comparing the predicted resulting trends to those previously discussed as known published conclusions within the literature review.
2) Determine the sensitivity of the first mode of vibration with respect to varying the tire's operating conditions due to its heavy influences on the rigid-ring model parameters.

The first mode of vibration, also referred to as a resonant frequency, is the frequency at which the tire system vibrates yielding a peak in amplitude, or the frequency at which vibration is experienced. There are several identifiable modes for a pneumatic tire; the first mode of vibration is the focus for this chapter, which is instigated only by a vertical motion of the tread without deformation. Hence, the tire is easily excited by road irregularities at the proper frequency. Tires are the first point of contact between the vehicle and the ground, thus any forces experienced at the tread due to this harmonic are transferred to the rim, through the suspension, and finally to the chassis where occupants will experience the effects of road irregularities. [4]

Each mode of vibration creates a distinctive shape transformation of the tire. The first modes of a tire is formed by the translational or rotational movement of the ring as a rigid structure. It may be surmised that the first harmonics are influencing factors for the ride comfort, stability, and handling properties of all types of vehicular models using pneumatic tires.

As Lardner et al. explains, to determine the modes of vibration, an experimental analysis of the forces exerted at the center of the tire spindle is required. The forces are measured in a time domain graph that is translated to a frequency domain graph through the use of a Fast Fourier Transform (FFT). What is important to understand is that the first peak on the frequency domain graph represents the rotational speed, this variable has no effect on the modes of vibration. The amplitudes of the mode of vibration decreases as the higher order of modes increases. This means that traditionally, the second peak on the frequency graph is the first mode of vibration, and the third peak representing the second mode of vibration will have a lower amplitude than the first mode of vibration. For this research, only the tire is considered; hence only the first mode of vibration is expected to be seen. When considering the longitudinal; x-axis, frequency domain graph, a third peak will appear after the first mode of vibration. This peak is not a representation of the second mode, it is a representation of the first mode of vibration in the vertical (z-axis). This means that the third peak will be higher than the second peak; this will become more evident within Figure 4-1. [4]

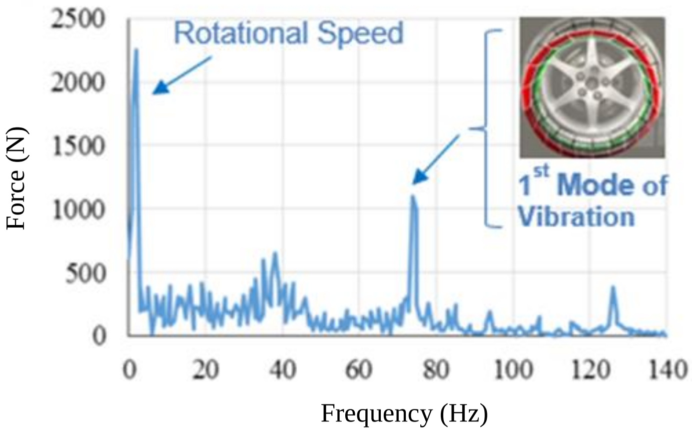

Figure 4-1: Example of First Mode of Vibration Analyzed in the Vertical Direction [4]

The analysis of vibrational dynamics of a tire may be broken down into two categories: out-of-plane, x-axis, and in-plane, z-axis) transmissibility detection because of the differential characteristics of these harmonics [4]. The drum-cleat test is a commonly accepted dynamic test used to authenticate the FEA tire modeling. The average mode frequency is determined to occur within a range of 80-90 Hz and the longitudinal first mode of vibration occurs within the range of 30-60 Hz according to previously published findings, surveying mostly passanger car tires.

4.2 Drum-Cleat Testing Procedure

A cleat impact instrument is a machine that measures a tires vibrational characteristics. A motor rotates a drum allowing the tire to rotate freely. Cleats are fixed to the rotating drum to excite the tire, in a similar manner as an impact hammer may be used to strike the tire instigating a vibrational excitement within the tire. Sensors are used to measure the exciting force and radial direction of the tire. A converter extracts the data in real time and an FFT is applied to determine the natural frequency of the tire. Figure 4-2 and Figure 4-3 are examples of a physical and virtual drum-cleat model set-up, respectively. [4]

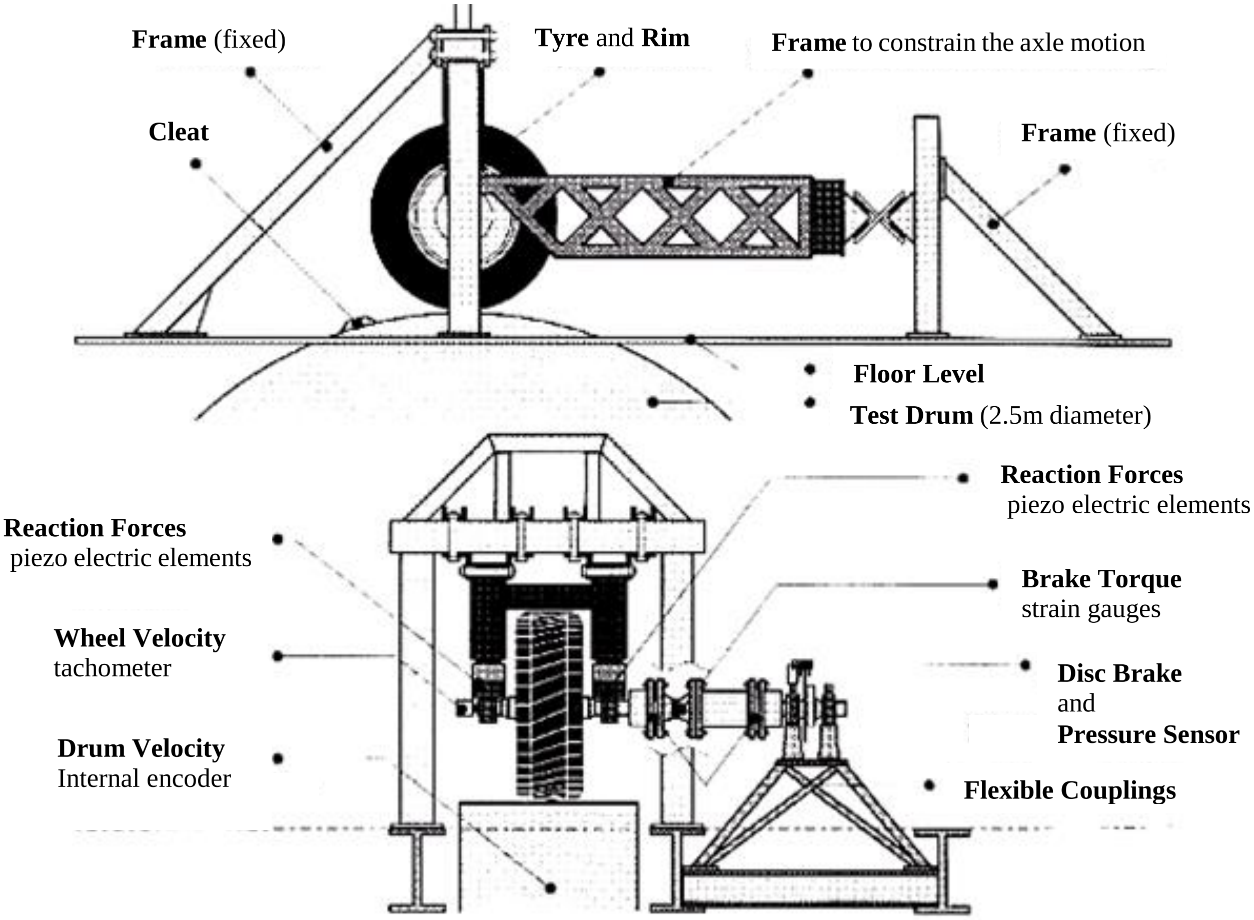

Figure 4-2: Example of Drum-Cleat Physical Testing Procedure [65]

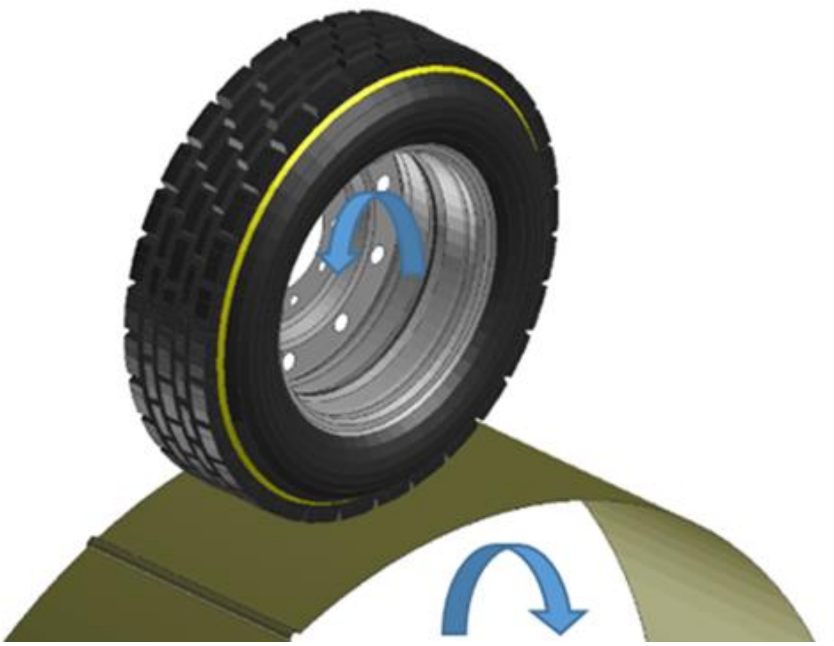

Figure 4-3: Drum-Cleat Testing Procedure

The main principle for this virtual drum-cleat experimentation, as described by Lardner et al., is to replicate a cleat impact instrument via a virtual 2.5m diameter circular drum that acts as an infinite long road. The virtual drum model has a 10 mm diameter cleat, or bump, with the purpose of exciting the tire, specifically the tread and carcass. The impact of the cleat thus causes the tire to vibrate. Through frequency analysis these vibrations determine the first mode of vibration of the tire. [4]

The drum is constrained as a rigid body and is free to rotate about the y-axis. A rotational velocity of 11.11 rad/s, or a linear velocity of 50 km/hr is applied (when constant speed is considered) to the centre spindle of the drum. It is through the rotation of the drum that the tire is rotated, presumably at the same linear velocity as the drum. The tire is fixed in all but the vertical and rotational directions, meaning that only the vertical tread and carcass responses are measured. Initially, the tire is given 0.1 seconds to settle upon the drum surface through the use of an applied sensor. The tire is free to move in only the vertical direction as the conditioning parameters of the inflation pressure and loading are applied. During this settling time, the tire is lowered onto the drum, after which, the tire is constrained as such that the rim is only allowed to rotate about y-axis and the tire is only allowed to move about the vertical direction. The forces exerted on the spindle of the tire are observed and measured in both the longitudinal and vertical directions. These forces are created as a time based data set; the FFT algorithm is then introduced to the time domain data to translate the data to a frequency domain data series. The frequency domain is used to determine and analyze the radial and vertical first modes of vibration(s) of the tire at varying parameters.

4.3 Drum-Cleat Results and Observations

The characteristics varied during the sensitivity analysis include investigating

- The influence of the tire inflation pressure between 55 psi, 85 psi, and 110 psi,
- Varying the linear speed of the tire from 5 to 125 km/h,
- And considering an applied loading between 3.34 kN (750 lbs.) and 40.03 kN (9,000 lbs.).

The dynamic properties of the tire, more specifically the vertical and horizontal modes of vibration, are important characteristics of the tire. The rim mounted tire may be represented as a mass-spring damper system. However, due to the structure of the tire, the majority of the mass is located near the outer edge of the tire, specifically the outer steel plies and tread. Therefore, the stiffness of the tire is controlled by both the sidewall material properties and the inflation pressure. The drum cleat procedure allows for the tread and belt to resonate vertically and horizontally to analyze the frequency at which the modes of vibration occur. These natural frequencies are important because the tire's internal damping has the ability of shifting these frequencies. More importantly, the determination of the frequencies allows for the calculations of the sidewall damping coefficient (α), and the vertical (k_{bz}) and residual (k_{vr}) stiffness of the tire.

The tire is inflated and loaded to the desired parameters and settled onto the drum cleat model. The section force in both the longitudinal (F_x) and vertical (F_z) directions are both measured from the spindle of the tire and the FFT algorithm provided by PAM-CRASH is applied to obtain the first modes of vibration(s) for comparison. Only one parameter is varied at a time with the other parameters maintaining the following conditions; 26.69 kN (6,000 lbs.), 110 psi, 50km/h.

Key assumptions are explained by Lardner and include considering that the rotational speed mode has no effect on the frequency of the first mode of vibration. Suspension and the vehicle chassis is neglected; therefore, only the first mode of vibration will be observed. The tire model was perfectly symmetric with homogenous properties. The tire's enveloping property is negligible; the small parabolic tire deformation caused by the drum cleat has no effect on the results. Furthermore, 3D displacements and forces due to the excitation of the tire are negligible, and the rim is assumed to rotate at the same linear velocity as the tire [4]. The vertical and longitudinal first mode of vibration is examined in Figure 4-4 to Figure 4-8 as the operating conditions are varied.

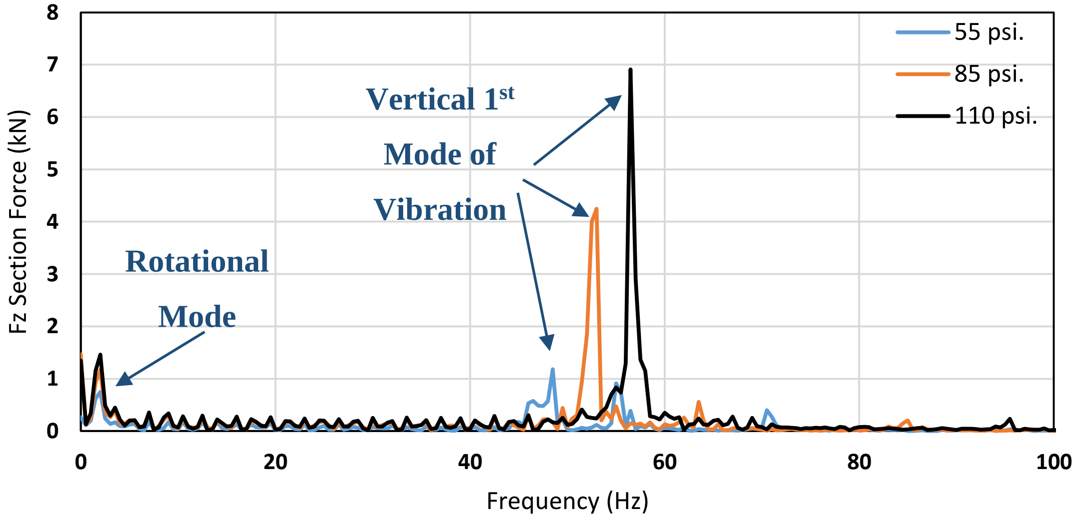

Figure 4-4: Example of the RHD Vertical First Mode of Vibration at 26.69 kN (6,000 lbs.) and Varying Inflation Pressure

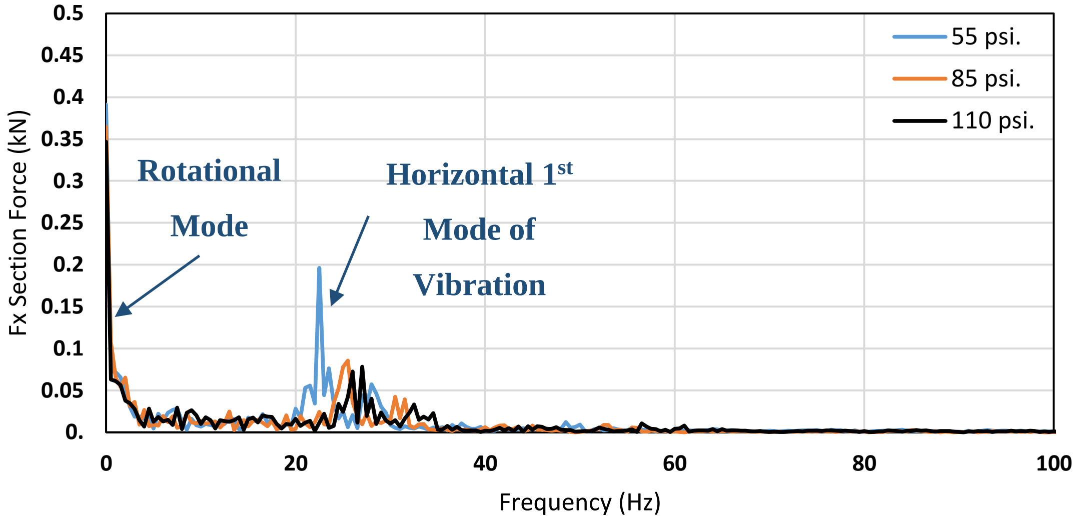

Figure 4-5: Example of the RHD Horizontal First Mode of Vibration at 26.69 kN (6,000 lbs.) and Varying Inflation Pressure

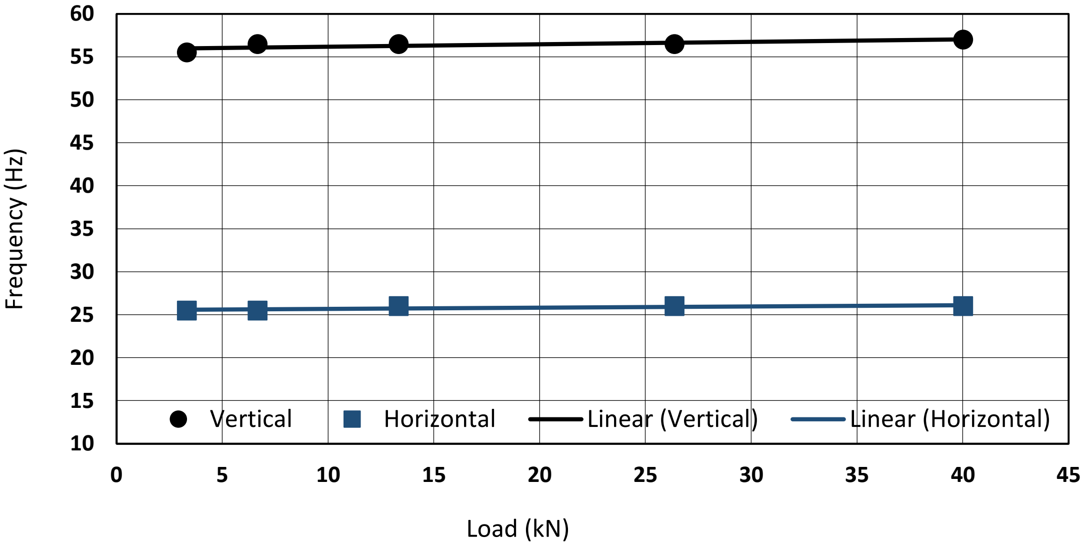

Figure 4-6: Influence of Applied Loading on the Vertical and Longitudinal First Modes of Vibrations

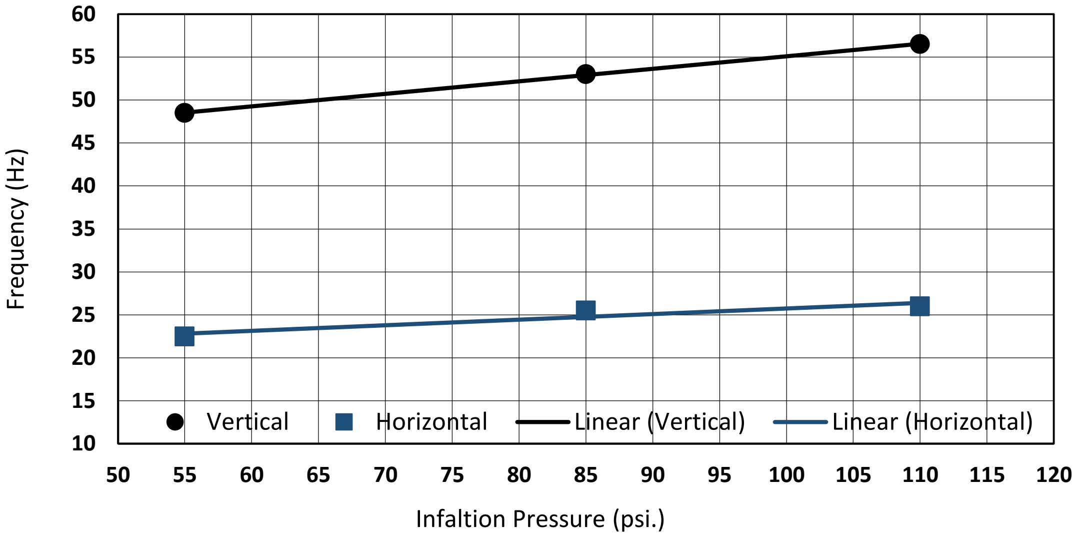

Figure 4-7: Influence of Inflation Pressure on the Vertical and Longitudinal First Modes of Vibrations

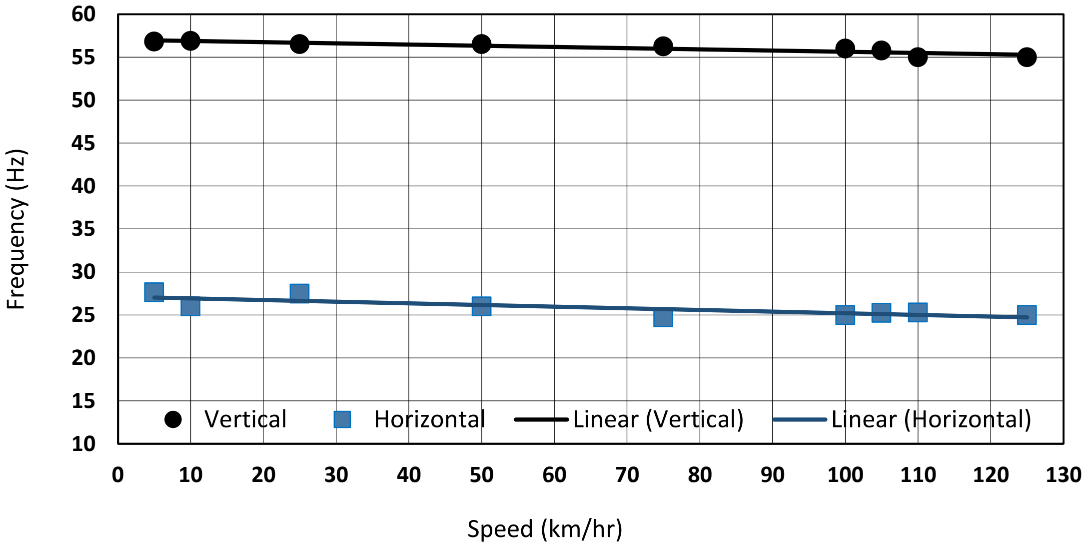

Figure 4-8: Influence of Linear Speed on the Vertical and Longitudinal First Modes of Vibrations

It is observed within Figures Figure 4-6 to Figure 4-8 that the vertical first mode of vibration of the RHD tire occurs within the range of 46-57 Hz and the longitudinal mode of vibration transpires at a lower frequency within the range of 21-26 Hz. These ranges support previous values determined within both the CHAPTER 2. Therefore, the purpose of this experiment to further validate the FEA wide base tire model for future research was a success.

4.4 Determination of the Sidewall Damping Coefficient

The sidewall damping coefficient is a predicted parameter that is introduced back into the FEA tire model, specifically within the sidewall region to obtain a realistic effect simulating the tire's damping effect during the off-road rigid-ring model parameter testing procedures. The mass-proportional sidewall damping coefficient is analytically described by Chang [24] to be determined using Equation 4-1.

$$\alpha = 2 \cdot \xi \cdot \omega = 2 \cdot \xi \cdot (2\pi f) \tag{4-1}$$

Where; ξ = 5 % = 0.05, the critical damping effect is assumed.

Table 4-1 presents the results showing that the first mode frequency is a heavily influential factor for the sidewall damping coefficient. Based on the previously determined influences, the average mode frequency of varying applied loadings was considered for each inflation pressure parameter. This is because the applied loading has a minimal influence on the nodal frequency compared to the effect of the inflation pressure.

Table 4-1: RHD Sidewall Damping Coefficient

Parameter	55 PSI	85 PSI	110 PSI	Units
Proportional Nodal Damping Factor (α)	29.155	32.802	35.564	rad/s

4.5 Chapter Summary

This chapter discussed the vertical and horizontal first mode at varying operating characteristics as a means to further validate the FEA tire model by comparing the virtually simulated results to be in agreement with the trends found in known literature. The most significant factor influencing the mode frequencies is the inflation pressure sharing a directly linear relation. Based on this analysis the proportional sidewall damping coefficient was determined based on the varying nodal frequency with respect to inflation pressure.

More importantly, the tread lines for the varying effects of the inflation pressure, speed, and applied load are confirming with previously determined results through other analytical, physical and virtual modeled methodologies. The observed trends are as follows;

- The vertical first mode of vibration occurs within the range of 46-57 Hz a
- The horizontal first mode of vibration transpires at a lower frequency within the range of 21-26 Hz.
- The applied loading on the spindle of the tire evidently has no significant influence on the first mode of vibration of the tire, however, it may be surmised that the relationship between the two parameters are linear and direct.
- Considering both the vertical and horizontal directions, the first mode of vibration is directly and linearly influenced by the inflation pressure of the tire.
- The linear speed has no obvious influence upon either the vertical or horizontal first modes of vibration of the RHD tire.

CHAPTER 5

DETERMINATION OF THE IN-PLANE OFF-ROAD RIGID-RING MODEL PARAMETERS

5.1 Chapter Introduction

The purpose of this chapter is to predict the in-plane off-road rigid-ring parameters of the RHD tire on dry sand SPH soft soil at varying operation conditions; varying the applied loading and inflation pressures of the tire, below, at, and above the recommended operating conditions. The applied loading is varying from 13.34 kN (3,000 lbs.), 26.69 kN (6,000 lbs.), and 40.03 kN (9,000 lbs.). The inflation pressure will be simulated at 0.379 MPa (55 psi), 0.586 MPa (85 psi), and 0.759 MPa (110 psi).

5.2 List of In-Plane Rigid-Ring Parameters

Although Zegelar and Pacejka's rigid-ring tire model was validated to predict the parameters of a pneumatic tire under most driving conditions, the model has one major disadvantage; it is only valid when the tire is driving over a rigid surface [10]. The in-plane off-road rigid-ring model implemented throughout this work is the same as the one proposed by Slade in 2009 [17].

The in-plane elastic sidewall is represented by both translational and rotational springs and dampers; all sidewall parameters are denoted with the subscript of 'b'. The subscript 'v' denotes parameters associated with the behaviour of the tread. The wheel rim and tread are considered to be rigid parts. The tread is specifically considered to be a rigid band. The tread stiffness and damping is represented as a spring and damper; k_{vr} and c_{vr}, respectively, located between the tread band and the road surface. [17]

The residual vertical stiffness, k_{vr} and damping,c_{vr} are introduced because the singular vertical and translational stiffness of the sidewall, k_{bz} andc_{bz}, are not enough to predict the dynamically complex response of the pneumatic tire. Both the residual vertical stiffness and damping parameters contribute to the motion of the wheel rim. Due to symmetry the vertical,k_{bz} stiffness is considered to be the same as the longitudinal stiffness,k_{bx}. [17]

The use of a rotational spring, $k_{b\theta}$, and damper$c_{b\theta}$, located between the tread band and wheel rim, is used to illustrate the rotational motion of the rigid tread band. The longitudinal slip stiffness,$k_{k,soil}$, is an additional parameter accounting for the additional flexibility of the soil and is presumed to act in series with the vertical residual stiffness of the tire. The longitudinal tread stiffness with respect to the tire is represented by a longitudinal spring,$k_{cx,soil}$, and damper $k_{k,soil}/v_{tr}$, together they represent the longitudinal slip that occurs between the tire and road surface during braking and accelerating. The in-plane rigid-ring model is presented within Figure 5-1 and the parameters are tabulated within Table 5-1.

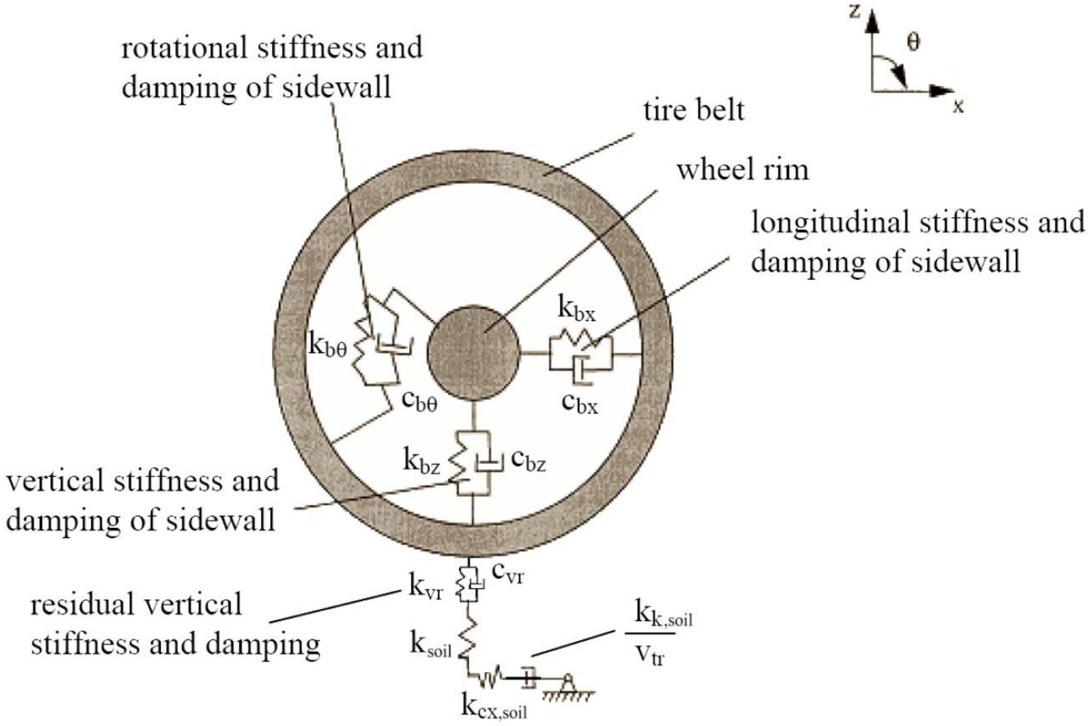

Figure 5-1: In-Plane Off-Road Rigid-Ring Model [17]

Table 5-1: List of In-Plane Off-Road Rigid-Ring Parameters

In – Plane Off-Road Rigid-ring Parameters	Symbol	Units
Total Vertical Stiffness	k_{tot}	kN/m
Sidewall Stiffness	k_{bz}	kN/m
Residual Vertical Stiffness	k_{vr}	kN/m
Vertical Damping Constant	c_{bz}	kN.s/m
Residual Damping Constant	c_{vr}	kN.s/m
Tire Damping Constant	c_{tot}	kN.s/m
Rotational Stiffness	$k_{b\theta}$	kN.m/rad
Rotational Damping Constant	$c_{b\theta}$	kN.m.s/rad
Soil Stiffness, Dry Sand	$k_{Dry\ Sand}$	kN/m
Total Equivalent Vertical Stiffness, Dry Sand	$k_{tot,\mathrm{Dry\ Sand}}$	kN/m
Longitudinal Tread Stiffness, Dry Sand	$k_{cx,\mathrm{Dry\ Sand}}$	kN/m
Longitudinal Tire Stiffness, Dry Sand	$k_{k,\mathrm{Dry\ Sand}}$	kN/unit slip
Longitudinal Tread Damping, Dry Sand	$k_{k,Dry\ Sand/v_{tr}}$	kN.s/m
Effective Contact Patch, Dry Sand	$2_{a,Dry\ Sand}$	m
Effective Rolling Radius, Dry Sand	$R_{e,\mathrm{Dry\ Sand}}$	m

5.3 Total Equivalent Vertical Stiffness, $k_{tot,Hard\ Surface}$

The vertical sidewall and residual stiffness,$k_{tot,Hard\ Surface}$, and soil stiffness are represented as a series of springs. Therefore, the total equivalent vertical stiffness of the soil requires that the total equivalent vertical stiffness on a hard surface, and residual and vertical stiffness be determined.

The total vertical stiffness describes the tire model's ability to resist deformation in the vertical and translational directions from a known applied force. The slope of vertical load deflection curve derives the total equivalent vertical stiffness, as Equation 5-1 describes; a simple load deflection test is applied to the tire to determine this parameter. The load test assumes the spindle of the tire to be only vertically free during loading ensuring a vertical displacement responsible for influencing only the two parameters the sidewall and residual stiffness. The ramped vertical loading is applied to the spindle of the tire after the tire is inflated and allowed a settling time of 0.3 seconds to settle onto the road surface. The virtual procedure is observed in Figure 5-2. A plot of vertical deflection to the applied load is created and the slope of the trends will solve for the total vertical stiffness as seen in Figure 5-3.

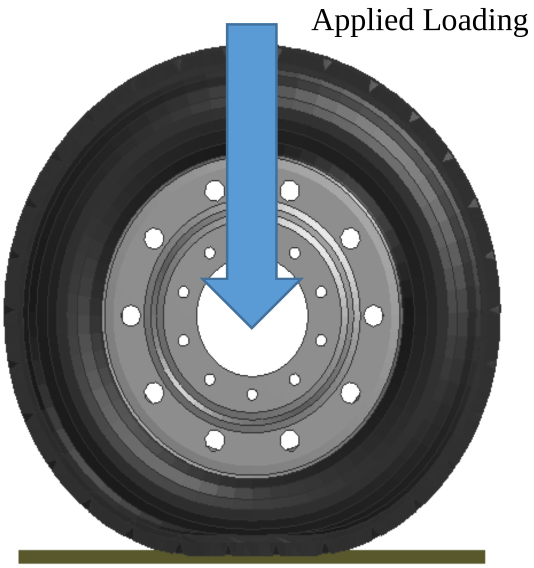

Figure 5-2: Load-Deflection Test on a Hard Surface

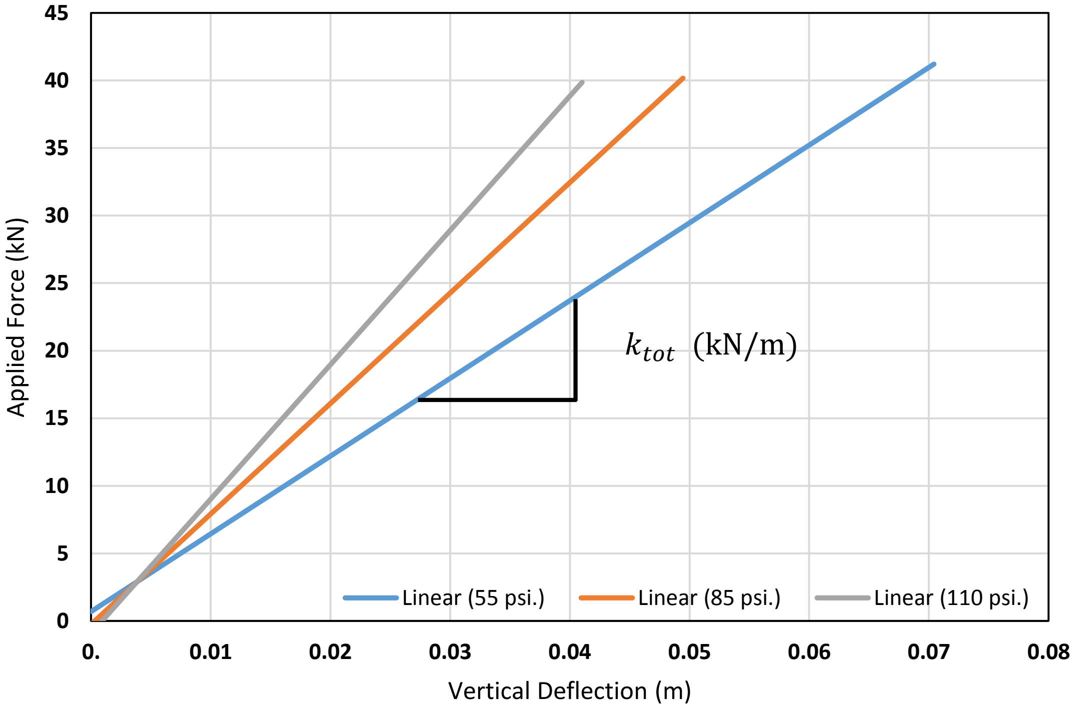

Figure 5-3: RHD Tire Load Deflection Relationship on a Hard Surface

The load deflection relationships for the RHD tire at varying inflation pressure are presented in Table 5-2. It is noted that the inflation pressure relationship is linear with respect to the total vertical stiffness; Equation 5-1. It may be assumed that the vertical stiffness is independent of load in the practical range of interest as the trends are mostly linear except for at extremely low loads on a hard surface [1].

$$k_{tot} = \frac{\text{Applied Loading}}{Vertical\ Defelction}\ kN/m \tag{5-1}$$

Table 5-2: RHD Total Vertical Stiffness on a Hard Surface

Parameter	55 PSI	85 PSI	110 PSI	Units
Total Vertical Stiffness (k_{tot})	575.45	817.91	993.65	kN/m

5.4 Vertical Stiffness and Residual Vertical Stiffness, k_{bz} and k_{vr}

Regardless of the road surface, the in-plane longitudinal and vertical stiffness, k_{bz} and k_{bx}, are considered to be one in the same due to the symmetry about the spindle of the tire. Recall that the vertical stiffness,k_{bz}, and residual stiffness, k_{vr}, are two springs in series that contribute to the vertical motion of the tire in parallel and represent the stiffness of the tread, describing the resistance of deflection within the sidewall and tread after excitation. Hence, these springs are located between the rigid tread band and the road. Therefore, the vertical and residual stiffness are required to be determined on a rigid road to calculate the soft soil parameters.

The dynamic drum-cleat test is used to determine the vertical and residual stiffness of the tire. The 2.5m diameter drum includes as 10mm cleat that upon impact will create the tire to vibrate. The tire is fixed in all but the vertical direction, meaning that only the vertical tread and carcass responses are measured. The tire is inflated to the desired inflation pressure and the vertical loading is applied. The tire is then rotationally accelerated by the drum to a linear equivalent velocity of 50km/hr. The excitation of the cleat impact forces the tire to resonate during which vertical forces at the spindle of the tire are measured to determine the natural frequency of the tire. Recall CHAPTER 4, from which Figure 5-4 is copied from, providing an example of the vertical first mode of vibration at 26.69 kN and the three inflation pressures, 55psi, 85 psi, and 100 psi.

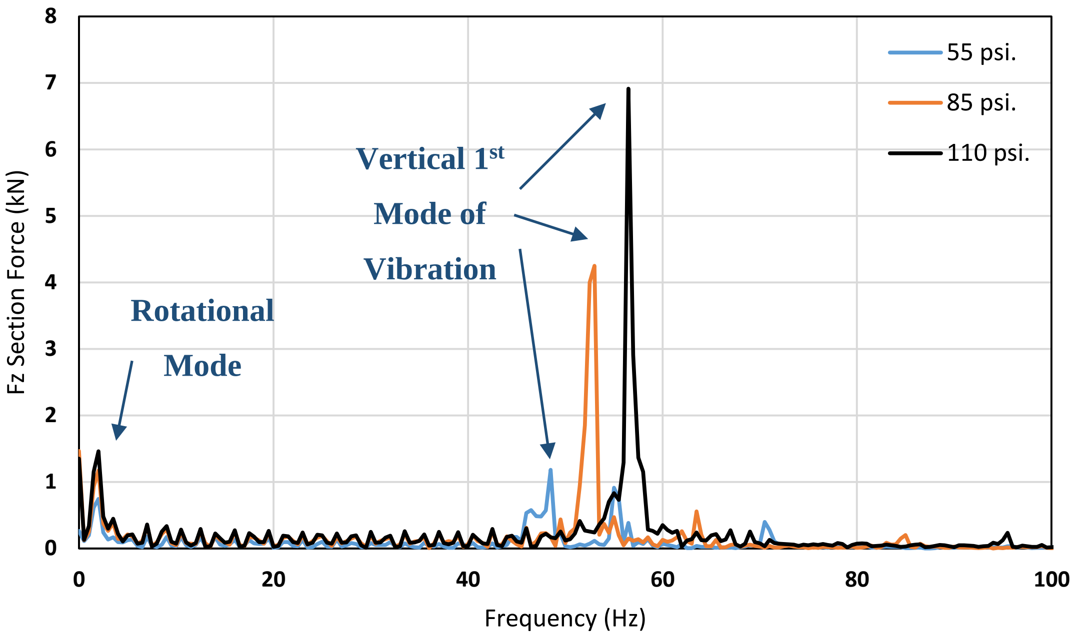

Figure 5-4: First Mode of Vibration at 26.69 kN (6,000 lbs.)

To determine the vertical and residual vertical stiffness using the natural frequency the relationship for springs in series is used within Equations 5-2 to 5-5, as previously determined by Chae [16];

$$\omega = \sqrt{\frac{k_{bz} + k_{vr}}{m_b}} \qquad 5\text{-}2$$

$$\therefore 2\pi f = \sqrt[2]{\frac{k_{bz} + k_{vr}}{m_b}} \qquad 5\text{-}3$$

$$k_{bz} + k_{vr} = (2\pi f)^2 \times m_b \qquad 5\text{-}4$$

$$\frac{1}{k_{tot}} = \frac{1}{k_{bz}} + \frac{1}{k_{vr}} \qquad 5\text{-}5$$

Where, ω represents the natural frequency (rad/s),

k_{bz} is the vertical sidewall stiffness (kN/m),

k_{vr} represents the residual vertical stiffness (kN/m),

k_{tot} symbolises the total vertical deflection (kN/m), f is the first mode frequency of in-plane vibration (Hz) (as determined within CHAPTER 4) and,

m_b is a representation of the mass of the tire belt, which is 43.4406 kg.

From the above calculations, the results to be shown in the following table, Table 5-3;

Table 5-3: RHD Vertical and Residual Stiffness Parameters

Parameter	Load kN	55 PSI	85 PSI	110 PSI	Units
First Mode Frequency (f)	13.345	46.002	51.396	56.502	Hz
	26.689	46.502	53.002	56.502	
	40.034	47.50	53.50	57.00	
Natural Frequency (ω)	13.345	289.038	322.931	355.014	rad/s
	26.689	292.179	333.022	355.014	
	40.034	298.451	336.150	358.141	
Total Vertical Stiffness (k_{tot})	13.345	575.450	817.910	993.650	kN/m
	26.689	575.450	817.910	993.650	
	40.034	575.450	817.910	993.650	
Sidewall Vertical Stiffness (k_{bz})	13.345	2912.050	3458.950	4170.420	kN/m
	26.689	2996.260	3773.410	4170.420	
	40.034	3166.121	3871.686	4277.627	
Residual Vertical Stiffness (k_{vr})	13.345	717.170	1071.210	1034.450	kN/m
	26.689	712.240	1044.260	1304.450	
	40.034	703.270	1036.975	1294.302	

It is summarized that the vertical and residual stiffness are dependent on the natural frequency of the system and therefore follow the same trends. As such, they have a directly proportional relationship with the inflation pressure but are not adversely influenced by the dynamic loading of the tire.

5.5 Total Vertical Damping and Residual Damping Constant, c_{tot} and c_{vr}

As discussed with the correlating springs, the longitudinal and vertical damping constants are considered equal due to symmetry about the spindle of the tire. The vertical, c_{tot}, and residual damping, c_{vr}, constants are two dampers in series and are responsible for the vertical damping of the tire.

In the free vertical vibration mode test on the drum-cleat, the in-plane sidewall and the residual damping are also connected to the tire belts in parallel, similar to the stiffness connection. Thus, the sum of the two damping constants is used in Equation 5-6; 5% of critical damping effect is used, which, that is observed in most tire response.

$$c_{bz} + c_{vr} = 2 \cdot \xi \cdot \sqrt{(k_{bz} + k_{vr}) \cdot m_b} \qquad 5\text{-}6$$

Where, c_{bz}: in-plane vertical damping constant of sidewall,

c_{vr}: residual damping constant in contact area,

ξ: damping ratio, assumed to be critical (5%),

m_b: mass of tire belt = 43.4406 kg.

Meanwhile, the residual damping constant can be calculated by using Equation 5-7;

$$c_{vr} = 2 \cdot \xi \cdot \sqrt{k_{vr} \cdot (m_b + m_a)} \qquad 5\text{-}7$$

Where, m_a: mass of the rim = 34.8 kg.

The total tire damping constant must be determined on the basis of two dampers in series; using Equation 5-8;

$$\frac{1}{c_{tot}} = \frac{1}{c_{bz}} + \frac{1}{c_{vr}} \qquad 5\text{-}8$$

The in-plane vertical damping constant of the sidewall and residual damping constant at the contact area are calculated at a tire load of 13.34 kN, 26.69 kN, and 40.03 kN, which are summarized in

Table 5-4. The in-plane vertical and longitudinal damping constants of the sidewall are considered to be the same regardless of the road surface type.

It is observed in Table 5-4 that the total vertical and residual damping constants are influenced by the inflation pressure of the tire, increasing with an increase in inflation pressure. Much the same as the respective stiffness values, the applied loading does not have a heavy influence on these parameters. This is because the total vertical and residual damping constant are functions of the tire's first mode of vibration.

Table 5-4: RHD Vertical and Residual Damping Constants

Parameter	Load kN	55 PSI	85 PSI	110 PSI	Units
Vertical Damping Constant (c_{bz})	13.345	0.506	0.487	0.532	kN.s/m
	26.689	0.523	0.543	0.532	
	40.034	0.560	0.560	0.550	
Residual Damping Constant (c_{vr})	13.345	0.75	0.915	1.010	kN.s/m
	26.689	0.746	0.904	1.010	
	40.034	0.742	0.901	1.006	
Total Tire Damping Constant (c_{tot})	13.345	0.302	0.318	0.348	kN.s/m
	26.689	0.307	0.340	0.348	
	40.034	0.319	0.345	0.355	

5.6 Rotational Stiffness and Damping Constant, $k_{b\theta}$ and $c_{b\theta}$

The rotational stiffness,$k_{b\theta}$, and damping constant,$c_{b\theta}$, determine the rotational motion of the rigid tread band. The static and isolated test procedure constrains the rim, suspended in space, so it is unable to rotate or translate and is not in contact with any road surface. The tread is considered rigid and only allowed to rotate with the plane of the tire. The tire is inflated and a 13.34 kN tangential force is applied to node on the rigid tread and under tread layer parts. The applied tangential force causes the tread band to rotate with respect to the rim. The tire sidewall stiffness ensures that a steady sate is reached at a certain angular displacement of the rim. Once a steady state rotation is achieved, the tangential force is removed causing the sidewall to oscillate rotationally. Figure 5-5 depicts a representation of the static test procedure described. Considering the steady state rotational displacement of the sidewall, the rotational stiffness,$k_{b\theta}$, may be determined using Equation 5-9 and data obtained from the graph illustrating the angular displacement with respect to time; Figure 5-6.

$$k_{b\theta} = \frac{Applied\ Moment}{Angular\ Displacement}\frac{kN.m}{rad} \tag{5-9}$$

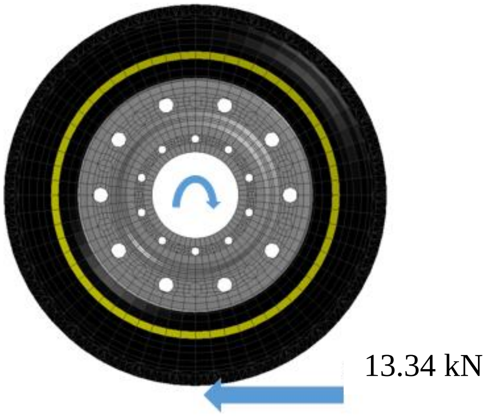

Figure 5-5: Rotational Stiffness and Damping Test Procedure

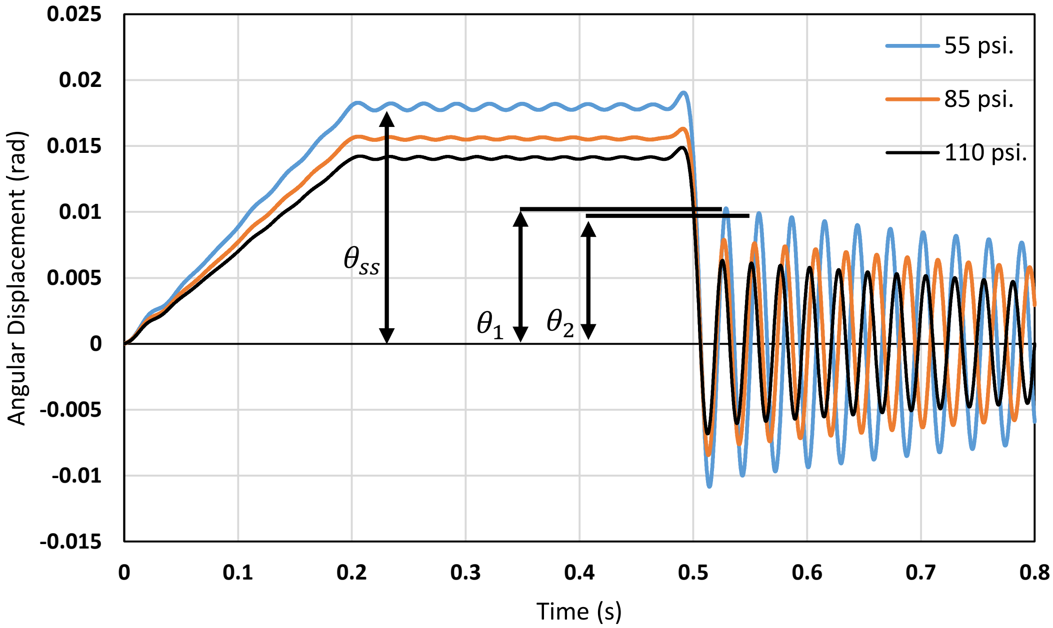

Figure 5-6: RHD Angular Displacement of the RHD Tread with Respect to Time

The logarithmic decrement (δ), and the damped period of vibration (τ), is calculated from the dissipating energy of the tread band's oscillation. Determining the magnitude of the tread bands angular displacement and decay over time allows the calculation of the damping constant using Equations 5-10 to 5-16;

Logarithmic Decrement:

$$\delta = ln\left(\frac{\theta_1}{\theta_2}\right) \tag{5-10}$$

Damping Ratio:

$$\xi = \frac{\delta}{\sqrt{4\pi^2 + \delta^2}} \tag{5-11}$$

Damped Period of Vibration:

$$\tau_d = t_2 - t_1 \tag{5-12}$$

Un-Damped Rotational Natural Frequency:

$$\omega_n = \frac{2\pi}{\tau_d\sqrt{1 - \xi^2}} \tag{5-13}$$

Damped Rotational Natural Frequency:

$$\omega_d = \frac{2\pi}{\tau_d} \tag{5-14}$$

Critical Damping Constant:

$$C_c = 2 \times I_{by} \times \omega_n \tag{5-15}$$

Where I_{by} is the moment of inertia of the tire belt, 12.073 kg-m^2

Rotational Damping Constant:

$$C_{b\theta} = \xi \times C_C \tag{5-16}$$

From the above mathematical procedure, the following values shown within Table 5-5 can be calculated. It is determined that the inflation pressure of the tire largely influences the rotational stiffness. However, the rotational damping constant is nearly constant with no large influence by the inflation pressure.

Table 5-5: Rotational Stiffness and Damping Constant Parameters

Parameter	55 PSI	85 PSI	110 PSI	Units
Steady State Displacement (θ_{ss})	0.018	0.016	0.014	rad
Rotational Stiffness ($k_{b\theta}$)	405.341	467.507	516.719	kN.m/rad
Logarithmic Decrement (δ)	0.036	0.034	0.033	-
Damping Ratio (ξ)	0.006	0.005	0.005	-
Damped Period of Vibration (τ_d)	0.029	0.027	0.026	s
Un-Damped Natural Frequency (ω_d)	217.525	233.670	246.483	rad/s
Critical Damping Constant (c_c)	5.252	5.642	5.952	kN.m.s/rad
Rotational Damping Constant ($c_{b\theta}$)	0.030	0.031	0.031	kN.m.s/rad

5.7 Total Equivalent Vertical Stiffness, $k_{tot,Dry\ Sand}$

To accommodate for the additional flexibility of the soil, another parameter,$k_{\ soil}$, is required. This parameter represents the vertical stiffness of the soil. Similar to the rigid-ring vertical stiffness, the spindle deflection or sinkage of the tire into the soil when plotted against the applied loading may determine the stiffness of the soil through analysis of the slope of the curve, Figure 5-7. The total equivalent vertical stiffness of the soil may be found through the relationship of the tire sidewall, tread residual, and soil stiffness as springs in series. The following Equations, 5-17 and 5-18, as developed by Slade [17] explain:

$$k_{\ Dry\ Sand} = \frac{\text{Applied Loading}}{Sinkage}\ \text{k}N/m \tag{5-17}$$

$$\frac{1}{k_{tot,Dry\ Sand}} = \frac{1}{k_{\ Dry\ Sand}} + \frac{1}{k_{bx}} + \frac{1}{k_{vr}} kN/m \tag{5-18}$$

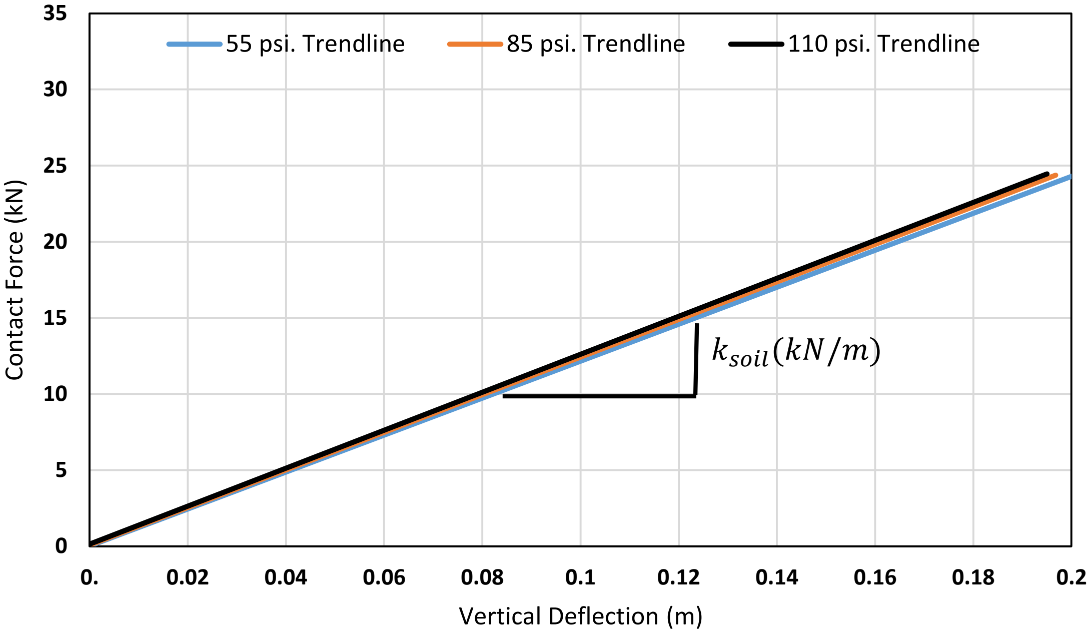

Figure 5-7: RHD Tire Load Deflection Relationship on Dry Sand

For the discussion of comparison, the total equivalent stiffness of the SPH dry sand soil is 110.72 kN/m at 110 psi, about one tenth of the total equivalent stiffness of the RHD tire on the rigid road which is 993.650kN/m at 110 psi. As mentioned, the given load range allows for the assumption that the vertical stiffness is independent of load [1]. More importantly, it appears that the dry sand soil stiffness is not heavily influenced by inflation pressure.

Equation 5-19 describes how the equivalent longitudinal tread stiffness,$k_{cx,Dry\ Sand}$, is calculated using half of the projected contact length, a$_{Dry\ Sand}$. As Slade [17] explains, the same equation as developed by Zegglarr and Pcjaka for describing the circumstances considering hard surface are adopted [10]. It may be noted in Figure 5-8 that the project half contact length and effective rolling radius are quantitatively measured from the simulation. It is concluded that the effective contact patch and rolling radius are load dependant; the inflation pressure does not have an effect on these parameters. The inflation pressure does, however, have a direct and linear relationship to the frequency at which the first mode of vibration occurs when oscillating on the drum-cleat model. The longitudinal tire and tread stiffness have a similar trend as they are directly influenced by the frequency of the first mode of vibration.

$$k_{cx,Dry\ Sand} = \frac{\mathrm{k}_{k,soil,Dry\ Sand}}{a_{Dry\ Sand}}\ \mathrm{k}N/m \qquad 5\text{-}19$$

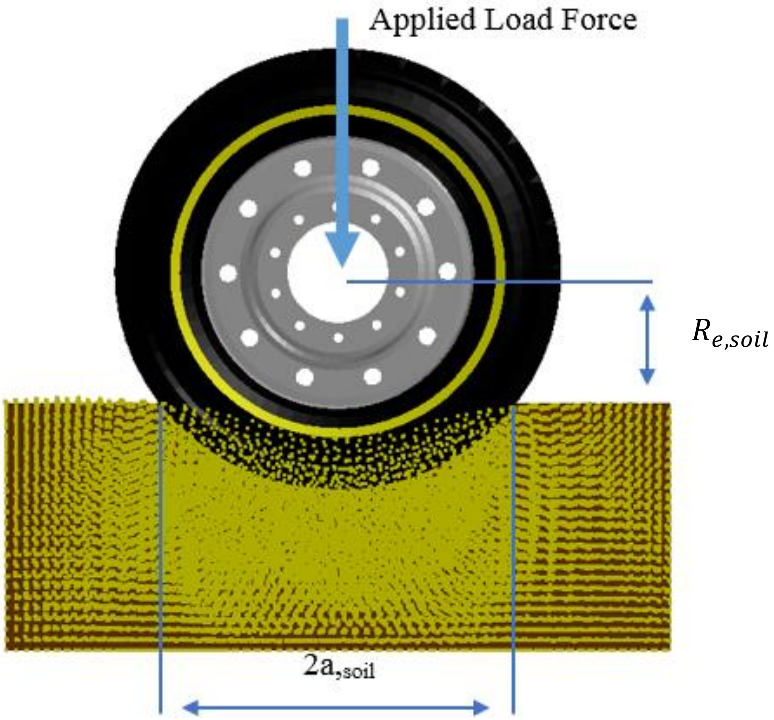

Figure 5-8: RHD Total Equivalent Vertical Stiffness Procedure on SPH Dry Sand

Table 5-6: RHD Total Equivalent Vertical Stiffness Parameters on Dry Sand

Parameter	55 PSI	85 PSI	110 PSI	Units
Soil Stiffness ($k_{,Dry\ Sand}$)	121.360	123.400	124.670	kN/m
Total Equivalent Vertical Stiffness ($k_{tot,Dry\ Sand}$)	100.223	107.223	110.772	kN/m

The trends for the soil total equivalent stiffness are the same for the hard surface parameters; the stiffness increases with inflation pressure but is assumed constant at varying applied loadings.

5.8 Longitudinal Tire Stiffness, $k_{k,Dry\ Sand}$

The longitudinal slip stiffness $k_{k,Dry\ Sand}$ spring is located between the tire and road surface, this parameter accounts for the longitudinal slip, or forces during braking and accelerating. It is assumed that the longitudinal slip stiffness is equal under either braking or acceleration conditions. It is assumed that the soil acts as a linear spring in series with the vertical residual stiffness of the tire over a specific load range.

A traction test is performed to determine the tire's ability to recover maximum traction after experiencing pure (100%) slip conditions. The tire is inflated and the loading is applied to the spindle of the tire. The tire is then rapidly accelerated to a rotational velocity of 20 rad/s or 50 km/hr and the tire is allowed to advance forward until a desired steady state speed is achieved. Figure 5-9 illustrates the traction test. The tire will experience zero slip in the beginning of the simulation due to the rapid acceleration of the tire. Therefore, the forces are measured until the rotational velocity reaches an equilibrium. The longitudinal force measured at the contact patch of the tire is measured; the longitudinal slip stiffness is defined as the slope of the longitudinal force plotted against the slip percentage of the tire as the slip approaches zero (0-10% slip). Equation 5-20 and Figure 5-10 describe this relation.

$$k_{k,Dry\ Sand} = \frac{\partial Longitudinal\ Force}{\partial Slip\%}\Big|_{Slip=0} \quad \frac{kN}{unit}slip \qquad 5\text{-}20$$

Figure 5-9: RHD Traction Test on SPH Dry Sand

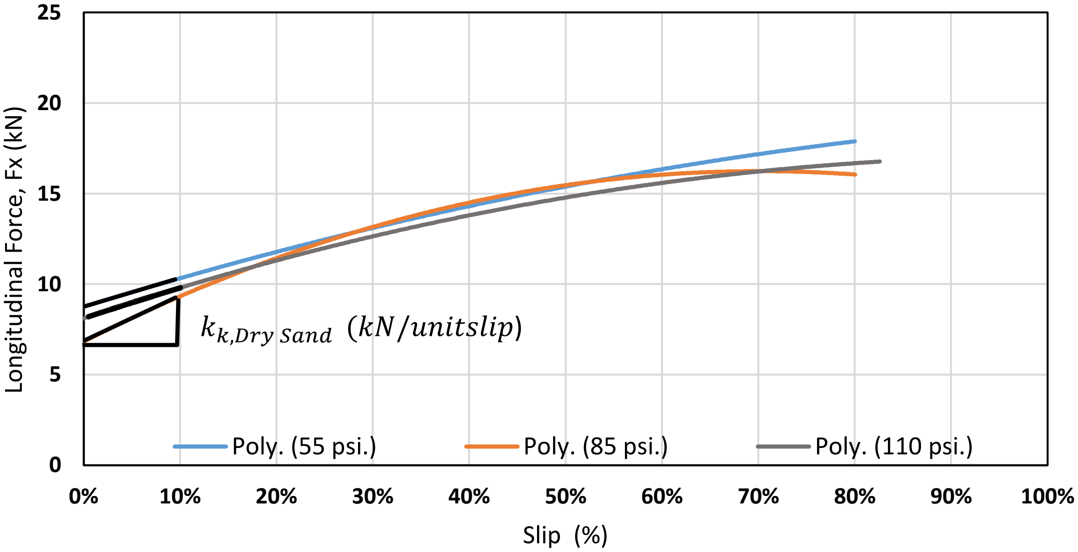

Figure 5-10: Longitudinal Force as a Function of Slip at 26.69 kN (6,000 lbs.)

The longitudinal tread damping is the ratio of the longitudinal tire stiffness to the steady state linear velocity measured at the tire center (v_{tr}). The longitudinal tread stiffness (k_{cx}) is the division of the longitudinal tire stiffness divided by half of the contact length, Equation 5-21; this relation was originally defined by Zegelaar and Pacejka [10]. The contact length is defined previously within Figure 5-8.

$$k_{cx,Dry\ Sand} = \frac{k_{k,Dry\ Sand}}{a}\frac{kN}{m} \qquad 5\text{-}21$$

Furthermore, Equation 5-21, for the longitudinal tread stiffness is only valid for slip ratios less than 0.1 during which the adhesion contact exists between the tire and road [10]. The following table, Table 5-7, summarizes the results:

Table 5-7: RHD Longitudinal Tire and Tread Stiffness Parameters on Dry Sand

Parameter	Load kN	55 PSI	85 PSI	110 PSI	Units
Longitudinal Tire Stiffness ($k_{k,\ Dry\ Sand}$)	13.345	13.249	8.492	10.557	kN/unit slip
	26.689	15.820	25.109	16.870	
	40.034	89.120	86.462	44.896	
Longitudinal Tread Stiffness ($k_{cx,\ Dry\ Sand}$)	13.345	39.727	25.734	31.513	kN/m
	26.689	40.710	65.644	43.818	
	40.034	209.202	204.644	106.515	
Projected Contact Length ($2a_{,Dry\ Sand}$) Recall: Figure 5-8: RHD Total Equivalent Vertical Stiffness Procedure on SPH Dry Sand	13.345	0.667	0.660	0.670	m
	26.689	0.772	0.765	0.770	
	40.034	0.852	0.845	0.843	
Effective Rolling Radius ($R_{e,Dry\ Sand}$)	13.345	0.402	0.394	0.407	m
	26.689	0.347	0.347	0.352	
	40.034	0.311	0.302	0.307	
Tread Speed ($v_{tr,Dry\ Sand}$)	13.345	10	10	10	m/s
	26.689	8.73	8.73	8.73	
	40.034	7.48	7.48	7.48	
Longitudinal Tread Damping ($k_{k,\ Dry\ Sand}/v_{tr}$)	13.345	3.973	2.573	3.151	kN.s/m
	26.689	1.812	2.876	1.932	
	40.034	5.352	11.914	6.00	

The longitudinal tire and tread stiffness and tread damping constants are directly and proportionally influenced by the applied loading but appear to have no major ainfluence in regard to the inflation pressure of the tire.

5.9 Chapter Summary

This chapter summarizes the in-plane off-road rigid-ring parameter predictions for the FEA RHD truck tire operating on a SPH Dry Sand model at three varying inflation pressures and applied loadings. The parameters may be observed within the following tables: Table 5-8, Table 5-9, and Table 5-10,

The total equivalent vertical stiffness increases with an increase in inflation pressure. However, it may be assumed that the vertical stiffness is independent of load in the practical range of interest as the trends are mostly linear except for at extremely low load [1]. It is summarized that the vertical and residual stiffness are dependant of the natural frequency of the system and therefore follow the same trends. They have a directly proportional relationship with the inflation pressure but are not adversely influenced by the dynamic loading of the tire. Furthermore, it is observed that the total vertical and residual damping constants are influenced by the inflation pressure of the tire, increasing with an increase in inflation pressure. Much the same as the respective stiffness values, the applied loading does not have a heavy influence on these parameters. It is determined that the inflation pressure of the tire largely influences the rotational stiffness. However, the rotational damping constant is nearly constant. The trends for the soil total equivalent stiffness are the same for the hard surface parameters; the stiffness increases with inflation pressure but is assumed constant at varying applied loadings.

In summary the effective contact patch and rolling radius are load dependant; the inflation pressure does not have an effect on these parameters. The inflation pressure does however have a direct and linear relationship to the frequency at which the first mode of vibration occurs when oscillating on the drum-cleat model. The longitudinal tire and tread stiffness have a similar trend as they are directly influenced by the frequency of the first mode of vibration. It may be concluded that the longitudinal tire, tread stiffness and tread damping constants are directly and proportionally influenced by the applied loading but appear to have no major influence in regard to the inflation pressure of the tire.

5.9.1 13.34 kN In-Plane Parameter Summary

Table 5-8: Summary of the In-Plane Off-Road Rigid-ring Parameter Predictions at 13.34 kN

13.34 kN In – Plane Off-Road Rigid-ring Parameters	55 PSI	85 PSI	110 PSI	Units
Total Vertical Stiffness (k_{tot})	575.45	817.91	993.65	kN/m
Sidewall Stiffness (k_{bz})	2912.050	3458.950	4170.420	kN/m
Residual Vertical Stiffness (k_{vr})	717.170	1071.210	1034.450	kN/m
Vertical Damping Constant (c_{bz})	0.506	0.487	0.532	kN.s/m
Residual Damping Constant (c_{vr})	0.750	0.915	1.010	kN.s/m
Tire Damping Constant (c_{tot})	0.302	0.318	0.348	kN.s/m
Rotational Stiffness ($k_{b\theta}$)	405.341	467.507	516.719	kN.m/rad
Rotational Damping Constant ($c_{b\theta}$)	0.030	0.031	0.031	kN.m.s/rad
Soil Stiffness, Dry Sand ($k_{Dry\ Sand}$)	121.360	123.400	124.670	kN/m
Total Equivalent Vertical Stiffness, Dry Sand ($k_{tot,Dry\ Sand}$)	100.223	107.223	110.772	kN/m
Longitudinal Tread Stiffness, Dry Sand ($k_{cx,Dry\ Sand}$)	39.727	25.734	31.513	kN/ m
Longitudinal Tire Stiffness, Soil ($k_{k,Dry\ Sand}$)	13.249	8.492	10.557	kN/unit slip
Longitudinal Tread Damping, Dry Sand ($k_{k,Dry\ Sand/v_{tr}}$)	3.973	2.573	3.151	kN.s/m
Effective Contact Patch, Dry Sand ($2_{a,Dry\ Sand}$)	0.667	0.660	0.670	m
Effective Rolling Radius, Dry Sand ($R_{e,Dry\ Sand}$)	0.402	0.394	0.407	m

5.9.2 26.69 kN In-Plane Parameter Summary

Table 5-9: Summary of the In-Plane Off-Road Rigid-ring Parameter Predictions at 26.69 kN

26.69 kN In – Plane Off-Road Rigid-Ring Parameters	55 PSI	85 PSI	110 PSI	Units
Total Vertical Stiffness (k_{tot})	575.450	817.910	993.650	kN/m
Sidewall Stiffness (k_{bz})	2996.260	3773.410	4170.420	kN/m
Residual Vertical Stiffness (k_{vr})	712.240	1044.260	1304.450	kN/m
Vertical Damping Constant (c_{bz})	0.523	0.543	0.532	kN.s/m
Residual Damping Constant (c_{vr})	0.746	0.904	1.010	kN.s/m
Tire Damping Constant (c_{tot})	0.307	0.340	0.348	kN.s/m
Rotational Stiffness ($k_{b\theta}$)	405.341	467.507	516.719	kN.m/rad
Rotational Damping Constant ($c_{b\theta}$)	0.030	0.031	0.031	kN.m.s/rad
Soil Stiffness, Dry Sand ($k_{Dry\ Sand}$)	121.360	123.400	124.670	kN/m
Total Equivalent Vertical Stiffness, Dry Sand ($k_{tot,Dry\ Sand}$)	100.223	107.223	110.772	kN/m
Longitudinal Tread Stiffness, Dry Sand ($k_{cx,Dry\ Sand}$)	40.710	65.644	43.818	kN/ m
Longitudinal Tire Stiffness, Soil ($k_{k,Dry\ Sand}$)	15.820	25.109	16.870	kN/unit slip
Longitudinal Tread Damping, Dry Sand ($k_{k,Dry\ Sand/v_{tr}}$)	1.812	2.876	1.932	kN.s/m
Effective Contact Patch, Dry Sand ($2_{a,Dry\ Sand}$)	0.772	0.765	0.770	m
Effective Rolling Radius, Dry Sand ($R_{e,Dry\ Sand}$)	0.347	0.347	0.352	m

5.9.3 40.03 kN In-Plane Parameter Summary

Table 5-10: Summary of the In-Plane Off-Road Rigid-ring Parameter Predictions at 40.03 kN

40.03 kN In – Plane Off-Road Rigid-Ring Parameters	55 PSI	85 PSI	110 PSI	Units
Total Vertical Stiffness (k_{tot})	575.450	817.910	993.650	kN/m
Sidewall Stiffness (k_{bz})	3166.121	3871.686	4277.627	kN/m
Residual Vertical Stiffness (k_{vr})	703.270	1036.975	1294.302	kN/m
Vertical Damping Constant (c_{bz})	0.560	0.560	0.550	kN.s/m
Residual Damping Constant (c_{vr})	0.742	0.901	1.006	kN.s/m
Tire Damping Constant (c_{tot})	0.319	0.345	0.355	kN.s/m
Rotational Stiffness ($k_{b\theta}$)	405.341	467.507	516.719	kN.m/rad
Rotational Damping Constant ($c_{b\theta}$)	0.030	0.031	0.031	kN.m.s/rad
Soil Stiffness, Dry Sand ($k_{Dry\ Sand}$)	121.360	123.400	124.670	kN/m
Total Equivalent Vertical Stiffness, Dry Sand ($k_{tot,Dry\ Sand}$)	100.223	107.223	110.772	kN/m
Longitudinal Tread Stiffness, Dry Sand ($k_{cx,Dry\ Sand}$)	209.202	204.644	106.515	kN/ m
Longitudinal Tire Stiffness, Soil ($k_{k,Dry\ Sand}$)	89.120	86.462	44.896	kN/unit slip
Longitudinal Tread Damping, Dry Sand ($k_{k,Dry\ Sand/v_{tr}}$)	5.352	11.914	6.00	kN.s/m
Effective Contact Patch, Dry Sand ($2_{a,Dry\ Sand}$)	0.852	0.845	0.843	m
Effective Rolling Radius, Dry Sand ($R_{e,Dry\ Sand}$)	0.311	0.302	0.307	m

CHAPTER 6

DETERMINATION OF THE OUT-OF-PLANE OFF-ROAD RIGID-RING MODEL PARAMETERS

6.1 Chapter Introduction

The purpose of this chapter is to predict the out-of-plane off-road rigid-ring parameters of the RHD tire on dry sand SPH soft soil (Dry Sand) at varying operation conditions. The applied loading is varying from 13.34 kN (3,000 lbs.), 26.69 kN (6,000 lbs.) and 40.03 kN (9,000 lbs.). The inflation pressure will change between 0.379 MPa (55 psi), 0.586 MPa (85 psi), and 0.759 MPa (110 psi).

6.2 List of Out-of-Plane Rigid-ring Parameters

The out-of-plane rigid-ring parameters uses translational and rotational springs and dampers to represent the elastic sidewall of the tire;k_{by}, and c_{by}. The rotational sidewall stiffness and damping,$k_{b\gamma}$, and, $c_{b\gamma}$, are represented by torsional springs and dampers. The residual vertical damping is the same as the respective in-plane parameter. The sidewall lateral stiffness and damping are represented by k_l, and c_l, respectively and have a similar test procedure based on the same theorems of the lateral slip within the in-plane model. The newly introduced parameters within the off-road rigid-ring model are to represent the vertical,k_{soil}, and longitudinal $k_{l,soil}$, flexibility of the soil. It is assumed that the vertical soil stiffness acts as a linear spring in series with the vertical and residual tire stiffness. The out-of-plane off-road rigid-ring model is illustrated in Figure 6-1 with its respective parameters tabulated within Table 6-1. [17]

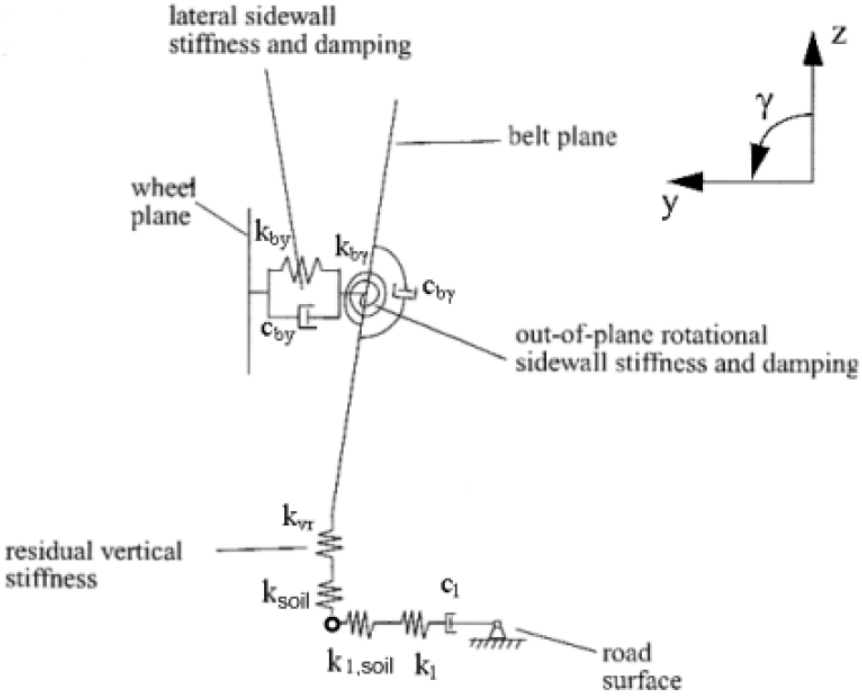

Figure 6-1: Out-Of-Plane Off-Road Rigid-Ring Model [17]

Table 6-1: List of Out-of-Plane Off-Road Rigid-Ring Model Parameters

Out-of-Plane Off-Road Rigid-ring Parameters	Symbol	Units
Translational Stiffness	k_{by}	kN/m
Translational Damping Constant	c_{by}	kN.s/m
Rotational Stiffness	$k_{b\gamma}$	kN.m/rad
Rotational Damping Constant	$c_{b\gamma}$	kN.s/rad
Lateral Tire Stiffness	k_l	kN/m
Lateral Damping Constant	c_l	kN.s/m
Total Lateral Slip Stiffness, Dry Sand	$k_{l,tot,Dry\ Sand}$	kN/m
Lateral Slip Stiffness, Dry Sand	$k_{l,Dry\ Sand}$	kN/m
Lateral Damping Constant, Dry Sand	$c_{l,Dry\ Sand}$	kN.s/m
Cornering Stiffness, Dry Sand	$k_{f,Dry\ Sand}$	kN/rad
Self-Aligning Torque Stiffness, Dry Sand	$k_{M,Dry\ Sand}$	kN.m/rad
Relaxation Length, Dry Sand	$\sigma_{,Dry\ Sand}$	m
Rolling Resistance Coefficient, Dry Sand	$RRC_{,Dry\ Sand}$	-

6.3 Translational Stiffness and Damping Constant, k_{by} and c_{by}

The purpose of the translational stiffness,k_{by}, and damping c_{by}, parameters are to predict the tire's ability to resist energy and deflection from the lateral direction. The virtual testing procedure for determining the translational parameters involves constraining the tire in space and setting the rim as a rigid body; the testing procedure is depicted within Figure 6-2. The tread base and tread band are also rigid bodies and constrained as such so that tire is only allowed motion in the lateral direction, unable to translate or rotate. The tire is inflated to the desired inflation pressure, after which, two lateral loads of 15 kN (3,372 lbs.) are applied, in the same direction, on the top and bottom of the tire on two select nodes of the rigid tread. After a steady state is obtained, the applied lateral loads are released. The tire carcass is laterally excited as the tread is translated a certain lateral distance due to the sidewall out-of-plane translational stiffness. The logarithmic decrement,δ, of the angular displacement, the steady state lateral displacement of the tread band ,y_{ss}, and the transient state of damping are obtained, and observed in Figure 6-3 to determine the translational stiffens and damping constants.

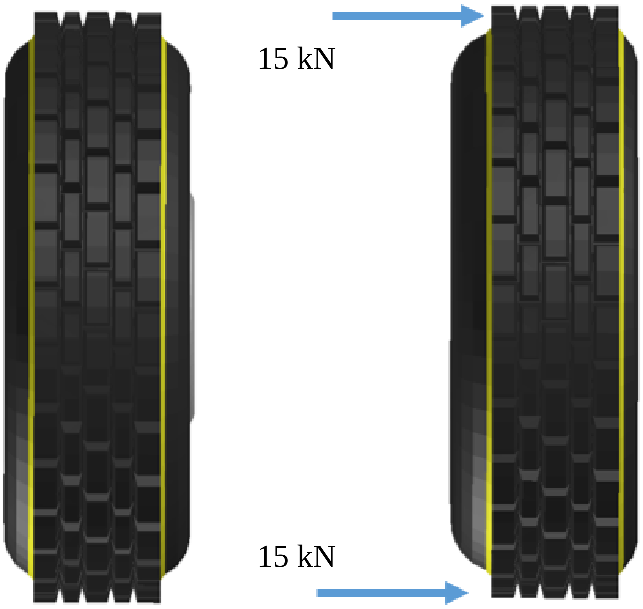

Figure 6-2: RHD Translational Stiffness Procedure

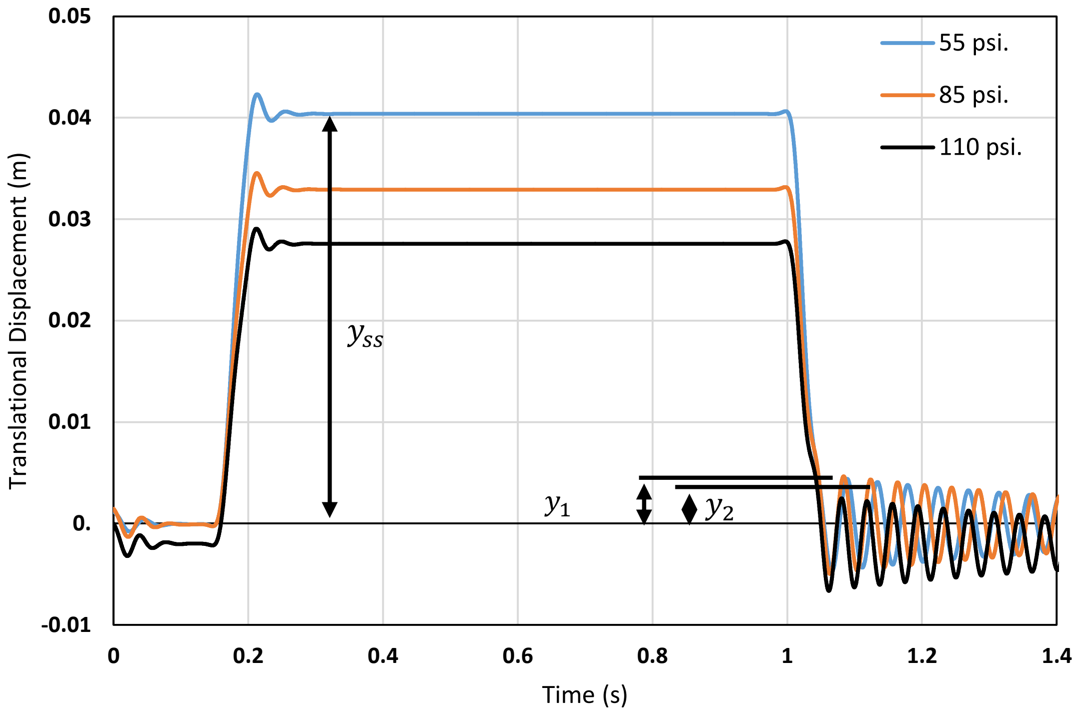

Figure 6-3: RHD Out-of-Plane Translational Displacement Response at 26.69 kN

The translational stiffness, k_{by}, can be determined using the steady state translational displacement of the sidewall and known applied lateral force within 6-1.

$$k_{by} = \frac{Lateral\ Force}{Lateral\ Displacement}\ kN/m \tag{6-1}$$

The sidewalls are the only parts allowed to elastically deform during this test procedure. The magnitude of the translational vibration decreases over time, allowing the adoption of the logarithmic decrement (δ) using the initial and successive amplitudes of the recorded oscillations as illustrated within Figure 6-3. From the logarithmic decrement, the dimensionless damping ratio (ξ) is determined. The timing of the initial and successive amplitudes is employed to determine the damped period of vibration (τ_d). From solving the damping ratio and damped period of vibration the un-damped (ω_n), translational natural frequency may be determined. The critical damping constant (c_c), is found to be the product of the mass of the tire belt and the un-damped natural frequency; the translational damping constant,c_{by}, is then determined as a function of the damping ratio and critical damping constant. Equations 6-2 to 6-8 explain the calculations described.

Logarithmic Decrement:

$$\delta = ln\left(\frac{y_1}{y_2}\right) \tag{6-2}$$

Damping Ratio:

$$\xi = \frac{\delta}{\sqrt{4\pi^2 + \delta^2}} \tag{6-3}$$

Damped Period of Vibration:

$$\tau_d = t_2 - t_1 \tag{6-4}$$

Un-Damped Translational Natural Frequency:

$$\omega_n = \frac{2\pi}{\tau_d\sqrt{1 - \xi^2}} \tag{6-5}$$

Damped Translational Natural Frequency:

$$\omega_d = \frac{2\pi}{\tau_d} \tag{6-6}$$

Critical Damping Constant:

$$C_c = 2 \times m_b \times \omega_n \tag{6-7}$$

Where m_b is the mass of the tire belt, 72 kg.

Translational Damping Constant:

$$C_{by} = \xi \times C_C \tag{6-8}$$

Since the applied load is independent of the vehicle load, it is assumed there is no difference when varying the applied loading. It may be observed that the inflation pressure directly influences the translational displacement and has a small influence on the translational damping constant. From the above mathematical procedure, the following values could be calculated within Table 6-2.

Table 6-2: Translational Stiffness and Damping Constant Parameters

Parameter	55 PSI	85 PSI	110 PSI	Units
Steady State Displacement (y_{ss})	0.040	0.033	0.029	m
Translational Stiffness (k_{by})	742.926	911.208	1017.603	kN/m
Logarithmic Decrement (δ)	0.075	0.068	0.065	-
Damping Ratio (ξ)	0.012	0.011	0.010	-
Damped Period of Vibration (τ_d)	0.045	0.040	0.038	s
Un-Damped Natural Frequency (ω_d)	139.612	156.332	166.306	rad/s
Critical Damping Constant (c_c)	20.104	22.512	23.948	kN.s/m
Translational Damping Constant (c_{by})	0.239	0.244	0.248	kN.s/m

6.4 Rotational Stiffness and Damping Constant, $k_{b\gamma}$ and $c_{b\gamma}$

The rotational sidewall stiffness,$k_{b\gamma}$, and damping , $c_{b\gamma}$, parameters are represented by torsional springs and dampers. The testing procedure is similar to the translational stiffness procedure as discussed within Section 6.3; however, the lateral forces of 15 kN (3,372 lbs.) are applied into the rigid tread base and parts in opposite directions. Once again, the rim is constrained as a rigid body, along with the tread band and tread base. The distinguishable difference is that the tire is constrained about the spindle. The procedure is highlighted within Figure 6-4. Due to the out-of-plane rotational stiffness of the sidewall the belt is rotated at a certain angle. The force is maintained until the rotational displacement reaches a steady state saturation. The lateral load is removed inducing a rotational vibration; this is seen within Figure 6-5.

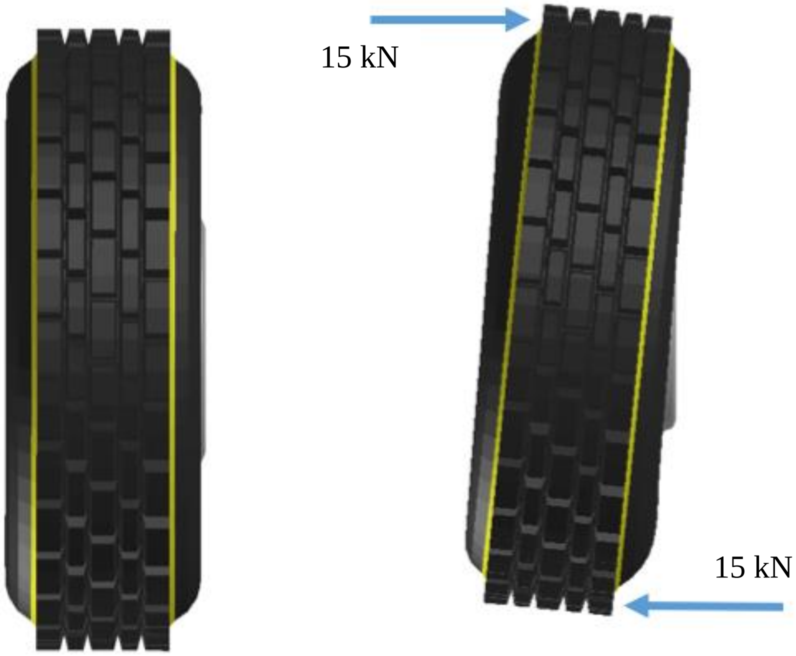

Figure 6-4: Rotational Stiffness Procedure

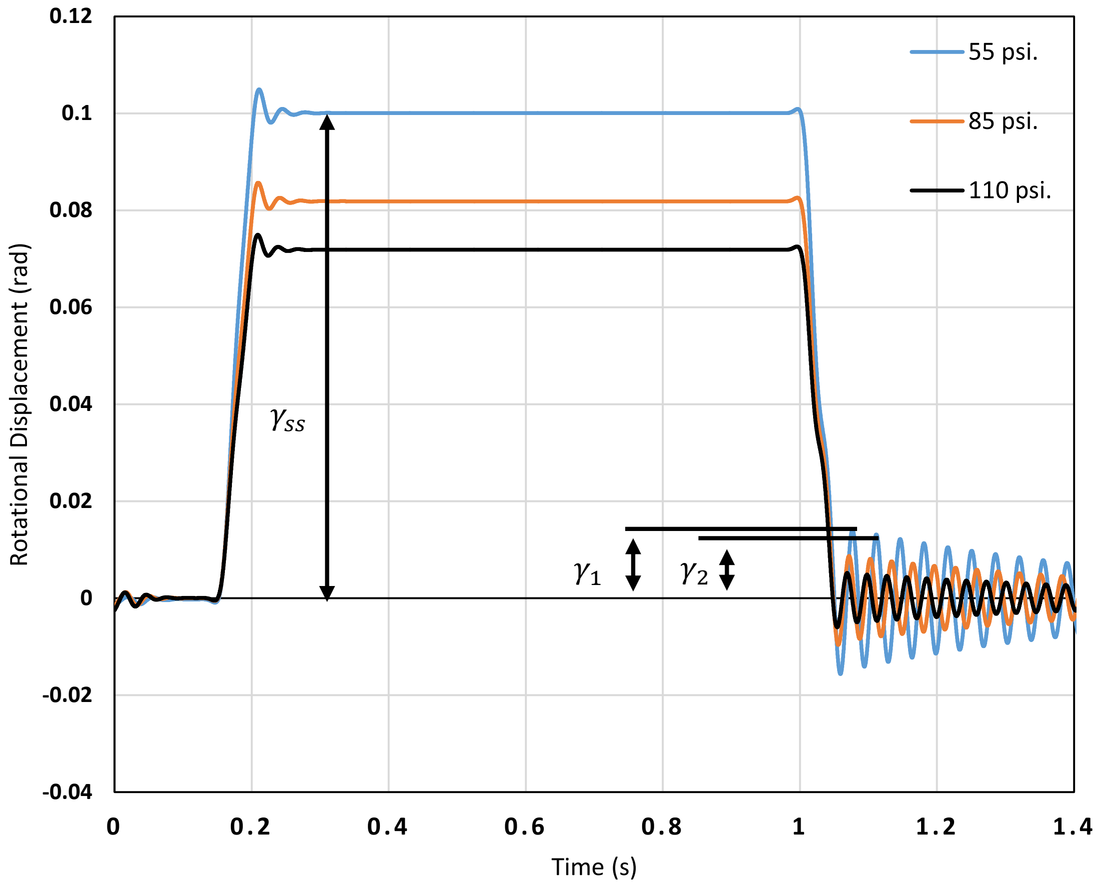

Figure 6-5: RHD Out-of-Plane Rotational Displacement Transient Response at 26.69 kN

Similar to the translational stiffness procedure, the rotational stiffness is the division of the applied moment by the angular displacement of the tread, Equation 6-9.

$$k_{b\gamma} = \frac{Applied\ Moment}{Angular\ Displacement}\ kNm/rad \tag{6-9}$$

An out-of-plane rotational vibration is experienced by the rigid tread band once the applied lateral forces are quickly removed and it is from the oscillation decay that the logarithmic decrement, the damping ratio, damped period of vibration, and damped and in-damped rotational frequencies that the translational damping of the sidewall are determined Equations 6-10 to 6-16.

$$\delta = ln\left(\frac{\gamma_1}{\gamma_2}\right) \tag{6-10}$$

$$\xi = \frac{\delta}{\sqrt{4\pi^2 + \delta^2}} \tag{6-11}$$

$$\tau_d = t_2 - t_1 \tag{6-12}$$

$$\omega_n = \frac{2\pi}{\tau_d\sqrt{1 - \xi^2}} \tag{6-13}$$

$$\omega_d = \frac{2\pi}{\tau_d} \tag{6-14}$$

$$C_c = 2 \times I_{bx} \times \omega_n \tag{6-15}$$

Where I_{bx} is the moment of inertia of the tire belt, 6.840 kg-m^2

Rotational Damping Constant:

$$C_{b\gamma} = \xi \times C_C \tag{6-16}$$

It is observed that the rotational stiffness and damping constants increases with an increase in inflation pressure. Table 6-3 lists the calculated predictions.

Table 6-3: RHD Rotational Damping Parameters

Parameter	55 PSI	85 PSI	110 PSI	Units
Steady State Displacement (y_{ss})	0.100	0.082	0.072	rad
Rotational Stiffness ($k_{b\gamma}$)	163.711	200.092	227.923	kN.m/rad
Logarithmic Decrement (δ)	0.075	0.068	0.061	-
Damping Ratio (ξ)	0.012	0.011	0.010	-
Damped Period of Vibration (τ_d)	0.035	0.031	0.029	s
Un-Damped Natural Frequency (ω_d)	180.530	202.658	217.386	rad/s
Critical Damping Constant (c_c)	2.470	2.772	2.974	kN.s/rad
Rotational Damping Constant ($c_{b\gamma}$)	0.029	0.030	0.029	kN.m.s/rad

6.5 Lateral Tire Stiffness and Damping Constant, k_l and c_l

The lateral tire stiffness, k_l, and damping, c_l, constants are a measurement of the reaction of the tire to externally applied lateral forces under specific load ranges. The lateral free vibration test is conducted by applying a 5 kN (1,124 lbs.) lateral load to the spindle of the tire to induce a lateral deflection. First, the tire is allowed a settling time to inflate to the desired inflation pressure and settle onto the road surface. The lateral force is applied after solid contact has been made between the tire and road surface, Figure 6-6 depicts the described procedure. The lateral load is applied until a steady state lateral displacement is achieved. When the lateral load is removed, the tire undergoes an out-of-plane translational vibration; the dissipating energy allows for the logarithmic decrement of angular displacements to be adopted to determine the lateral stiffness and damping constants of the RHD tire. An example of the results is shown within Figure 6-7.

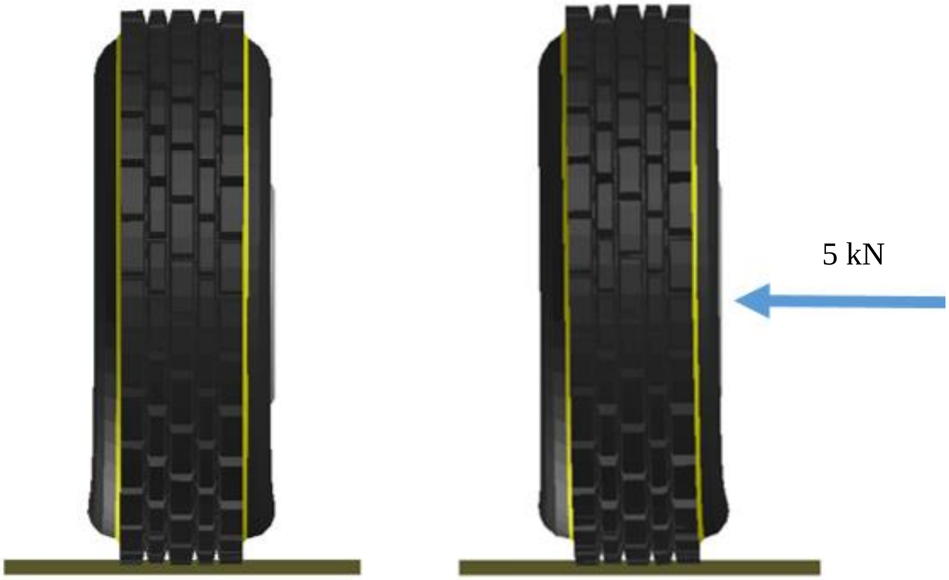

Figure 6-6: RHD Lateral Free Vibration Test Procedure

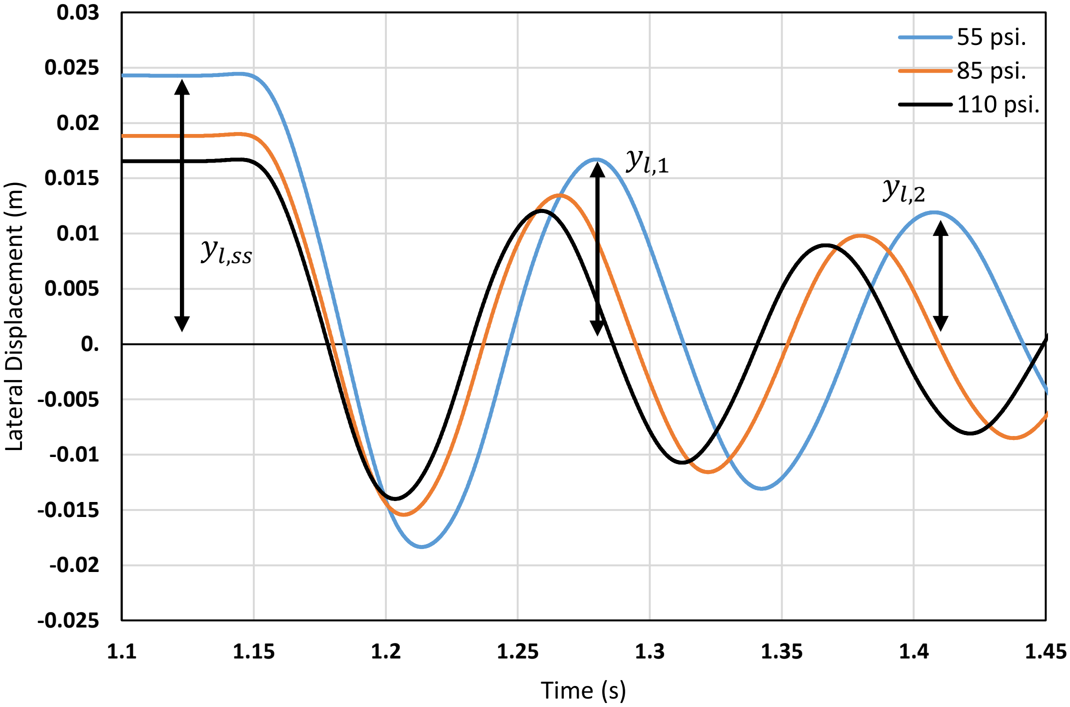

Figure 6-7: RHD Lateral Free Vibration at 26.69 kN

From the above plot, Figure 6-7, the maximum displacement values can be tabulated and used in the following formula, Equation 6-17 to calculate the lateral tire stiffness, k_l;

$$k_l = \frac{Lateral\ Force}{Lateral\ Drisplacement}\ kN/m \tag{6-17}$$

As used previously, Equations 6-18 to 6-24 adapt the logarithmic decrement of lateral displacements to solve for the lateral damping constant:

$$\delta = ln\left(\frac{y_{\mathrm{l},1}}{y_{\mathrm{l},2}}\right) \tag{6-18}$$

$$\xi = \frac{\delta}{\sqrt{4\pi^2 + \delta^2}} \tag{6-19}$$

$$\tau_d = t_2 - t_1 \tag{6-20}$$

$$\omega_n = \frac{2\pi}{\tau_d\sqrt{1 - \xi^2}} \tag{6-21}$$

$$\omega_d = \frac{2\pi}{\tau_d} \tag{6-22}$$

$$C_c = 2 \times m_{wheel} \times \omega_n \tag{6-23}$$

Where m_{wheel} is the mass of the tire and rim, 106.8 kg

$$C_l = \xi \times c_c \tag{6-24}$$

From the above mathematical procedure, the following values were able to be calculated within Table 6-4. It is determined that the lateral slip stiffness and damping constants are directly proportional to inflection of the applied inflation pressure and applied vertical loadings

Table 6-4: Lateral Damping Constant Parameters at 3,000lbs.

Parameter	Load (kN)	55 PSI	85 PSI	110 PSI	Units
Steady State Displacement ($y_{l,ss}$)	13.345	0.022	0.018	0.016	m
	26.689	0.023	0.018	0.016	
	40.034	0.024	0.016	0.011	
Lateral Slip Stiffness (k_l)	13.345	222.626	270.345	309.621	kN/m
	26.689	212.397	265.420	302.202	
	40.034	211.665	320.227	439.576	
Logarithmic Decrement (δ)	13.345	0.331	0.297	0.293	-
	26.689	0.356	0.315	0.298	
	40.034	0.367	0.323	0.313	
Damping Ratio (ζ)	13.345	0.053	0.047	0.047	-
	26.689	0.057	0.050	0.047	
	40.034	0.058	0.051	0.050	
Damped Period of Vibration (τ_d)	13.345	0.125	0.112	0.106	s
	26.689	0.128	0.114	0.108	
	40.034	0.133	0.120	0.109	
Un-Damped Natural Frequency (ω_d)	13.345	50.529	56.304	59.498	rad/s
	26.689	49.120	55.128	58.449	
	40.034	47.313	52.447	57.910	
Critical Damping Constant (c_c)	13.345	10.793	12.027	12.709	kN.s/m
	26.689	10.492	11.775	12.485	
	40.034	10.123	11.218	12.385	
Lateral Slip Damping Constant (c_l)	13.345	0.568	0.567	0.591	kN.s/m
	26.689	0.594	0.590	0.591	
	40.034	0.591	0.576	0.616	

6.6 Lateral Tire Stiffness and Damping Constant, $k_{l,Dry\ Sand}$ and $c_{l,Dry\ Sand}$

The lateral tire stiffness,$k_{l,Dry\ Sand}$, procedure for a soft soil is identical to that as described for the previous lateral vibration test conducted on a hard surface. The procedure is initiated with a rapid inflation pressure followed by a settling time allowing the tire to settle in the soil with the applied vertical load. Similar to the rigid road procedure, a lateral force of 5kN is applied to the center of the tire in a cyclic fashion allowing the tire carcase to resonate, as illustrated below in Figure 6-8. The proceeding Figure 6-9 observes the steady state lateral displacement and transient state of damping response from the tire on dry sand.

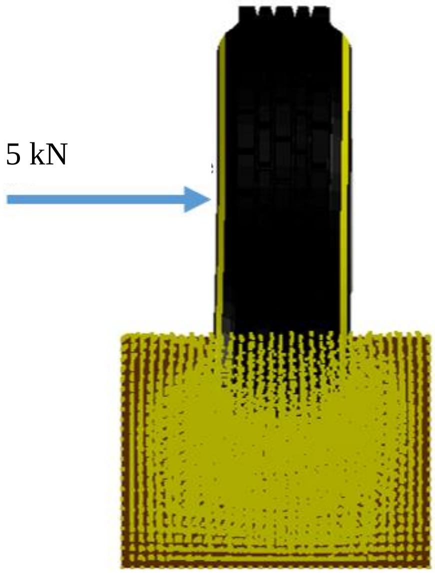

Figure 6-8: RHD Lateral Stiffness Predictions on Dry Sand

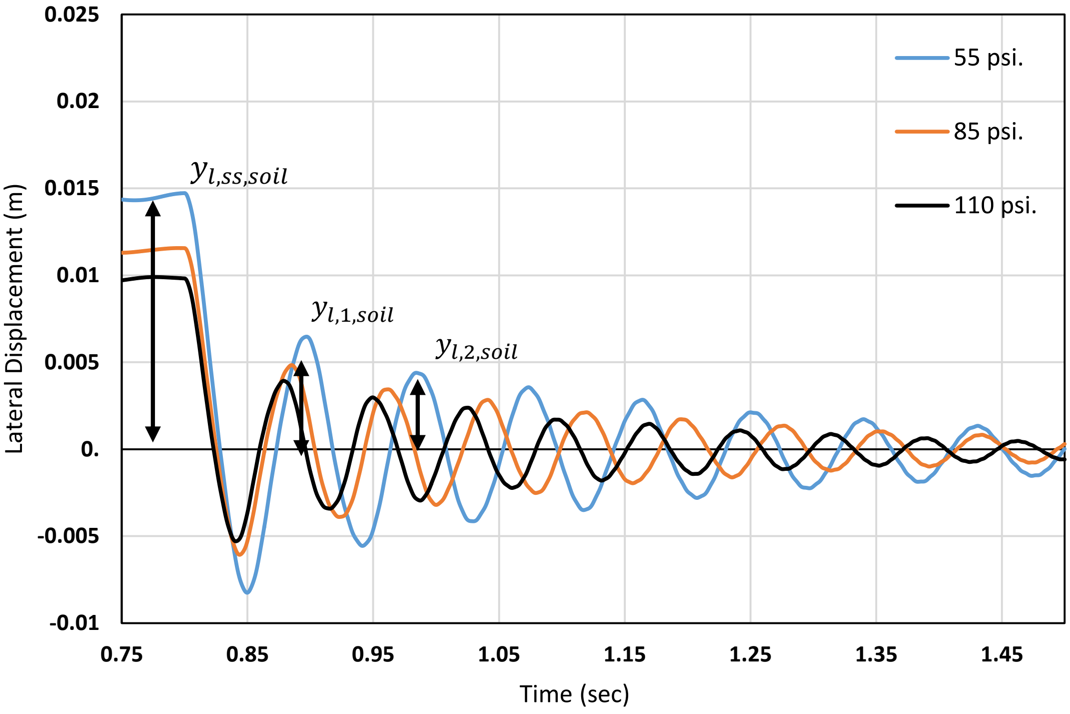

Figure 6-9: RHD Lateral Free Vibration at 26.689 kN on Dry Sand

Through graphical analysis the maximum displacement distance of the tire carcase, $y_{l,ss,Dry\ Sand}$, is tabulated to determine the total equivalent lateral tire stiffness, $k_{l,tot,Dry\ Sand}$, as the quotient of the applied lateral force (5 kN), by the lateral displacement. The equivalent lateral tire stiffness is determined from the total equivalent stiffness were expressed by Slade and are shown in Equations 6-25 and 6-26. [17]

$$k_{l,tot,Dry\ Sand} = \frac{Lateral\ Force}{Lateral\ Drisplacement}\ kN/m \tag{6-25}$$

$$\frac{1}{k_{l,Dry\ Sand}} = \frac{1}{k_{l,tot,Dry\ Sand}} - \frac{1}{k_{l,Rigid\ Road}} \tag{6-26}$$

Such that;

$k_{l,tot,Dry\ Sand}$ = Total equivalent lateral stiffness of the tire on SPH dry sand,

$k_{l,Rigid\ Road}$ = Lateral tire stiffness on rigid road and,

$k_{l,Dry\ Sand}$ = Lateral stiffness of tire on SPH on dry sand

When the applied lateral force is removed from the spindle of the tire, the tire experiences an out-of-plane translational vibration. Adopted from the hard surface calculations, the logarithmic decrement of the lateral displacements obtains two neighbouring peak values, $y_{l,1,soil}$ and $y_{l,2,soil}$ to determine the contact area slip stiffness and damping. The longitudinal slip damping constant, $c_{l,Dry\ Sand}$, may be determined through the use of Equations 6-27 to 6-33;

$$\delta = ln\left(\frac{y_{l,1,Dry\ Sand}}{y_{l,2,Dry\ Sand}}\right) \tag{6-27}$$

$$\xi = \frac{\delta}{\sqrt{4\pi^2 + \delta^2}} \tag{6-28}$$

$$\tau_d = t_2 - t_1 \tag{6-29}$$

$$\omega_{n,Dry\ Sand} = \frac{2\pi}{\tau_d\sqrt{1-\xi^2}} \tag{6-30}$$

$$\omega_{d,Dry\ Sand} = \frac{2\pi}{\tau_d} \quad \text{6-31}$$

$$C_{c,Dry\ Sand} = 2 \times m_{wheel} \times \omega_{n,Dry\ Sand} \quad \text{6-32}$$

Where m_{wheel} is the mass of the tire and rim, 106.8 kg

$$C_{l,Dry\ Sand} = \xi \times C_{C,Dry\ Sand} \text{ (kN s/m)} \quad \text{6-33}$$

Table 6-5: Lateral Damping Tire Calculations on SPH Soft Soil 1 (Dry Sand)

Parameter	Load (kN)	55 PSI	85 PSI	110 PSI	Units
Steady State Displacement ($y_{l,ss,soil}$)	13.345	0.022	0.017	0.015	m
	26.689	0.017	0.012	0.010	
	40.034	0.016	0.012	0.010	
Lateral Tire Stiffness ($k_{l,tot,soil}$)	13.345	228.893	293.970	342.964	kN/m
	26.689	294.062	408.207	502.069	
	40.034	309.157	417.247	511.948	
Equivalent Lateral Tire Stiffness ($k_{l,soil}$)	13.345	8131.692	3364.134	3184.766	kN/m
	26.689	764.810	758.800	759.136	
	40.034	671.213	1377.180	3109.470	
Logarithmic Decrement (δ)	13.345	0.667	0.679	0.638	-
	26.689	0.687	0.581	0.495	
	40.034	0.779	0.771	0.609	
Damping Ratio (ξ)	13.345	0.106	0.107	0.101	-
	26.689	0.109	0.092	0.079	
	40.034	0.123	0.122	0.096	
Damped Period of Vibration (τ_d)	13.345	0.103	0.100	0.086	s
	26.689	0.092	0.079	0.074	
	40.034	0.083	0.069	0.066	
Un-Damped Natural Frequency (ω_n)	13.345	61.573	63.252	73.510	rad/s
	26.689	68.855	79.961	85.735	
	40.034	76.176	92.264	96.068	
Critical Damping Constant ($c_{c,soil}$)	13.345	13.152	13.511	15.702	kN.s/m
	26.689	14.707	17.080	18.313	
	40.034	16.271	19.708	20.520	
Out-of-Plane Slip Constant ($c_{l,soil}$)	13.345	1.388	1.452	1.585	kN.s/m
	26.689	1.598	1.572	1.438	
	40.034	2.001	2.401	1.980	

It is observed in Table 6-5 that the lateral tire stiffness increases with an increase of inflation pressure but decreases with an increase in applied loading. The damping parameters on both hard surface and dry sand are directly influenced by the inflation pressure and applied loading, increasing in tandem.

6.7 Steering Characteristics on Dry Sand, $k_{f,Dry\ Sand}$

The cornering stiffness,$k_{f,Dry\ Sand}$, of the RHD tire is determined through a steady state steering experiment. The experiment procedure is depicted within Figure 6-10 consists of an applied vertical load to the tire spindle to simulate the vehicle weight and loading of 13.34 kN, 26.69 kN, and 40.03 kN (3,000 lbs., 6,000 lbs., and 9,000 lbs.). The tire inflation pressure varied from 110 psi, 85 psi, and 55 psi with an applied linear tire speed (applied to the tire spindle also) of 10 km/h. The lateral and horizontal forces at the tire-soil contact area are analyzed as the tire steering rates change from 0, 4, 8, and 12 degrees. Figure 6-11 and Figure 6-12 are illustrations of obtained results.

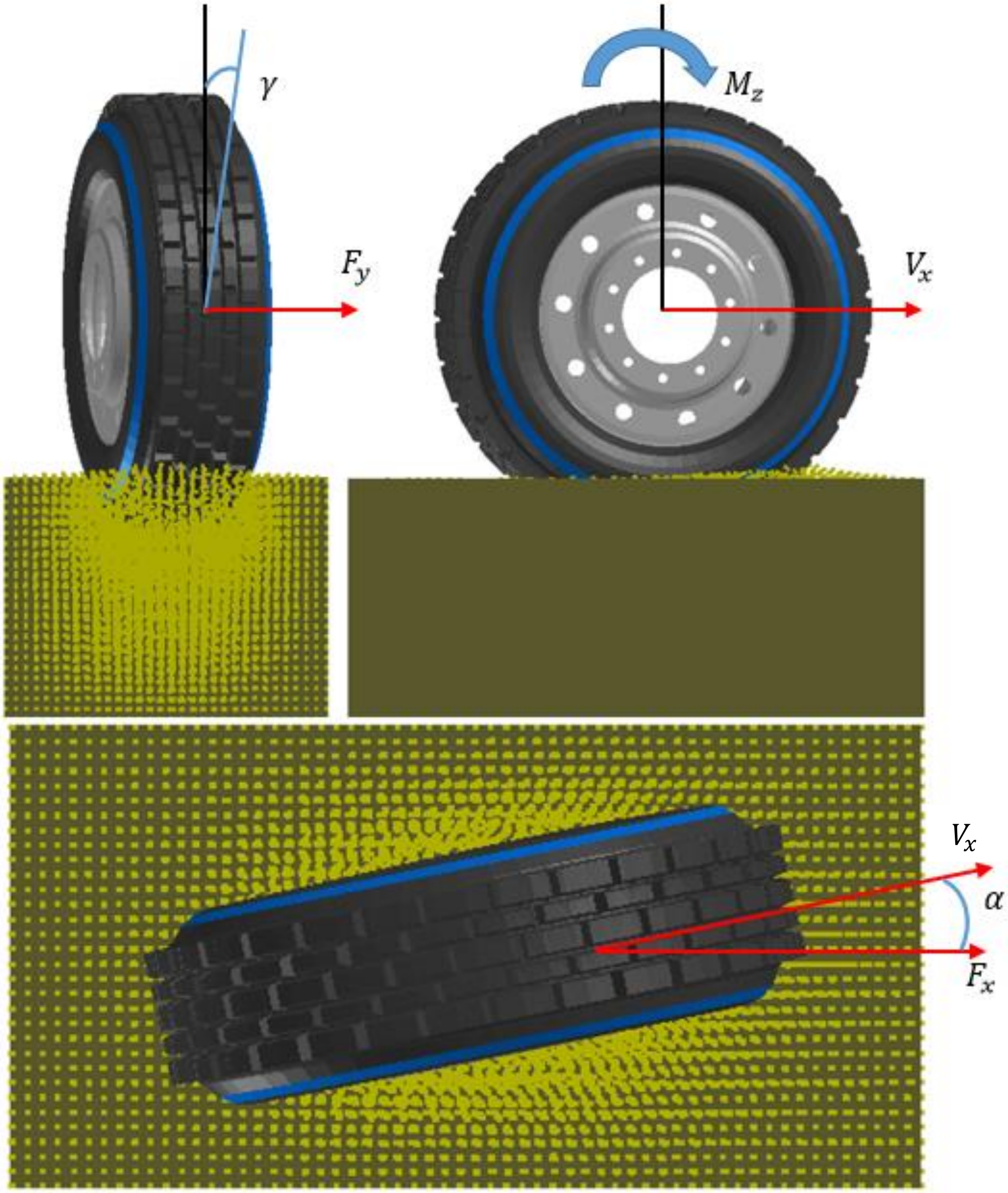

Figure 6-10: RHD Cornering Stiffness Procedure on Dry Sand

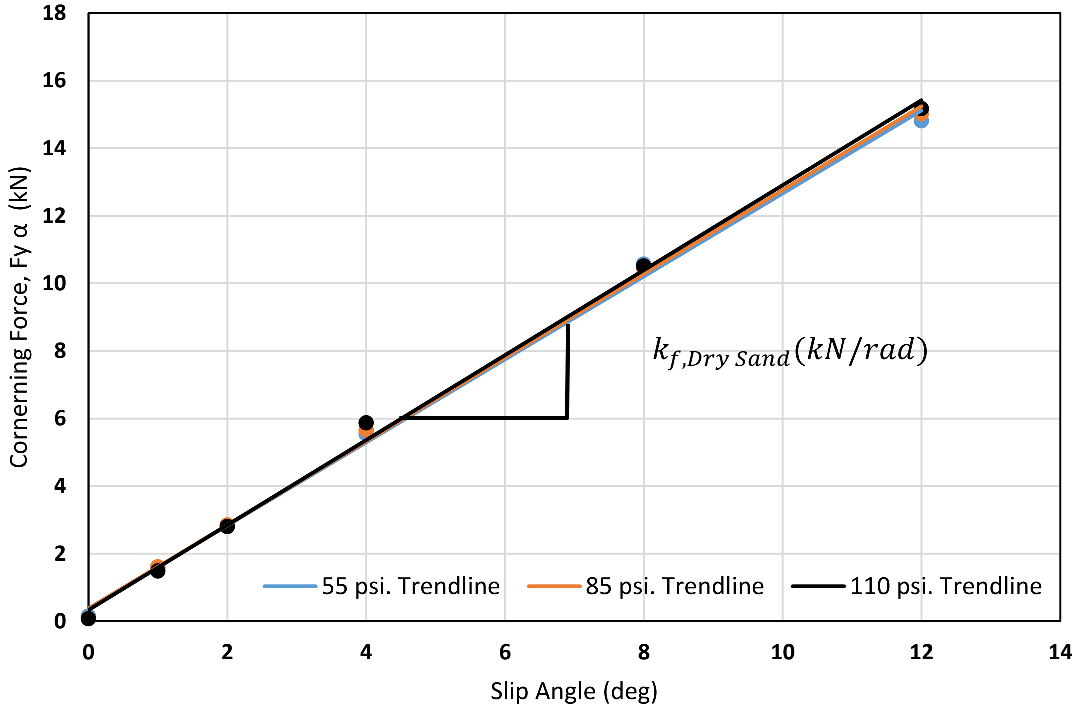

Figure 6-11: Cornering Stiffness as a Function of the Slip Angle at 26.69 kN on Dry Sand

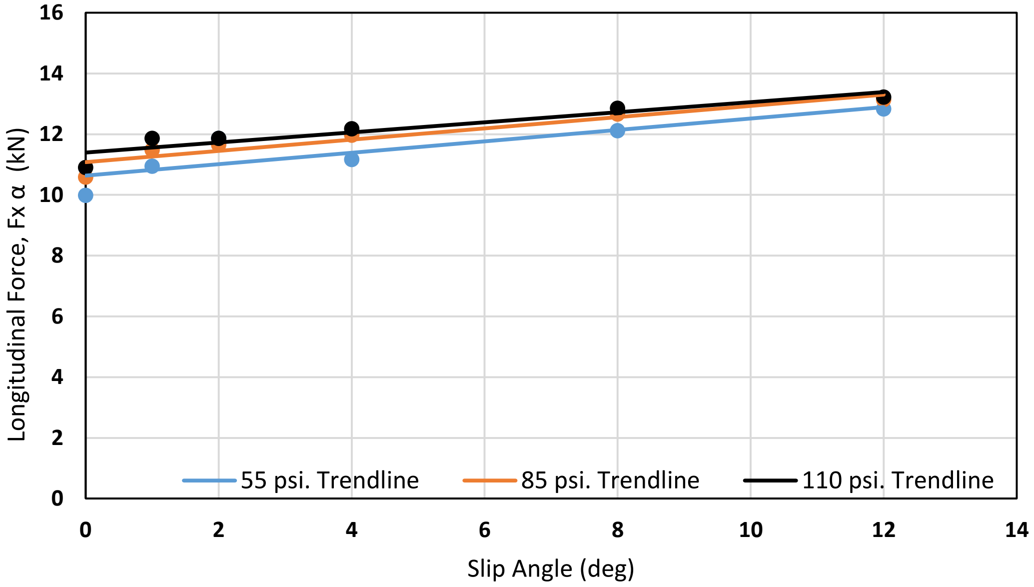

Figure 6-12: The Longitudinal Force as a Function of the Slip Angle at 26.69 kN on Dry sand

Since the soft soil curves have a linear trend, the slope is taken from the linear trend between a slip angles of 0-12 deg. It is noted that the slip angle is defined as the angle between the longitudinal axis of the wheel and its direction of travel [1]. The cornering stiffness is the derivative of the lateral force,$F_{y,Dry\ Sand}$, with respect to the slip angle,$\alpha_{Dry\ Sand}$, evaluated at a zero-slip angle; when the slip angle is greater than zero the force acting on the tire is the lateral force, as Equation 6-34 describes. The same method of calculations is used for the 85 psi and 55 psi parameter predictions.

$$k_{\ f,Dry\ Sand} = \frac{\partial\ F_{y,SPH\ Dry\ Sand}}{\partial\ \alpha_{Dry\ Sand}}|_{\alpha=0} \qquad 6\text{-}34$$

Table 6-6: Cornering Stiffness on SPH Soft Soil 1 (Dry Sand) at 3,000lbs.

Parameter	Load (kN)	55 PSI	85 PSI	110 PSI	Units
Cornering Stiffness ($k_{f,Dry\ Sand}$)	13.345	44.834	45.917	44.639	kN/rad
	26.689	70.376	71.01	72.044	
	40.034	90.845	97.156	97.672	

Table 6-6 makes it evident that the cornering stiffness linearly increases with an increase in slip angle and the force increases with an increase in applied loading but does not significantly increase with an increase in inflation pressure.

6.8 Self-Aligning Moment Stiffness on Dry Sand, $M_{z,Dry\ Sand}$

During the same procedure as the cornering stiffness test, as described within Section 6.7 , the moment,$M_{z,Dry\ Sand}$, about the contact patch is also analytically observed within Figure 6-13. The torque stiffness,$k_{M,Dry\ Sand}$ is the summation for the linear slope of the moments and pneumatic trail.

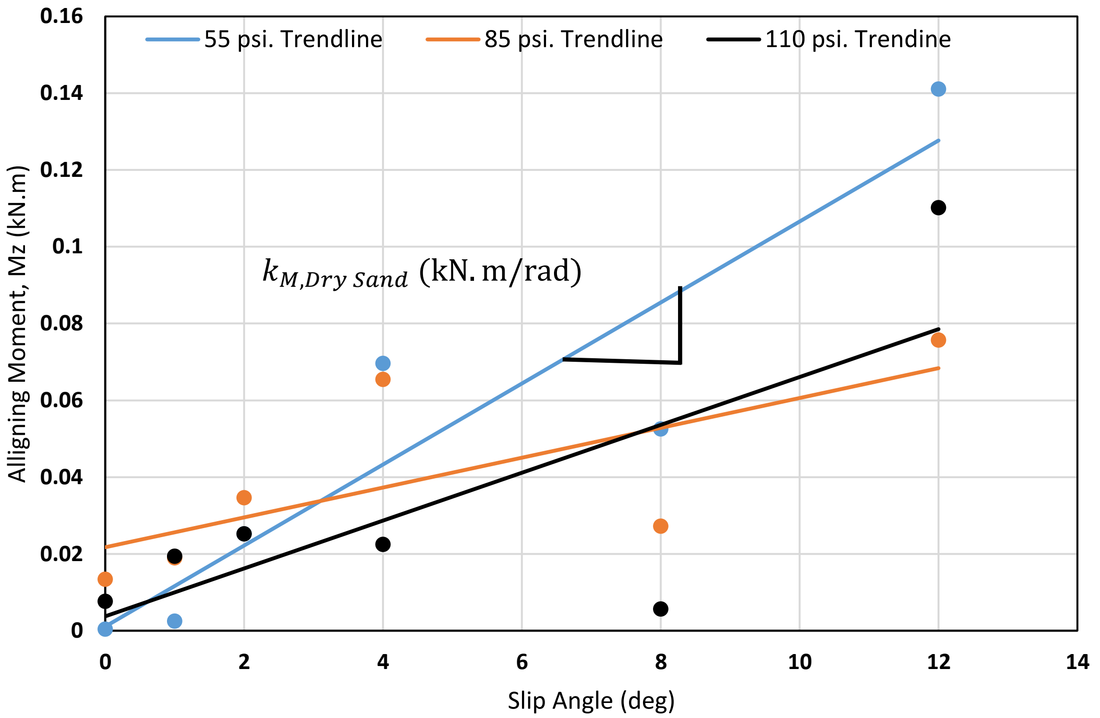

Figure 6-13: RHD Self-Aligning Moment at 26.69 kN on Dry Sand

The self-aligning moment stiffness is the slope of the self-aligning moment ($M_{z,Dry\ Sand}$) verses slip angle as displayed within Equation 6-35 ;

$$k_{\ M,Dry\ Sand} = \frac{\partial\ M_{y,Dry\ Sand}}{\partial\ \alpha_{sDry\ Sand}}|_{\alpha=0} \qquad 6\text{-}35$$

As observed in Table 6-7, the self-aligning torque stiffness appears to have no noticeable trend with respect to the inflation pressure and applied loading. Further investigation of the soil model and of the tire-soil interaction is required to understand this phenomenon.

Table 6-7: RHD Self-Aligning Stiffness on Dry Sand

Parameter	Load (kN)	55 PSI	85 PSI	110 PSI	Units
Self-Aligning Torque Stiffness ($k_{M,Dry\ Sand}$)	13.345	0.602	0.372	0.304	kN.m/rad
	26.689	0.521	0.223	0.355	
	40.034	0.791	0.075	0.384	

6.9 Relaxation Length on Dry Sand, $\boldsymbol{\sigma_{Dry\ Sand}}$

The relaxation length,σ, is the ratio of the cornering stiffness,$k_{f,Dry\ Sand}$, by the total equivalent lateral stiffness,$k_{l,tot,Dry\ Sand}$. The relaxation length is the length in which the tire must travel to overcome the initial resistive forces and reach steady state cornering values. The total equivalent lateral stiffness is determined and described in detail in the previous Section 5.3. In summary, the lateral tire stiffness experiment applies and releases a 5kN lateral load to the spindle of the tire in a cyclic fashion allowing the tire carcase to resonate. The results are determined using Equation 6-36 and summarized in Table 6-8.

$$\sigma_{Dry\ Sand} = \frac{k_{f,Dry\ Sand}}{k_{Lltot,Dry\ Sand}}\ m \qquad 6\text{-}36$$

Table 6-8: RHD Relaxation Length on Dry Sand

Parameter	Load (kN)	55 PSI	85 PSI	110 PSI	Units
Relaxation Length ($\sigma_{Dry\ Sand}$)	13.345	0.196	0.156	0.130	m
	26.689	0.239	0.174	0.143	
	40.034	0.304	0.233	0.191	

6.10 Rolling Resistance Coefficient on Dry Sand, $\boldsymbol{RRC_{Dry\ Sand}}$

The rolling resistance coefficient is obtained through a similar testing procedure as the previous cornering stiffness experiment, but at 1/10th the applied speed, by analyzing the resistive forces acting on the tire-soil contact patch (F_x), and vertical loading on the tire (F_z); Equation 6-37 and Figure 6-14 illustrate the relationship of the rolling resistance coefficient on dry sand.

$$RRC_{Dry\ Sand} = \frac{F_x}{F_z} \qquad 6\text{-}37$$

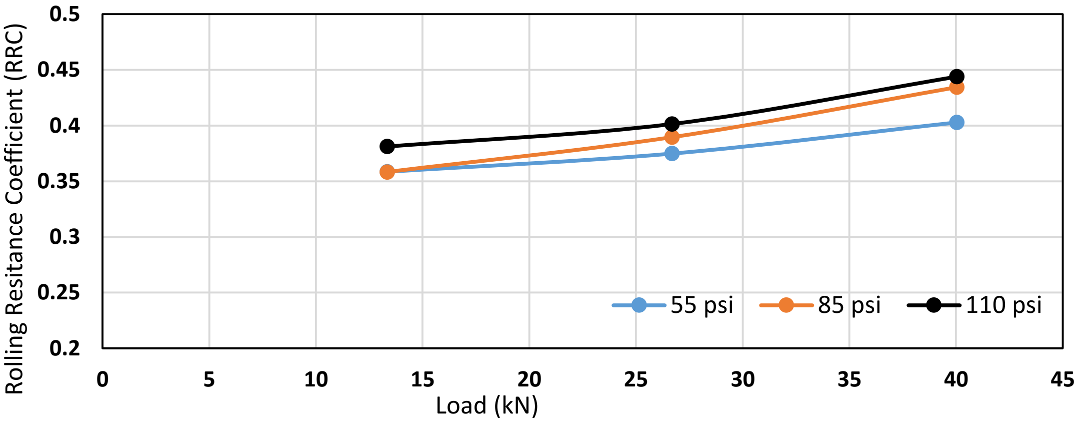

Figure 6-14: Rolling Resistance Coefficient on Dry Sand

Table 6-9: Rolling Resistance Coefficient on SPH Soft Soil 1 (Dry Sand)

Parameter	Load (kN)	55 PSI	85 PSI	110 PSI	Units
Rolling Resistance Coefficient ($RRC_{Dry\ Sand}$)	13.345	0.352	0.345	0.336	-
	26.689	0.408	0.396	0.374	
	40.034	0.471	0.460	0.426	

The rolling resistance coefficient is summarised within Table 6-9 and appears to increase with load but has no direct correlation with the inflation pressure. It may be assumed that an increase in inflation pressure increases the rolling resistance of the tire on dry sand. These trends are supported by Wong's conclusions with the variation of the rolling resistance on different road surfaces [1].

6.11 Chapter Summary

This chapter summarized that the translational and rotational stiffness and damping constant parameters are linearly dependant on the inflation pressure of the tire. Yet, the applied loading is not assumed to be an influential factor. The lateral stiffness and damping parameters yield identical trends. The lateral stiffness and damping constant on a hard surface is linearly proportional to either operating conditions. The cornering stiffness increases linearly with both the load and inflation pressure conditions. It is noted that the cornering stiffness is mostly load dependant as the inflation pressure is only noticeably influential at high loads. Because the relaxation length is a function of the cornering stiffness and lateral stiffness, the relaxation length is dependent on the applied tire loading. Finally, the rolling resistance coefficient is highly dependent by both the applied loading and inflation pressure conditions. Table 6-10, Table 6-11, and Table 6-12 summarize the predicted out-of-plane off-road rigid-ring model parameters.

6.11.1 13.34 kN Out-of-Plane Parameter Summary

Table 6-10: Summary of the Out-of-Plane Off-Road Rigid-ring Parameter Predictions at 13.34 kN

13.34 kN Out-of-Plane Off-Road Rigid-ring Parameters	55 PSI	85 PSI	110 PSI	Units
Translational Stiffness (k_{by})	742.926	911.208	1017.603	kN/m
Translational Damping Constant $(c_{b\gamma})$	0.239	0.244	0.248	kN.s/m
Rotational Stiffness $(k_{b\gamma})$	163.711	200.092	227.923	kN.m/rad
Rotational Damping Constant $(c_{b\gamma})$	0.029	0.030	0.029	kN.m.s/rad
Lateral Tire Stiffness (k_l)	222.626	270.345	309.621	kN/m
Lateral Damping Constant (c_l)	0.568	0.567	0.591	kN.s/m
Total Lateral Slip Stiffness, Dry Sand $(k_{l,tot,Dry\ Sand})$	228.893	293.970	342.964	kN/m
Lateral Slip Stiffness, Dry Sand $(k_{l,Dry\ Sand})$	8131.692	3364.134	3184.766	kN/m
Lateral Damping Constant, Dry Sand $(c_{l,Dry\ Sand})$	1.388	1.452	1.585	kN.s/m
Cornering Stiffness, Dry Sand $(k_{f,Dry\ Sand})$	44.834	45.917	44.639	kN/rad
Self-Aligning Torque Stiffness, Dry Sand $(k_{M,Dry\ Sand})$	0.602	0.372	0.304	kN.m/rad
Relaxation Length, Dry Sand $(\sigma_{,Dry\ Sand})$	0.196	0.156	0.130	m
Rolling Resistance Coefficient, Dry Sand $(RRC_{,Dry\ Sand})$	0.352	0.345	0.336	-

6.11.2 26.69 kN Out-of-Plane Parameter Summary

Table 6-11: Summary of the Out-of-Plane Off-Road Rigid-ring Parameter Predictions at 26.69 kN

26.69 kN Out-of-Plane Off-Road Rigid-ring Parameters	55 PSI	85 PSI	110 PSI	Units
Translational Stiffness (k_{by})	742.926	911.208	1017.603	kN/m
Translational Damping Constant $(c_{b\gamma})$	0.239	0.244	0.248	kN.s/m
Rotational Stiffness $(k_{b\gamma})$	163.711	200.092	227.923	kN.m/rad
Rotational Damping Constant $(c_{b\gamma})$	0.029	0.030	0.029	kN.m.s/rad
Lateral Tire Stiffness (k_l)	212.397	265.420	302.202	kN/m
Lateral Damping Constant (c_l)	0.594	0.590	0.591	kN.s/m
Total Lateral Slip Stiffness, Dry Sand $(k_{l,tot,Dry\ Sand})$	294.062	408.207	502.069	kN/m
Lateral Slip Stiffness, Dry Sand $(k_{l,Dry\ Sand})$	764.810	758.800	759.136	kN/m
Lateral Damping Constant, Dry Sand $(c_{l,Dry\ Sand})$	1.598	1.572	1.438	kN.s/m
Cornering Stiffness, Dry Sand $(k_{f,Dry\ Sand})$	70.376	71.010	72.044	kN/rad
Self-Aligning Torque Stiffness, Dry Sand $(k_{M,Dry\ Sand})$	0.521	0.223	0.355	kN.m/rad
Relaxation Length, Dry Sand $(\sigma_{,Dry\ Sand})$	0.239	0.174	0.143	m
Rolling Resistance Coefficient, Dry Sand $(RRC_{,Dry\ Sand})$	0.408	0.396	0.374	-

6.11.3 40.03 kN Out-of-Plane Parameter Summary

Table 6-12: Summary of the Out-of-Plane Off-Road Rigid-ring Parameter Predictions at 40.03 kN

40.03 kN Out-of-Plane Off-Road Rigid-ring Parameters	55 PSI	85 PSI	110 PSI	Units
Translational Stiffness (k_{by})	742.926	911.208	1017.603	kN/m
Translational Damping Constant $(c_{b\gamma})$	0.239	0.244	0.248	kN.s/m
Rotational Stiffness $(k_{b\gamma})$	163.711	200.092	227.923	kN.m/rad
Rotational Damping Constant $(c_{b\gamma})$	0.029	0.030	0.029	kN.m.s/rad
Lateral Tire Stiffness (k_l)	211.665	320.227	439.576	kN/m
Lateral Damping Constant (c_l)	0.591	0.576	0.616	kN.s/m
Total Lateral Slip Stiffness, Dry Sand $(k_{l,tot,Dry\ Sand})$	309.157	417.247	511.948	kN/m
Lateral Slip Stiffness, Dry Sand $(k_{l,Dry\ Sand})$	671.213	1377.180	3109.470	kN/m
Lateral Damping Constant, Dry Sand $(c_{l,Dry\ Sand})$	2.001	2.401	1.980	kN.s/m
Cornering Stiffness, Dry Sand $(k_{f,Dry\ Sand})$	90.845	97.156	97.672	kN/rad
Self-Aligning Torque Stiffness, Dry Sand $(k_{M,Dry\ Sand})$	0.791	0.075	0.384	kN.m/rad
Relaxation Length, Dry Sand $(\sigma_{,Dry\ Sand})$	0.304	0.233	0.191	m
Rolling Resistance Coefficient, Dry Sand $(RRC_{,Dry\ Sand})$	0.471	0.460	0.426	-

CHAPTER 7

CONCLUSIONS AND FUTURE WORK

7.1 Conclusions

This thesis successfully predicts the in-plane and out-of-plane off-road rigid-ring parameters of an FEA RHD truck tire on a SPH soft soil representing dry sand. These parameters are described at varying operating conditions; applied vertical loading, 13.34 kN (3,000 lbs.), 26.69 kN (6,000 lbs.), and 40.03 kN (9,000 lbs.) and inflation pressure at 55 psi, 85 psi, 110 psi.

Further validation of the FEA tire model is concluded by quantifying the vibrational mode trends to be in agreement with previously published literature. It is determined that the tire's inflation pressure has the most substantial impact on the first mode of vibration of the three operating conditions analyzed within the scope of the drum-cleat sensitivity analysis; the relationship between the mode frequency and inflation pressure is directly linear. Neither the applied loading nor the linear speed of the tire have a substantial influence on the nodal frequency. The first vertical mode of vibration of the RHD tire occurs within the range of 46-57 Hz, and the horizontal first mode of vibration occurs between 21-26 Hz. The frequency analysis enabled for the determination of the proportional RHD sidewall damping coefficient, with respect to inflation pressure, which is re-submitted into the FEA tire model during rigid-ring testing procedures on dry sand.

The in-plane off-road rigid-ring RHD parameters were successfully predicted on an SPH dry sand soft soil model at three varying inflation pressures and applied loadings. All majority in-plane parameters are strongly influenced by the inflation pressure of the tire, the relationship with respect to the inflation pressure is directly linear. This is because the in-plane parameters are products of relationships derived with respect to the first mode of the tire. The longitudinal tire and tread stiffness and damping constants are the parameters which are not heavily influenced by the inflation pressure of the tire but rather these parameters have a linear relationship with respect to the applied loading of the tire. In perspective the vertical sidewall and residual stiffness and damping constants, and the rotational stiffness and damping constants are constant regardless of the road surface the tire is traversing. The total equivalent vertical stiffness on soft soil (Dry Sand) is not as heavily influenced by the inflation pressure compared to the total vertical stiffness on soft soil, with the soft soil vertical stiffness increasing by a total of 10 kN over a difference of 55 psi. However, the hard surface total vertical stiffness nearly doubles over the same increase in inflation pressure. For perspective, at the maximum inflation pressure tested, 110 psi, the dry sand total vertical stiffness is nearly nine times smaller than that determined on the hard surface. This is a predictable trend as the soft soil deforms under vertical loading. The longitudinal force evidently increases with an increase in slip percentage; whereas it is expected that on a hard surface the slip would reach a peak.

The out-of-plane off-road rigid-ring parameters were also successfully predicted at varying operating conditions. The translational and rotational stiffness and damping constants are not dependent on the road surface or applied loading but are linearly proportional to the inflation pressure of the tire. The lateral stiffness and damping values on the hard surface is linearly proportional to either operating conditions. When considering the lateral stiffness on dry sand the parameters are inversely proportional to either the applied loading or inflation pressure conditions. For perspective, the lateral stiffness on dry sand is at a minimal of three times higher than that of the corresponding values tested on a hard surface. This is accounted for by the compression of the soil by the tire during the experience of a lateral force. In regards to the steering characteristics, the cornering stiffness has a direct and linear relationship with respect to both the applied loading and inflation pressure conditions. However, the cornering stiffness is primarily load dependent because the inflation pressure is only noticeably influential at high vertical loads. More importantly, it is observed that the soil builds in front of the tire, creating what is called a bulldozing effect, during high slip angles. The additional lateral force of the soil exerted onto the tire during cornering maneuvers may contribute to higher than expected results. This may be solved through investigation of the cohesion of the soil model. Because the relaxation length is a function of the cornering stiffness and lateral stiffness, the parameter is also another function linearly dependant on the varied operating conditions. Furthermore, the rolling resistance coefficient is directly proportional with respect to linearity of either the applied loading or inflation pressure of the tire.

The main outcomes of this research are summarised in the following points;

- The investigation of a new FEA RHD (U.O.I.T 2017) truck tire on a recently developed SPH (Dry Sand) soil model was successfully completed.
    - The in-plane and out-of-plane off-road rigid-ring model was populated.
    - The parameters will facilitate a full vehicle model for industry partners (Volvo).
- The influence of varying the tire's operating conditions (applied tire loading and inflation pressure) on the tire-soil interactions and on the off-road rigid-ring parameters has been determined.
    - The off-road rigid-ring parameters have a direct linear relation with the tire's operating conditions on SPH soft soil (Dry Sand).
    - It is worthy to note that the inflation pressure is only noticeably influential at high vertical loads when considering the cornering stiffness.
    - At this present time the author is unable to quantify these observations to state of the art because previous soil interactions were limited to FEA soil modeling techniques and were further limited to single, or static, tire operating conditions.
- The tire-soil interactions between an FEA RHD truck tire and a SPH (Dry Sand) soil model offered insight.
    - A Bulldozing phenomenon is observed. This phenomenon was also noted with respect to literature of an FEA soil model (Sandy Loam) [17]; however the phenomenon is drastically more visible within the SPH (Dry Sand) model presented within this work(s).
    - Some resulting steering characteristic parameters (cornering stiffness and self-aligning moment stiffness) are difficult to measure and appear to be lower than anticipated when qualitatively comparing to off-road models incorporating FEA soil modeling techniques.
    - This prompts further investigation of the SPH modeling techniques to confirm if the above mentioned occurrences are simply accurate to a more detailed soil model as provided with SPH modeling techniques or if it

indicates a miss interpretation or representation of the actual soil within the newly developed SPH model.

The main outcomes are such that the discussed research gaps within CHAPTER 1 have been occupied with bridges of information. However, due to the individuality of this research it is extremely difficult to quantify comparisons to state of the art. Combined with the discoveries mentioned above further investigations and future works(s) to complete the gaps in entirety is advised. Please refer to the following section (Section 7.2) for recommendations on future work(s).

7.2 Future Work

It is recommended that the SPH soft soil (Dry Sand) modeling techniques undergoes further investigation to complete the bridging of the research gaps due to lack of state of art. Specifically highlighting concerns of uncertainty of the accuracy of the soil model needs to be addressed. It is recommended that the soil model be validated with physical testing measurements of an RHD truck tire driving over a dry sand; transducers may be used to take these measurements. However, due to the expense of obtaining the required equipment for such an extensive physical experiment a laboratory soil sample test may suffice in combination with laboratory testing of the tire to be compared to specific rigid-ring parameters, specifically parameters only in need of static testing.

When considering the SPH soil model used within this thesis it has some short comings; the soil model does not yet accurately represent the damping effects of the soil. Soil properties should be accurately investigated with real tri-axle testing of physical soil samples to determine specific soil parameters. Specifically, the soil cohesion requires further investigation along with the application of the soil properties defined within PAM-CRASH material card functions is in need of further understanding. More importantly, the friction coefficient was assumed to be a generic value and should be determined via experimental measurements. Furthermore, the use of PAM-OPT may be used to explore the optimisation of the soil material properties.

Another possible method of confirming the tire-soil interaction model is to compare the predicted parameters to another software output, such as MATLAB or LS-DYNA. More importantly, the off-road rigid-ring model parameters needs to consider the probability of accounting for the soil damping, likely with the introduction of a damper in parallel to the soil stiffness parameter. Furthermore, the alternative isolated parameter testing methodologies for the steering characterises should be considered in future work. Future investigation of SPH modeling techniques may include the modeling of water for tire hydroplaning studies, or even mixed tire-soil-water interactions in the interest of investigating steering and traction characteristics on flooded surfaces.

PUBLICATIONS

Lardner, K., El-Gindy, M., Oijer, F., Johansson, I. et al., "Determining the Vertical and Longitudinal First Mode of Vibration of a Wide Base FEA Truck Tire," SAE Technical Paper 2016-01-1308, 2016, doi:10.4271/2016-01-1308.

*Note: Portions of the listed publication have been used within this thesis. All writings and simulations within the mentioned publication was completed by the author of this thesis and the publication works are continued in the work of this thesis. Technical support and advice has been received by the listed co-authors for both works.

REFERENCES

[1] J. Y. Wong, Theory of Ground Vehicles 3rd Edition, Toronto : John Wiley & Sons, Inc. , 2001.

[2] Continental Tire , "History of the Passenger Tire," Continental Tire , 2017. [Online]. Available: http://www.continentaltire.com/content/history-passenger-tire. [Accessed 11 06 2017].

[3] Michelin, "History of the Michelin Group," Michelin , 2017. [Online]. Available: http://www.michelin.com/eng/michelin-group/profile/history-of-the-michelin-group. [Accessed 11 06 2017].

[4] K. Lardner, El-GIndy, Moustafa, F. Oijer and Johansson I , "Determining the Vertical and Longitudinal First Mode of VIbration of a Wide BAse FEA Truck Tire," in *SAE technical Paper 2016-01-1308*, Detroit, Michigan, 2016.

[5] Michelin , "How is a tire made?," 2017. [Online]. Available: http://www.michelinman.com/US/en/help/how-is-a-tire-made.html. [Accessed 11 06 2017].

[6] K. M. Captain, A. B. Boghani and D. N. Wormley, "Analytical Tire Models for Dynamic Vehicle Simulation," *Vehicle System Dynamics,* vol. 8, no. 1, pp. 1-32, 1979.

[7] D. C. Davis, "A Radial-Spring Terrain-Enveloping Tire Model," *Vehicle System Dynamics,* vol. 4, no. 1, pp. 55-69, 1975.

[8] M. Takayama and K. Yamagishi, "Simulation Model of Tire Vibration," *Tire Science and Technology* , vol. 1, no. No. 1, pp. 38-49, 1984.

[9] M. Loo, "A Model Analysis of Tire Behavior Under Vertical Loading and Straight-Line Free Rolling," *Tire Science and Technology* , vol. 13, no. 2, pp. 67-90, 1985.

[10] P. W. Zegelaar and H. B. Pacejka, "Dynamic Tyre Responses to Brake Torque Variations," *Vehicle System Dynamics,* vol. 27, no. S1, pp. 65-79, 1997.

[11] S.-J. Kim and A. R. Savkoor, "he Contact Problem of In- Plane Rolling of Tires on a Flat Road," *Vehicle System Dynamics,* vol. 27, no. S1, pp. 189-206, 1997.

[12] S. Bruni, F. Cheli and F. Resta, "On the Identification in Time Domain of the Parameters of a Tyre Model for the Study of In-Plane Dynamics," *Vehicle System Dynamics,* vol. 27, no. S1, pp. 136-150, 1997.

[13] D. J. Allison and R. S. Sharp, "On the low frequency in-plane forced vibrations of pneumatic tyre/wheel/suspension assemblies," *Vehicle System Dynamics,* vol. 27, no. S1, pp. 151-162, 1997.

[14] A. J. C. Schmeitz, S. T. H. Jansen, H. B. Pacejka, J. C. Dsvis, N. N. Jota, C. G. Liang and G. Lodewijks, "Application of a semi-empirical dynamic tyre model for rolling over arbitrary road profiles," *International Journal of Vehicle Deisgn,* vol. 36, no. 2-3, pp. 194-215.

[15] J. R. Allen, Rigid Ring Quater-Vehicle Model for Durability and Ride Comfort Predictions, Pennsylvania: The Pennsylvania State University, 2007, p. 75.

[16] S. Chae, Nonlinear Finite Element Modeling And Analysis of A Truck Tire, Pennsylvania: The Pennsylvania State Univeristy, 2006, p. 206.

[17] J. L. Slade, Development of a New Off-Road Rigid Ring Model for Truck Tires Using Finite Element Analysis, The Pennsylvania State Univeristy , 2009 , p. 89.

[18] R. N. Yong, E. A. Fattah and P. Boosninsuk, "Analysis and predictio of tyre-soil interaction and performance using finite elements," *Journal of Terramechanics* , vol. 15, no. 1, pp. 43-63, March 1978.

[19] Y. Nakajima and J. Padovan, "Numerical Simulations of Tires Sliding Events Involving Impacts with Holes and Bumps," *Tire Science and Technology,* vol. 14, no. 2, pp. 125-136, 1986.

[20] T. B. Rhyne, R. Gall and L. Y. Chang, "Influence of Rim Rum-Out on the Nonuniformity of Tire-Wheel Assemblies," *Tire Scence and tecnology,* vol. 22, no. 2, pp. 99-120, 1994.

[21] T. Hiroma, S. Wanjii, T. Kataoka and Y. Ota, "Stress analysis using fem on stress distribution under a wheel conisdering friction with adhesion between a wheel and soil," *Journal of Terramechanics,* vol. 34, no. 4, pp. 255-233, October 1997.

[22] X. Yan, "Nonlinear Three-Dimensional Finfite Element Analysis of Steady Rolling Radial Tires," *Journal of Reinfoeced Plastics and Compositie s,* vol. 22, no. 8, pp. 733-750, 2003.

[23] X. Yan, "Finite Element Formulation of Tire with Static Foundation Contact and Its Application," *Journal of Reinforced Plastics and Composites,* vol. 24, no. 16, pp. 1671-1696, 2005.

[24] Y. P. Chang, Nonlinear Rotating Tire Modeling for Transient Response Simulations, Ph. D. Thesis, Univerity Park, PA, 2002.

[25] R. Ali, M. El-GIndy, D. Ranvir, T. Mukesh, F. Oijer and I. Johansson, "Prediction of Tire Ground Interaction Using FEA Truck Tire Models," in *ASME 2012*

International Design Engineering Technical Confrences and Computers and Information in Engineering Confrence , 2012.

[26] P. Kindt, P. Sas and W. Desmet, "Three-dimesnional Ring Model for the Prediction of the Tyre structural Dynamic Behaviour," *Procedings of ISMA2008,* pp. 4155-4170, 2008.

[27] A. C. Reid, "Development and Optamization of a Wide Base FEA Truck Tire Model for Prediction of Tire-Road Interactions," Univerity of Onario Institute of Technology, Oshawa, Ontario, 2015.

[28] M. G. Bekker, Theory of Land Locomotion, AnnArbor: The University of Michigan Press, 1956.

[29] M. G. Bekker, Off-the-Road Locomotion, AnnArbor: University of Michigan Press, 1960.

[30] M. G. Bekker, Introduction to Terrain-Vehcile Systems, AnnA rbor: The University of Michigan Press, 1969.

[31] Z. Jamosi and B. Hanamoto, "The Analyitical Determination of Drawbar Pull as a Function of Slip for Tracked VEhicles in Deformable Soils," in *1st International Conference on Terrain-Vehicle Systems,* Turin, Italy, 1961.

[32] M. S. Osman, "The Measurment of Soil Shear Strength," *Journal of Terramechanics* , vol. 1, no. 3, pp. 54-60, 1964.

[33] R. D. Wismer and H. J. Luth, "Off-Road Prediction for Wheeled Vehicles," *Journal of Terramechanics* , vol. 10, no. 2, pp. 49-61, 1973.

[34] W. W. Brixius, "Traction Prediction Equations for Bias Ply Tires Paper No. 87-1662," *ASAE,* 1987.

[35] R. N. Yong, A. F. Youssef and E. A. Fattah, "Vane-Cone Measurments for Assesment of Tractive Performance in Wheel-Soil Interaction," in *5th International Conference of the ISTVS,* Detroit, USA, 1975.

[36] R. Alcock, Wittig and V. , "An Emperical Method of Predicting Traction," *Journal of Terremechanics* , vol. 29, no. 4-5, pp. 381-394, 1992.

[37] J. Y. Wong, Terramechanics and Off-Road Vehicles, Elsevier, 1989.

[38] A. Okello, "A Review of Soil Strength Measurment Techniques for Prediction of Terrain Vehicle Performance," *Journal of Agriculural Engineering Research,* vol. 50, pp. 129-155, 1991.

[39] M. Grahn, "Prediction of Sinkage and Rolling Resistance for Off-the-Road Vehicles Considering Penetration," *Journal of Terramechanics,* vol. 28, no. 4, pp. 339-347, 1991.

[40] E. Masad, "Stress-Strain Model for Clays with Anisotropic Void Ratio Distribution," *International Journal for Numerical and Analystical Methods in Geomechanics,* vol. 22, no. 5, pp. 393-416, 1998.

[41] N. A. Al-Shayea, "A Plastic-DAmage Model for Stress-Strain Behaviour of Soils," *International Journal of Damafe Mechanics,* vol. 12, no. 4, pp. 304-329, 2003.

[42] S. A. Shoop, "Finite Element Modeling of Tire-Terrain Interaction," U.S. Army Engineer Research and Development Center, Hanove, 2001.

[43] C. W. Fevers, "Improved FEM Simulation Model for Tire-Soil Interaction," *Journal of Terramechanics,* vol. 41, no. 2-3, pp. 87-100, 2004.

[44] J. P. Hamblleton and A. Drescher, "Modeling wheel-induced rutting in soils: Identification," *Journal of Terramechanics* , vol. 45, no. 6, pp. 201-211, 12 2008.

[45] J. P. Hambleton and A. Drescher, "Modeling wheel-indiced rutting in soils: Rolling," *Journal of Terramechanics,* vol. 46, no. 2, pp. 35-47, 2009.

[46] R. C. Chiroux, W. A. Foster, C. E. Johnson, S. A. Shoop and R. L. Raper, "Three-Dimensional FInite Elment Ansalysis of Soil Interaction with a Rigid Wheel," *Applied Mathematics and Computation,* vol. 162, no. 2, pp. 707-722, 2005.

[47] B. Schlatter, A PEdagogical tool using smoothed particle hydrodynamics to model fluid flow past a system of cylinders, Dual MS Project, Oregon State University, 1999.

[48] P. H. L. Groenenboom, "Numerical Simulation of 2D and 3D Hypervelocity Impact Using the SPH Option in PAM-SHOCK," *International Journal of Impact Engineering* , vol. 20, no. 1-5, pp. 309-323, 1997.

[49] R. A. Clegg, J. Sheridan, C. J. Hayhurst and N. J. Francis , "The Application of SPH Techniques in AUTODYN-2D to Kinetic Penetrator Impacts on Mutli-Layered Soil and Concrete Targets," *8t International Symposium on Interaction of the Effects of Munitions with Structures,* pp. 22-25, April 1997.

[50] M. Frauud, R. Destefanis, D. Palmieri and M. Marchetti, "SPH Simulations of Debris Impacts Using Two Deifferent Computer Codes," *International Journal of Impact Engineering* , vol. 23, no. 1-1, pp. 249-260, 1999.

[51] M. A. McCarthy, J. R. Xiao, C. T. McCarthy, A. Kamoulakos and J. Ramos, "Modelling of Bird Strike on an Aircraft Wing Leading Edge Made from

Fibre Metal Laminates - Part 2: Modelling of Impact with SPH Bird Model," *Applied Composite Materials,* vol. 11, no. 5, pp. 317-340, 2004.

[52] A. F. Johnson and M. Holzapfel, "Numerical Prediction of Damage in Composite Structures from Soft Body Impacts," *Journal of Materials Science,* vol. 41, no. 20, pp. 6622-6630, 2006.

[53] K. Maeda, H. Sakai and M. Sakai, "Development of Seepage Failure Analysis Method of Ground with Smoothe PArticle Hydrodynamics," *Structural Eng./Earthquake Eng., JSCE,* vol. 23, no. 2, pp. 307s-319s, 2006.

[54] H. H. Bui, R. Fukagawa and K. Sako, "Smoothed Particle Hydrodynamics for Soil Mechanics," *Numerical Methods in Geotechnical Engineering,* 2006.

[55] H. H. Bui, K. Sako and R. Fukagawa, "Numerical Simulation of Soil-Water Interaction Using Smoothed Particle Hydrodynamics (SPH) Method," *Journal of Terramechanics,* vol. 44, pp. 399-346, 2007.

[56] H. H. Bui, K. Sako, R. Fukagawa and J. C. Wells, "SPH-Based Numerical Simulations for Large Deformation of Geomaterial Considering Soil-Structure Interaction," in *12th International Conference of International Association for Computer Methods and Advances in Geoomechanics (IACMAG),* Goa, India, 2008.

[57] H. H. Bui, R. Fukagawa, K. Sako and S. Ohno, "Lagrangian Meshfree Particles Method (SPH) for Large Deformation and Failure Flows of Geomaterial Using Elastic-Plastic Soil Constitutive Model," *International Journal for Numerical and Analytical Methods in Geomechanics* , vol. 32, pp. 1537-1570, 2008.

[58] H. H. Bui, R. Fukagawa, K. Sako and J. C. Wells, "Slope Stability Analysis and Discontinuous SLope Failure Simulation by Elasto-Plastic Smoothed Particle Hydrodynamics (SPH)," *Geotechnique,* vol. 61, no. 7, pp. 565-574, 2011.

[59] H. H. Bui and R. Fukagawa, "An Improved SPH Method for Saturated Soils and its;s Applications to Investigate the Mechansims of Embankment Failure: Case of Hydrostatic Pore-Water Pressure," *International Journal for Numerical and Analytical Methods in Geomechanics,* 2011.

[60] R. S. Dhillion, Development of Truck Tire-Terrain Finite Element Analysis Models, Oshawa, On: University of Ontario Institute of Technology, 2013.

[61] P. H. Groenenboom and B. K. Cartwright, "Hydrodynamics and Fluid-Structure Interaction by Coupled SPH-FE Method," *Journal of Hydraulic Research,* vol. 48, no. S1, pp. 61-73, 2010.

[62] R. Lescoe, Improvement of Soil Modeling in a Tire-soil Interaction Using Finite Elwmwnt Analysis and Smoothed Particle Hydrodynamics, The Pennsylvania State University , 2010.

[63] M. Marjani, Development of FEA Wide-Base Truck Tire and Soil Interaction Models, Oshawa, Ont.: University of Ontario Institute of Technology, 2016, p. 105.

[64] M. Marjani, M. El-Gindy, D. Phillips, F. Oijer and I. Hohansson, "FEA Tire Modeling and Validation Techniques, DETC2015-46514," in *Proceedings of the ASME 2015 International Design Engineering TEchnical COnferences & Computers and Information in Engineering Confrence IDETC/CIE 2015*, Boston, MA, USA , 2015.

[65] "Investigation of Tyre Vibration," [Online]. Available: https://www.tut.fi/ms/muo/tyreschool/moduulit/moduuli_8/hypertext_2/1/1_3.html#1_3_4 . [Accessed 13 01 2015].

[66] H. B. Pacejka, Tyre and Vehicle Dynamics, Butterworth-Heinemann, 2006.

[67] H. Pacejka, "Analysis of Tire Properties," *Mechanics of Pneumatic Tires, edited by Clark, Published by the U.S. Department of Transportation,* 1981.

[68] L. E. Kung, W. Soedel and T. Y. Yang, "Free Vibration of a Pneumatic Tire-Wheel Unit Using a Ring on anElastic Foundation and a Finite Elemeny Model," *Journal of Sound and Vibration,* vol. 207, no. 2, pp. 181-194, 1986.

[69] S. Chae, Nonlineat Finite Element Modeling And Analysis of A Truck Tire A Thesis in Materials, Pennsylvania: The Pennsylvania State Univeristy, 2006, p. 206.